CHARACTERIZATION OF IN-SITU STRESS AND PERMEABILITY IN FRACTURED RESERVOIRS

FINAL REPORT

for Period May 22, 2002–June 30, 2006

by

Daniel R. Burns
and
M. Nafi Toksöz

Earth Resources Laboratory
Department of Earth, Atmospheric, and Planetary Sciences
Massachusetts Institute of Technology
Cambridge, MA 02139

September 25, 2006

Prepared for
THE U.S. DEPARTMENT OF ENERGY
AWARD NUMBER DE-FC26-02NT15346

This technical progress report was prepared with the support of the U.S. Department of Energy, under Award No. DE-FC26-02NT15346. However, any opinions, findings, conclusions, or recommendations expressed herein are those of the authors and do not necessarily reflect the views of the DOE.

DISCLAIMER

Abstract

Fracture orientation and spacing are important parameters in reservoir development. This project resulted in the development and testing of a new method for estimating fracture orientation and two new methods for estimating fracture spacing from seismic data. The methods developed were successfully applied to field data from fractured carbonate reservoirs. Specific results include: the development a new method for estimating fracture orientation from scattered energy in seismic data; the development of two new methods for estimating fracture spacing from scattered energy in seismic data; the successful testing of these methods on numerical model data and field data from two fractured carbonate reservoirs; and the validation of fracture orientation results with borehole data from the two fields.

Researchers developed a new method for determining the reflection and scattering characteristics of seismic energy from subsurface fractured formations. The method is based upon observations made from 3D finite difference modeling of the reflected and scattered seismic energy over discrete systems of vertical fractures. Regularly spaced, discrete vertical fractures impart a ringing coda type signature to seismic energy that is transmitted through or reflected off of them. This signature varies in amplitude and coherence as a function of several parameters including: 1) the difference in angle between the orientation of the fractures and the acquisition direction, 2) the fracture spacing, 3) the wavelength of the illuminating seismic energy, and 4) the compliance, or stiffness, of the fractures. This coda energy is the most coherent when the acquisition direction is parallel to the strike of the fractures. It has the largest amplitude when the seismic wavelengths are tuned to the fracture spacing, and when the fractures have low stiffness. The method uses surface seismic reflection traces to derive a transfer function that quantifies the change in the apparent source wavelet before and after propagating through a fractured interval. When a 3D seismic survey is acquired with a full range of azimuths, the variation in the derived transfer functions allows identification of subsurface areas with high fracturing and determines the strike of those fractures. The method was calibrated with model data and then applied it to data from two fractured carbonate reservoirs giving results that agree with well data and fracture orientations derived from other measurements.

In addition, two approaches for estimating fracture spacing from scattered seismic energy were developed. The first method relates notches in the amplitude spectra of the scattered wavefield to the dominant fracture spacing that caused the scattering. The second uses conventional frequency-wavenumber (FK) filtering to isolate the backscattered signals and then recovers an estimate of the fracture spacing from the dominant wavelength of those signals. The methods were applied to Emilio Field data, resulting in the fracture spacing estimates of about 30-40 meters in both cases.

Table of Contents

Report Contributors:

D. R. Burns
X. Campman
S. Chi
R. Rao
M. N. Toksoz
M. E. Willis
Y. Zhang

Executive Summary

The major result of this project has been the development, testing, and application of a processing and analysis method for extracting fracture information from scattered wavefield signals in seismic data. The method, referred to as the Scattering Index Method, has several important characteristics. First, the method is robust and computationally inexpensive. Second, the method uses a normalization or differential approach that compares the scattering signal above and below an interval of interest in the data. Such an approach is expected to remove any overburden or acquisition footprint from the resulting estimates. Finally, the method has been tested on an extensive suite of synthetic model results as well as several different field data sets with encouraging results. Fracture orientation and fracture density estimates from the Emilio Field (an offshore fractured carbonate reservoir in the Adriatic Sea) agree with FMI logs and borehole breakout data in several wells in the field. The results from analysis of data over an onshore fractured carbonate field in the Middle East were also in agreement with FMI logs from several wells.

Two approaches have been developed to estimate fracture spacing (that is, average spacing between fracture corridors) from spectral analysis of pre-stack seismic data containing scattered wave signals. One method interprets the notches in the amplitude spectra, the other uses FK analysis to isolate backscattered energy and estimate fracture spacing from the wavenumber values of the peak energy. Both methods were applied to the Emilio Field data resulting in spacing estimates of 30-40 m.

In support of these major developments we also investigated ways of using borehole acoustic logs to estimate in-situ stress values, since this stress field will impact fracture apertures and flow estimates. Finally, we also investigated possible approaches for converting seismically derived fracture orientation and spacing information into permeability values for use in reservoir simulators.

II. Introduction

The purpose of this project is to develop and implement large-scale numerical models to quantify the effects of fracture parameter variations on seismic reflection signals and in-situ stress variations on flexural modes in boreholes. These models will be used as the basis of data analysis and inversion routines for estimating the heterogeneous fracture distribution in fractured reservoirs from seismic and borehole field data. Fracture property distributions estimated from seismic data can be used to estimate the permeability tensor in the reservoir for input to reservoir simulators.

The objective of the project is schematically displayed in Figure 1. 3-D seismic data, because of its wide spatial coverage, provides us with an image of the reservoir with resolution in the range of tens of meters. These data are processed to enhance coherent reflections that allow us to map reservoir structure and fault patterns. If we can develop methods to extract information about the distribution and orientation of fractures that are present, the information will be very beneficial to future drilling decisions and production plans. Furthermore, if this seismically derived fracture model (panel 'B" of Figure 1) can be converted into flow properties (by knowledge of fracture spacing, aperture, and connectivity network), then the flow properties of the reservoir can be estimated (panel 'C' of Figure 1). These data can then be used in reservoir simulators to predict reservoir behavior (with comparisons to production history for validation).

The results of this project can be summarized schematically in Figure 2. These plots are the results of our analysis methods on field data from the Emilio Field, an offshore fractured carbonate reservoir. The left panel shows the fault locations as derived from standard interpretation of the 3-D seismic data. The far right panel shows the distribution and orientation of fractures in the reservoir as derived from our scattering index methods developed under this contract. This panel is equivalent to panel 'B' in Figure 1. The orientations of the fractures determined by this method have been validated against borehole data (FMI logs and borehole breakouts) and other seismic analysis methods (amplitude versus offset and azimuth (AVOA), and shear wave birefringence analysis). The center panel of Figure 2 shows the fracture spacing estimates derived from our FK analysis and Spectral Notch methods that were developed under this contract. This panel provides information that is similar to panel 'C' in Figure

1. Fracture spacing will be related to permeability values; however, permeability values will also be a function of fracture apertures and connectivity.

We explored several approaches for converting seismically derived fracture information into permeability estimates. The first was to use a statistical approach derived from the work of Oda (1985) and adapted by Brown and Bruhn (1998). In this approach the distribution of fracture orientations, obtained from the seismic data together with estimates of the fracture length and aperture, are used to derive an equivalent permeability tensor. The fracture network can also be subject to an imposed in-situ stress field (from borehole acoustic logs, for example, as summarized in a later section) that will alter the permeability tensor through closing of fractures in certain orientations. Figure 3 shows an example of the estimated permeability tensors for the Emilio Field based on an assumed aperture value (from core data) and fracture length. A second approach that was investigated was to model Stoke's flow numerically in a fracture network and from those models estimate an equivalent permeability value. This approach provided physical insight into the nature of flow in fracture networks, but proved somewhat untenable in looking at complex 3-D fracture networks. Each of these approaches will be summarized briefly in later sections of the report.

Although we were not able to complete the full cycle as shown in Figure 1, we have completed many of the critical steps. A full history matching of the reservoir performance using our estimated fracture properties was not completed, however a qualitative comparison is possible by comparing relative production variations from different wells with our results. The well locations shown in Figure 2 can be compared to the variations in fracture density. For example, the well shown by a 'blue' dot is by far the most productive well in the field and it is situated in an area of more intense fracturing as shown by our analyses.

The following sections of the report contain summaries of the results of our studies. The appendices contain some newly published papers and conference abstracts. A list of all publications is also provided.

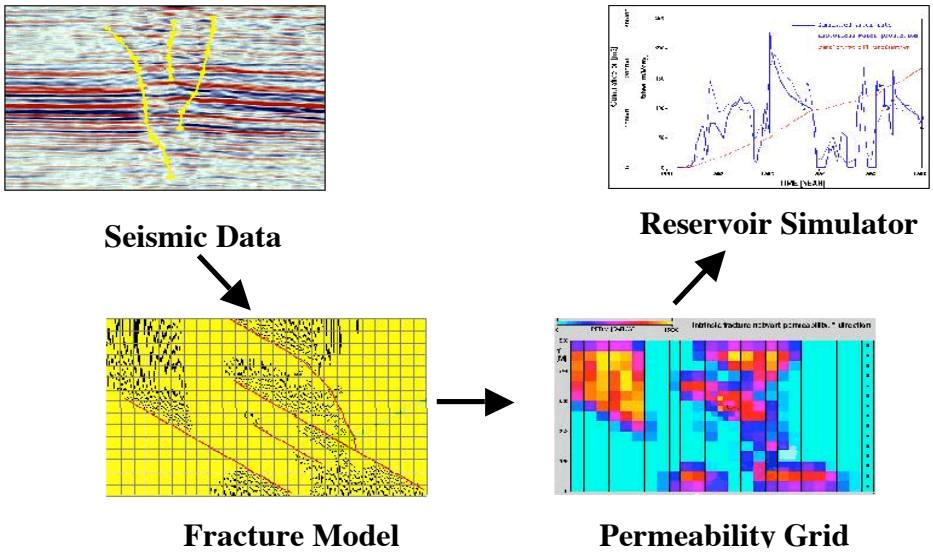

Figure 1. Schematic display of the project objectives. Surface 3-D seismic data is used to estimate the spatial distribution of fracture parameters (e.g., fracture density, spacing, orientation). A model is used to convert such fracture parameters into permeability values, which are input to reservoir simulators for history matching.

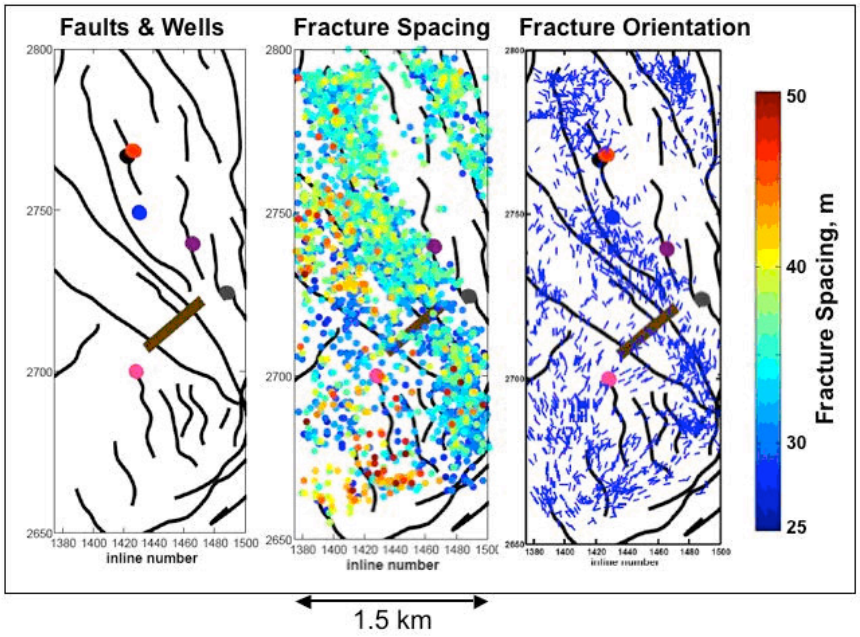

Figure 2. Scattered wavefield analysis of 3-D seismic data volume in a fractured carbonate reservoir (Emilio field). The left panel shows the seismic faults and well locations. The right panel shows the spatial distribution of fracture density and orientation (the direction of each line segment gives the orientation estimate). The center panel shows the estimated spacing of fracture corridors, with the spacing values given by the color bar on the far right.

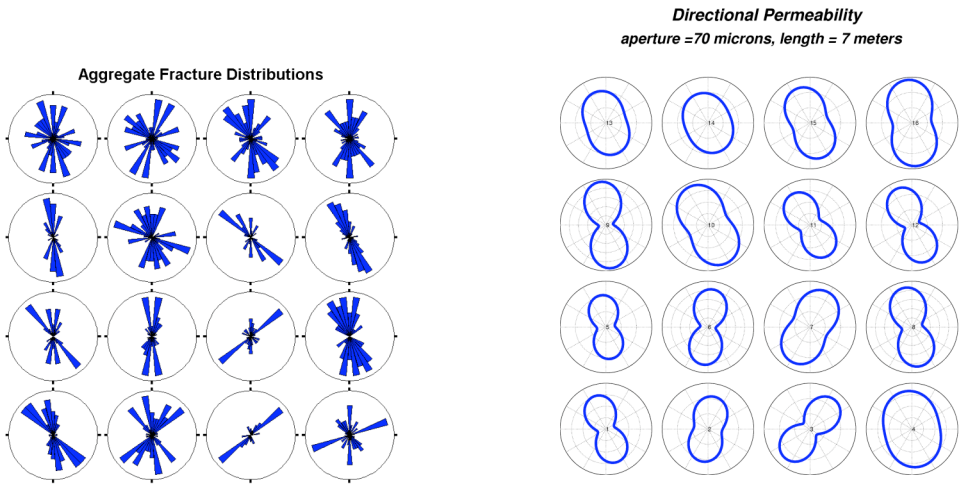

Figure 3. Left panel: angular histograms plots of the fracture distributions estimated from the Emilio Field data. The top of each plot represents fractures aligned north. Right panel: estimated permeability tensor computed from the Oda model as adapted by Brown (personal communication). Fracture apertures and lengths were assumed to be 70 microns and 7 meters respectively. The aperture value was based on mean fracture apertures measured in cores from the field site.

III. Technical Results and Discussion – Summaries

A system of aligned fractures effects propagating seismic waves in several ways. If the fractures and fracture spacing are small relative to the seismic wavelength, then the fractures cause the reservoir rock to behave like an equivalent anisotropic medium with a symmetry axis normal to the strike of the 'open' fractures. The resulting seismic anisotropy will therefore be related to the fluid flow directions in the reservoir. We can develop analysis methods to estimate the orientation of these open fractures as well as the fracture density from seismic measurements. In particular, seismic reflections from the top and bottom of a fractured reservoir will display different amplitude variations with offset (AVO) as a function of the orientation of the seismic source-to-receiver direction relative to the orientation of the fractures. Such measurements are referred to as amplitude variations with offset and azimuth (AVOA). This is this most popular and well-developed method of fracture analysis from seismic data (e.g., Lynn et al., 1996; Mallick et al., 1998; Ruger, 1998). As part of our project we developed an inversion method for estimating fracture orientation and density from measured AVOA from reservoir reflectors that builds off of these previous efforts (Minsley et al., 2004). This

method was tested on field seismic data from the Emilio Field to provide a baseline on fracture orientation in the field, and as a comparison and validation with previously published work in the field (Vetri et al., 2002; Gaiser et al., 2002).

If, however, the fractures and fracture spacing are closer in size to the seismic wavelength, then the fractures will scatter the seismic energy causing a more complex seismic signature. When we think about these larger scale features we are focusing on the major fracture corridors within a reservoir. Such features will represent the corridors controlling the majority of flow within the reservoir and therefore are critical to reservoir performance. The scattered wave energy results in a seismic signature that varies as a function of the orientation of the seismic acquisition relative to the fracture orientation. This scattered seismic energy also provides information about the fracture orientation and fracture spacing or density. The major result of this project has been the development, testing, and application of a processing and analysis method for extracting fracture information from these scattered wavefield signals in seismic data. The method, referred to as the Scattering Index Method, has several important characteristics. First, the method is robust and computationally inexpensive. Second, the method uses a normalization or differential approach that compares the scattering signal above and below an interval of interest in the data. Such an approach is expected to remove any overburden or acquisition footprint from the resulting estimates (which is a serious concern with AVOA results). Finally, the method has been tested on an extensive suite of synthetic model results as well as several different field data sets with encouraging results. In addition two approaches have been developed to estimate fracture spacing (that is, average spacing between fracture corridors) from spectral analysis of the pre-stack seismic data.

In support of these major developments we also investigated ways of using borehole acoustic logs to estimate in-situ stress values, since this stress field will impact fracture apertures and flow estimates. Finally, we also investigated possible approaches for converting seismically derived fracture orientation and spacing information into permeability values for use in reservoir simulators.

In the following sections we summarize our major results. First, the numerical modeling methods that were developed and tested will be treated, followed by the

Scattering Index Method and spectral analysis method developments. A section summarizing the field data results will follow. Finally a brief summary of our results in borehole acoustics and permeability estimation will be covered.

III.A Numerical modeling

Large-scale numerical modeling codes have been one of main tools in developing and testing our fracture characterization methods. Because these codes have formed such an important part of our research, significant effort was put into the development, testing, and implementation of these codes. During the course of the project three different codes were used. First, the 3-D finite difference elastic wave propagation code developed at the Lawrence Berkeley Lab (Nihei et al., 2002) was used. Second, a similar code, developed at MIT, was used. This code was also adapted to include the effects of intrinsic attenuation. Both of these codes include anisotropy and were run on computer clusters.

Finally, we have adapted our 3-D elastic, anisotropic finite difference code in two additionally ways. First, we implemented the rotated staggered grid (RSG) method developed by Saenger (2004). The RSG method can more accurately represent large contrasts of elastic moduli between the fractures and surrounding formation. Second, we applied the perfectly matched layer (PML) absorbing boundary condition to minimize boundary reflections (Marcinkovich and Olsen, 2003). Like the previous codes, the results generated by this code were compared to other numerical results as well as analytic and integral method modeling codes for validation. The RSG code was also tested with a single fracture model to illustrate its improved handling of complex, high-contrast interfaces. Standard-staggered-grid (SSG) finite difference schemes, even with 4^{th} order accuracy in space and 2^{nd} order accuracy in time, may generate artificial numerical noise or become unstable when very high contrast interfaces are present (Nihei et al., 2004). This is because the SSG needs to average the shear moduli of cells around the high contrast interface at each time step. To address this issue we use the rotated-staggered-grid method (RSG), which is 2^{nd} order accurate both in space and time. To illustrate, Figure 4 compares the snapshots of seismic wave propagation calculated by each of these two schemes for the same model: a single large fracture filled with gas

embedded in a homogeneous and isotropic medium. Numerical noise is present when the SSG scheme is used, but not with the RSG scheme.

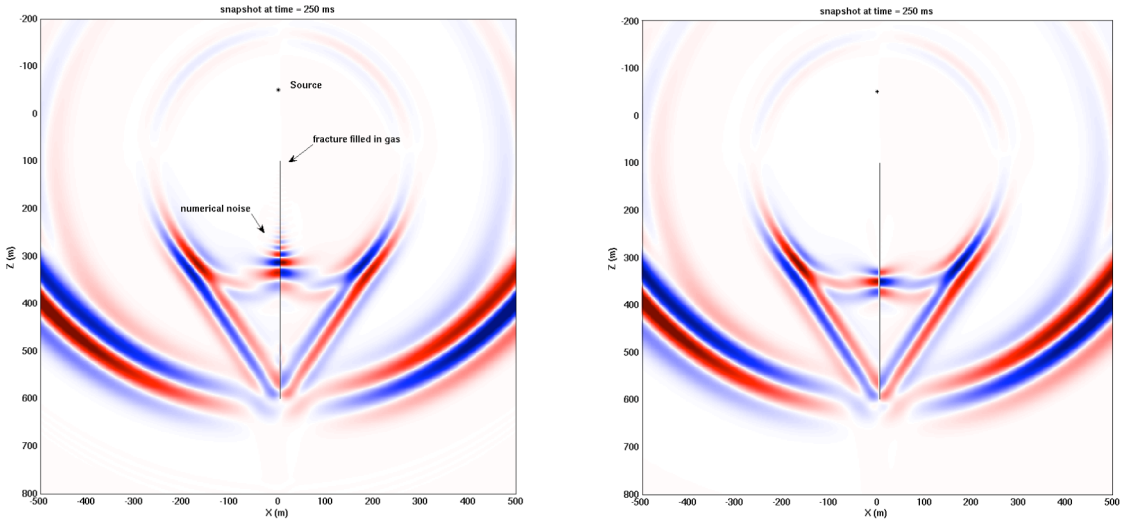

Figure 4. Wavefront snapshots of seismic wave propagation calculated by the standard staggered grid (SSG) scheme (left) and rotated staggered grid scheme (right) for the same model: a single large fracture filled with gas embedded in a homogeneous and isotropic medium. Numerical noise is present along the fracture when the SSG scheme is used, but not with the RSG scheme.

When using either the SSG or RSG modeling methods, we used the Coates-Schoenberg scheme (Coates and Schoenberg, 1995). to represent the presence of fractures within a given finite difference cell. In this scheme, a finite difference cell containing a fracture is replaced with an equivalent anisotropic material whose properties are dependent on the fracture orientation and properties. With this approach we developed a range of simple models where a fractured reservoir is represented as a homogeneous background medium containing parallel vertical fracture zones separated by different amounts of spacing. Each fracture zone would be one grid cell wide (5 m grid size in most of our models), and each such grid cell would use the Coates-Schoenberg formulation for its properties. These grid cells should be thought of as a fracture zone, or corridor, containing thin fractures. The key defining parameter for these grid-cell fracture zones is the compliance of the cell, which we refer to as fracture

compliance. The amount of seismic scattering will be directly related to the fracture compliance values used.

Although most of our models were based on a single set of parallel vertical fractures (see the next section for more details on the model geometries), we also investigated the effect of multiple fracture sets on seismic scattering (Chi and Campman, 2005; Chi et al., 2006). The Coates-Schoenberg formulation is quite general as it allows for modeling multiple intersecting sets of fractures with arbitrary orientations. However, in order to fully benefit from this flexibility, the finite-difference code must allow for fairly arbitrary anisotropy (at least monoclinic). Chi and Campman (2005) developed a scheme for adapting the finite difference codes to handle such situations, and Chi et al. (2006) added this feature to the code and modeled a number of multiple fracture set situations, which will be shown in the next section. A more detailed paper describing these results in included in the Appendix.

III.B Seismic scattering from fractures: model basis/synthetics

Our canonical fractured reservoir model consists of a simple reservoir geometry consisting of five horizontal layers. All the layers except for the third layer are homogeneous and isotropic elastic media. The third layer is 200-m thick and contains parallel, vertical fractures that are as tall as the layer, one grid cell thick (5m), and run the entire width of the model (Figure 5). Table 1 lists the properties of each layer. We generated a series of models with the following fracture spacings: no fractures, 10m, 25m, 35m, 50m, and 100m. More complex models were also considered: one with two sets of fractures with different spacing and orientation and the other with a Gaussian distribution of spacing. All models use a 40Hz Ricker wavelet as the seismic source.

Table 1. Parameters for model

Layer	Thickness (m)	Vp (m/s)	Vs (m/s)	Density (g/cc)
1	200	3000	1765	2.2
2	200	3500	2060	2.25
3	200	4000	2353	2.3
4	200	3500	2060	2.25
5	200	4000	2353	2.3

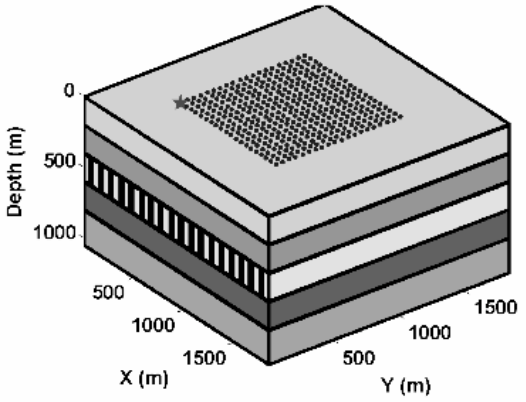

Figure 5. Model geometry.

Figure 6 shows the geometry and results for a model with a single set of vertical fractures with 50m spacing. The seismic shot gather oriented normal to the fractures shows complex forward and back-scattering below the reservoir level, while the shot gather parallel to the fractures shows a more organized semi-parallel set of arrivals consisting of forward scattering and multiplied scattered waves that are guided along the fracture strike. It is this difference in scattering as a function of orientation that will be exploited by the Scattering Index Method.

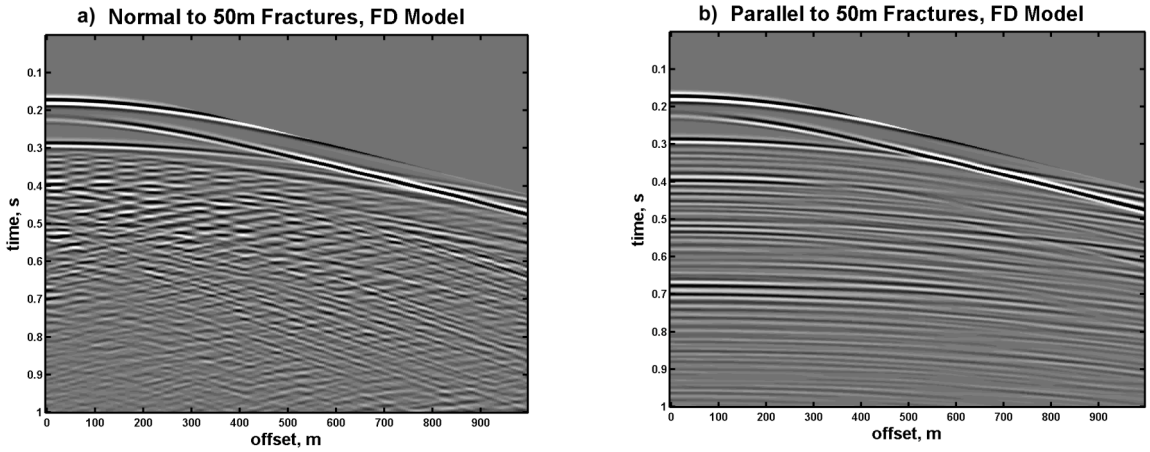

Figure 6. Vertical component of the 3D Finite difference modeling for 50m fracture spacing from Willis et al. (2004a, b): a) shows the shot record acquired normal to the fractures, b) shows the shot record acquired parallel to the fracture direction.

The Scattering Index Method is based on the observation that if we perform normal moveout corrections and stack the data shown in Figure 6, the scattered energy will 'stack out' (that is, be canceled due to the different phases present) normal to the fractures, but will 'stack in' (that is, be reinforced due to the similar phases present) parallel to the fractures. This is shown more clearly in Figure 7 that shows the same shot records for the 50m fracture spacing case together with a velocity analysis to the right of each record. The velocity analysis shows the stacked energy (color contours) as a function of different stacking velocities. Normal to the fracture direction there is no coherent stackable energy in or below the reservoir level (300 ms), while for the parallel case, there are many coherent events that can be seen primarily below the base reservoir.

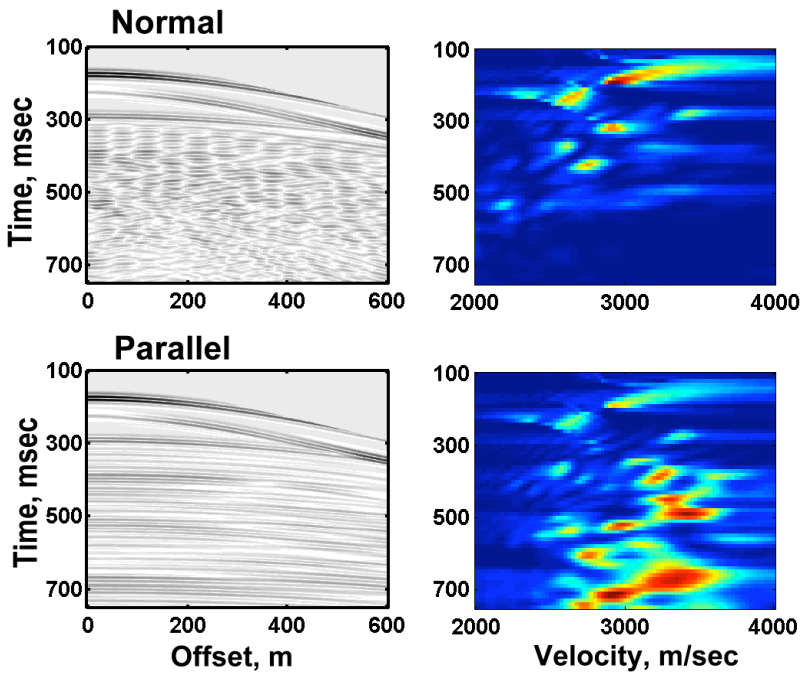

Figure 7. Left two plots show the seismic shot records for the model with 50m fracture spacing. The top left plot show the shot record normal to fractures, left bottom plot shows the shot record parallel to the fractures. The right two plots show the velocity spectra for the corresponding shot records on the left.

Because in field data observing these scattered wavetrains will be difficult due to the nearly continuous nature of the subsurface reflectivity, we need a way to identify and characterize these differences in scattered energy. In addition, if there are fractured zones or other scatterers in the overburden, those scattered waves will contaminate, or overprint, the scattered energy from our zone of interest in the reservoir. So our analysis approach starts with the concepts from existing methods of seismic wavelet estimation to obtain two apparent (or temporally local) source wavelets from the reflection time series – one from above the fractured zone (the "input" wavelet) and one below it (the "output" wavelet). These wavelets are represented by their autocorrelations obtained from windowed portions of the reflection time series above and below the fractured zone of interest. We then compute the time domain transfer function between the autocorrelations of the two extracted wavelets. The transfer function is computed by deconvolving the autocorrelation of the input wavelet from the autocorrelation of the output wavelet. This transfer function characterizes the effect of scattering in the interval of interest, between the two windowed portions of the trace (see previous report). A simple pulse shaped transfer function

indicates no scattering, while a long ringing transfer function captures the scattering within the reservoir interval. It is important to note that any contamination from scattering above the interval will be present in both the input and output extracted wavelets and thus will be excluded from the transfer function. If the method is applied to data stacked in different azimuthal directions, the interval transfer function should exhibit greater ringing in the direction parallel to fracturing. The left panel of Figure 8 shows the results of applying NMO and stacking the model traces in different azimuthal directions. The trace labeled "normal" corresponds to the stack of the traces in the top left plot of Figure 7. The trace labeled "parallel" corresponds to the stack of traces in the bottom left plot of Figure 7. In between these two traces are those stacked traces corresponding to 10 degree increments between normal and parallel directions to the fractures. (For comparison, the bottom trace labeled "control" is the trace from the model with no fractures.) The right panel of Figure 8 shows the transfer functions derived for the stacked traces in the left panel of the same figure. We can see that the transfer functions are all compact and similar to the non-fractured case (labeled "control") for orientations that are not parallel to the fractures. However, for azimuthal stacks oriented parallel to the fractures, the transfer function contains significant energy at non-zero lag values.

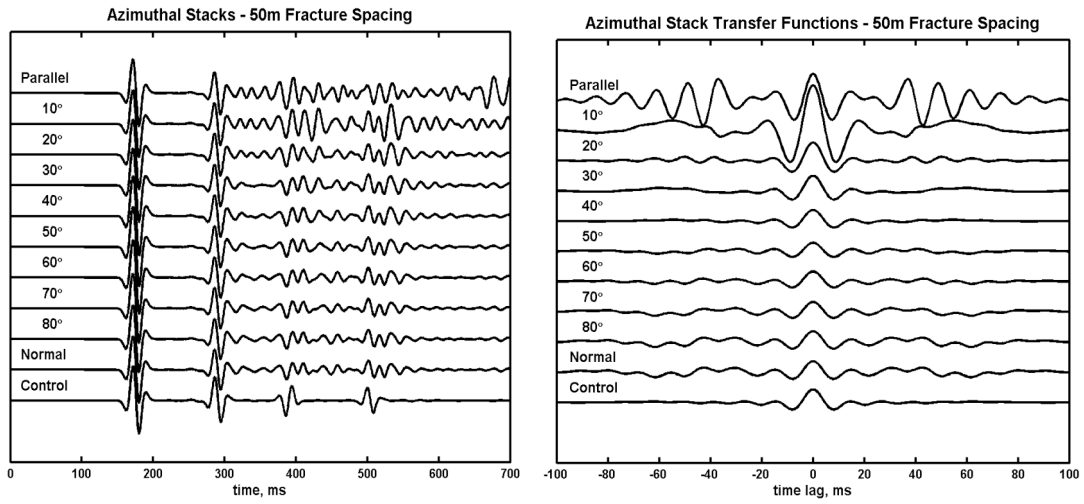

Figure 8. Left Panel: a plot showing the azimuthal stacks of traces from the 50m fracture spacing model. The traces represent azimuth stacks starting in the direction parallel to fracturing (top), and then increasing in 10 degree increments until normal to the fractures. The bottom trace shows the stack for the model without a fractured layer. Right panel: a plot showing the transfer functions corresponding to the azimuthal stacks in the left panel.

Scattering Index

In order to quantify the amount of transfer function ringiness or non-compactness, we created a Scattering Index, SI, defined by:

$$SI = \sum_{t=0}^{m} | t_i | i^n$$

where i is the time lag, t_i is the transfer function (time domain) amplitude at lag i, n is an exponent, typically equal to unity, and m is a lag at which there is no more significant energy in the transfer function. (It is also possible to normalize the scattering index based upon its energy and interval time sample or other such criteria.) The more the transfer function rings, the larger the value of the Scattering Index. If the transfer function is a simple spike (i.e. representing no scattering) then the Scattering Index attains a value of zero.

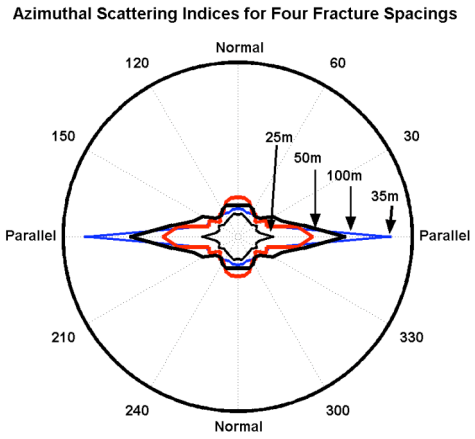

Figure 9. Polar plot of the azimuthal variation of Scattering Indices derived from the transfer functions of the 25, 35, 50 and 100m fracture spacing models. The Scattering Index is largest in the direction parallel to the fracture orientation. The largest scattering index is for the 35m fracture spacing, while the smallest shown is for the 25m spacing. (Quadrants 2 through 4 were created from the measurements in quadrant 1.)

Figure 9 shows the scattering index values for models run with 25, 35, 50 and 100m fracture spacings. These results show that there is a clear maximum of the scattering index in the parallel direction. It is also clear that in the non-parallel directions the scattering index is not zero but fluctuates about a smaller, but fairly consistent, value.

For this set of models, the 35m spacing produces the largest value due to a tuning effect from the particular values of P and S wave velocity and source wavelet frequency.

Non-regular spacing and multiple fracture sets

One of the first questions to be answered is whether this methodology is applicable for fracture systems that are not perfectly regular or have multiple sets of fractures. We generated two models to address these questions. Figure 10 shows the azimuthal stacks for the case of uniform 35m fracture spacing and the corresponding transfer functions. Figure 11 shows the same plots for a model with the spacing of the fractures having a Gaussian distribution with a mean of 35m and standard deviation of 10m. In both cases the strong ringing of the stack and the transfer function are still present in the direction parallel to the fractures.

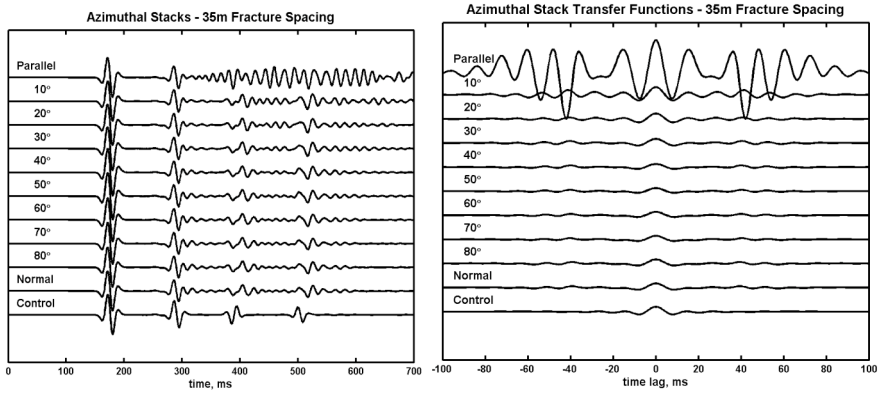

Figure 10. Left panel: azimuthal stacks for a model with uniform 35m spacing of fractures. Right panel: the transfer functions corresponding to the same stacks.

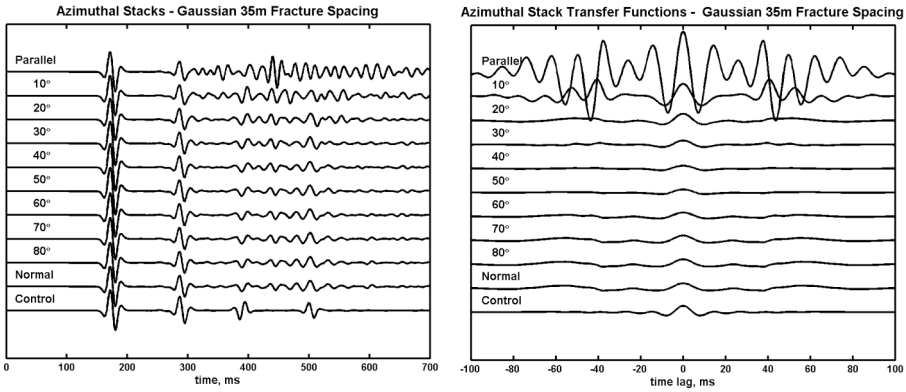

Figure 11. Left panel: azimuthal stacks for a model with a Gaussian distribution of fracture spacings with a mean of 35m and a standard deviation of 10m. Right panel: the transfer functions corresponding to the same stacks.

Multiple fracture sets

We recently (Chi et al., 2006, Appendix) developed and implemented a method for including the effects of multiple fracture sets in the RSG 3-D finite difference models. Figure 12 shows examples of the geometry of a model with orthogonal and non-orthogonal fracture sets in a three layered reservoir model. In addition to investigating these two geometries, models were also generated for cases where the spacing and compliance of the intersecting fracture sets was different. For the orthogonal sets of fractures Figure 13 shows the shot gathers at 0, 45, and 90 degrees, and Figure 14 shows a snapshot of the wavefield as it interacts with the fractured layer. Analysis of these model results show that wavefield scattering is still present and the azimuthal variations in scattering are still interpretable. For example, with orthogonal intersecting fracture sets the scattering index will have two maxima, one in the direction parallel to one set, and one parallel to the other with a minimum at 45 degrees. When the two compliances are different, the scattering index is proportional to the compliance values. For non-orthogonal fracture sets, the interpretation is more complicated, although the fracture orientations can still be picked up in the scattering indices. Figure 15 and 16 show the azimuthal stacks and scattering index plots for each of these situations. Chi et al. (2006) and Zhang et al. (2006) (Appendix) provide more details about these modeling results.

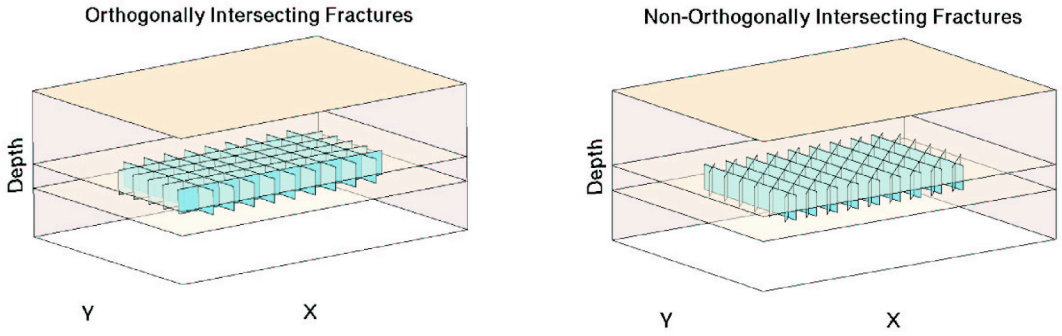

Figure 12. Geometry of the fractured reservoir model with orthogonal fracture sets (left panel) and non-orthogonal fracture sets (right panel)

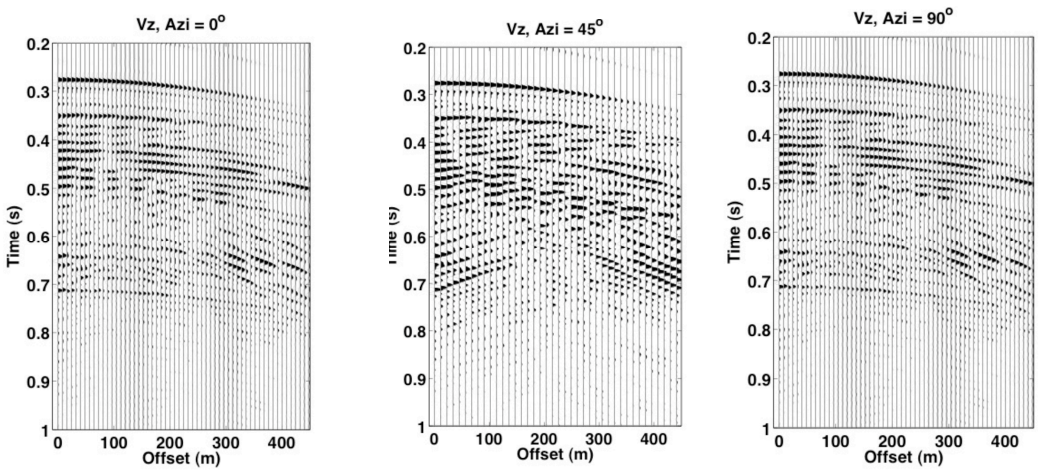

Figure 13. Shot gathers generated by the 3-D RSG model for the case of a fractured reservoir containing two sets of orthogonal fractures with the same spacing and compliance at 0 degrees (parallel to one set of fractures, left panel), 45 degrees (center panel), and 90 degrees (parallel to the second set of fractures, right panel).

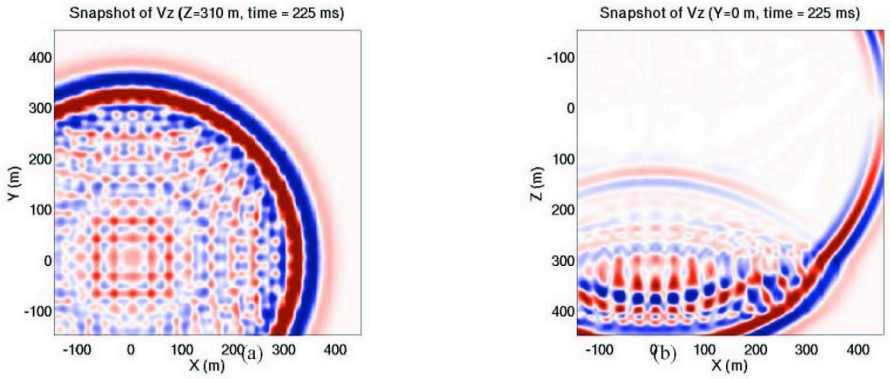

Figure 14. Wavefield snapshot of numerical model data for orthogonal fracture sets. Map view (left panel) and cross section at 0 degrees (right panel).

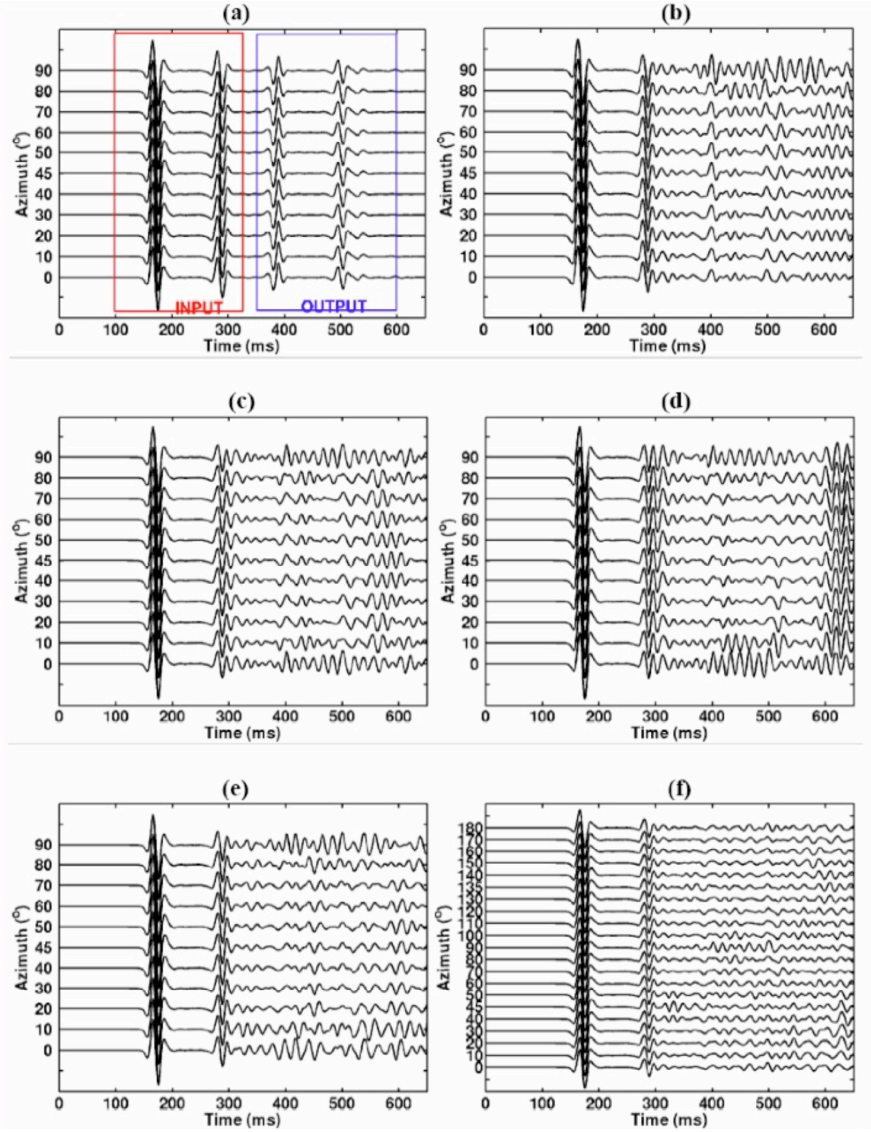

Figure 15. Azimuthal stacks for different multifracture models: a) no fractures, b) single fracture set 35m spacing, c) orthogonal fracture sets at 35m spacing, d) orthogonal fracture sets at 35m spacing, fractures at 0 degrees have 4x the compliance of the 90 degree fractures, e) orthogonal fracture sets with same compliance, fractures at 0 degrees spaced at 35m, fractures at 90 degrees spaced at 50m, f) non-orthogonal fracture sets (45 degree orientation), 35m spacing.

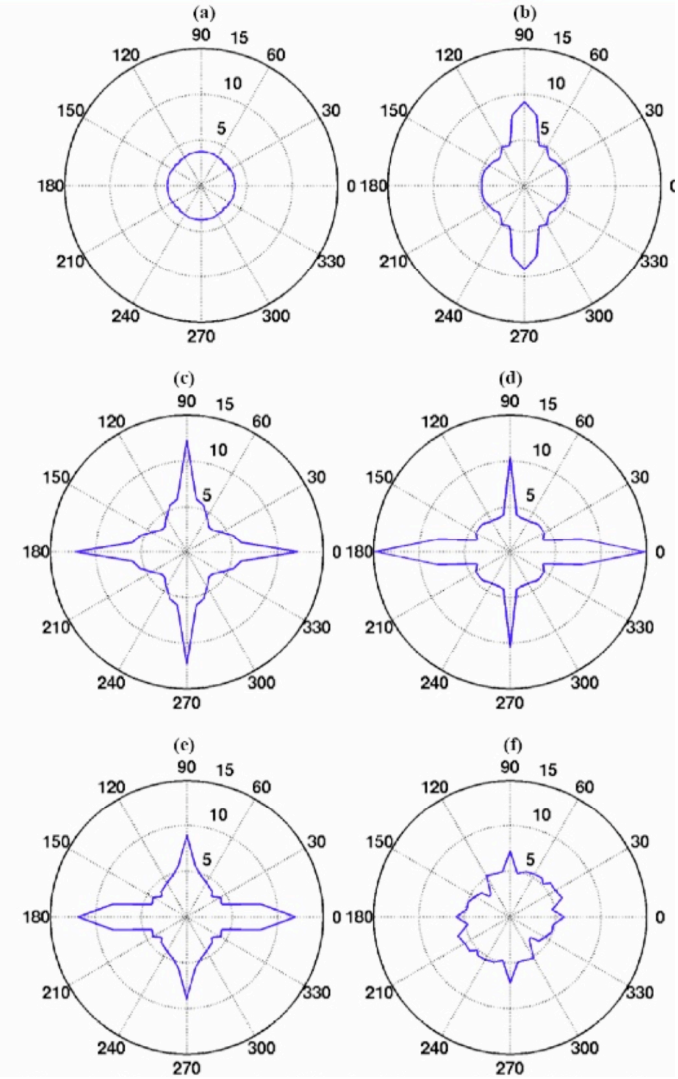

Figure 16. Scattering index plots for the same multifracture models as shown in Figure 15: a) no fractures, b) single fracture set 35m spacing, c) orthogonal fracture sets at 35m spacing, d) orthogonal fracture sets at 35m spacing, fractures at 0 degrees have 4x the compliance of the 90 degree fractures, e) orthogonal fracture sets with same compliance, fractures at 0 degrees spaced at 35m, fractures at 90 degrees spaced at 50m, f) non-orthogonal fracture sets (45 degree orientation), 35m spacing.

Fracture Spacing estimation

Fracture spacing is an important parameter in reservoir development. We have developed two approaches for estimating fracture spacing from scattered seismic energy. The first relates notches in the amplitude spectra of the scattered wavefield to the dominant fracture spacing that caused the scattering (Willis et al., 2005a). The second uses conventional FK filtering to isolate the backscattered signals and then recovers an estimate of the fracture spacing from the dominant wavelength of those signals (Grandi et

al., 2005; Zhang et al., 2006). The first method is based on the observation that discrete, vertically aligned fracture systems impart one or more notches in the spectral ratios of stacked reflected seismic traces. This apparent attenuation is due to the azimuth dependant scattering introduced by the fractures. The most prominent notch is located at the frequency where the P wavelength is about twice the fracture spacing. The frequency location of the notches can be used to determine the fracture spacings. Azimuth stacks with an orientation parallel to the fractures tend not show these spectral notches – allowing for another way to detect the fracture orientation.

In the second method we analyze the seismic data in the frequency-wavenumber (FK) domain. In our studies on the scattering effects of discrete fractures on synthetic seismic data we have observed the presence of both forward and backscattered signals. In particular, the backscattered signals (the energy that is propagating back towards the source) appear to be a maximum when the acquisition direction is normal to the fractures and a minimum when the direction is parallel to the fractures. In the FK domain we can separate the backscattered energy and determine the fracture spacing from its dominant wavenumber (i.e., wavelength). FK analysis for fracture spacing estimation was successfully applied to numerical model results, with particular focus on PS converted waves. Because S wave arrivals have shorter wavelengths than P waves, these PS arrivals have higher resolution and therefore can provide estimates of finer scale fracture spacing.

Spectral Notch Method

This process follows directly from the transfer function calculation used for the Scattering Index Method for each azimuth stack trace: (1) identify a target depth range (the fractured layer) to investigate; (2) extract a window of data containing reflections which are above this fractured layer (denoted as the 'input'); (3) extract a window of data below the fractured layer (denoted as the 'output') containing reflections which includes the scattered energy; (4) take the autocorrelation of the extracted windows; (5) window the auto-correlations to focus on the source wavelet near zero lag; and (6) compute the spectra ratio of the lower and upper windowed autocorrelations from the amplitude spectrum of the time domain transfer function (see Willis et al, 2004a, b; 2005).

The mean of the corresponding amplitude spectra of the 50m fracture spacing model for azimuths within 40 degrees of normal to fracture strike is shown in Figure 17. On this display a deep notch in the spectrum at about 35 Hz can be seen. Since there is no attenuation in the model we would expect to see a nearly flat spectral ratio over the bandwidth of about 10 to 80 Hz. This is not the case. At this particular frequency energy in the propagating signal happens to cancel out due to the time delay of a P wave traveling between two fractures and creating a null. The notch at about twice the fracture spacing is characteristic of all the models studied.

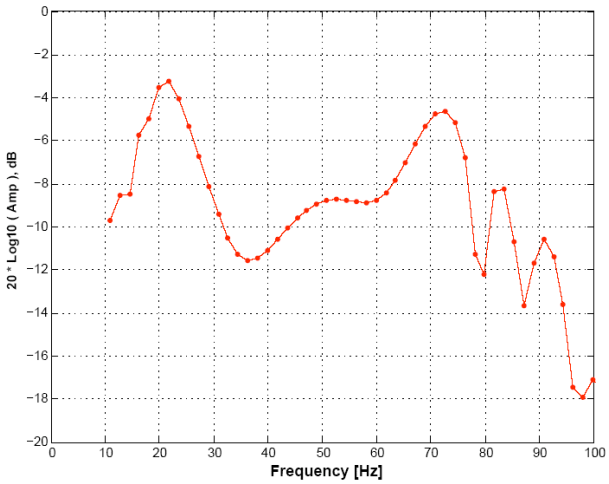

Figure 17. The mean of the spectral ratios for the 50m fracture case for azimuth stacks with orientations within 40 degrees of normal to the fracture strike. The vertical axis is in dB.

The notch effect is reduced for azimuths close to the fracture strike direction. This is due to the fractures acting like mechanical polarizers, channeling energy away from the normal direction, towards the parallel direction. Hence, in the parallel direction, there is in fact an amplification, or a peak in the spectral ratios. Thus, this azimuth sensitive behavior of the spectral ratios also provides fracture orientation. Lynn (2004b) noted holes in the spectra of shear components and attributed them to interference of backscattered energy.

FK Method

We derived a methodology to determine orientation and average spacing of discrete fractures based on the analysis of seismic scattered energy (or coda) in the frequency-wavenumber (FK) domain. In the FK domain it is relatively easy to identify

(and therefore separate) events with different apparent velocities in the seismic data. In our studies on the scattering effects of discrete fractures on synthetic seismic data we have observed the presence of both forward and backscattered signals. In particular, the backscattered signals (the energy that is propagating back towards the source) appear to be a maximum when the acquisition direction is normal to the fractures and a minimum when the direction is parallel to the fractures. Since these signals are generated at the fractures, they also contain information related to the spacing of the fractures.

To test this method model data was generated numerically for a variety of fracture spacings. The modeled data are collected according to source-receiver azimuth and subsequently transformed into the FK domain via a 2-D Fourier transform. Backscattered energy falls into the negative wavenumber quadrant of the FK plane (right panels of Figure 18). Two observations are made of the FK characteristics of azimuthal gathers at the fractured level: (1) the energy in the negative wavenumber quadrant is a maximum for source-receiver azimuth normal to fractures and is a minimum along the fracture strike direction; and (2) the distribution of energy in this quadrant varies according to fracture spacing such that backscattered signal from shorter fracture spacings contains higher frequencies-wavenumbers (Figure 19).

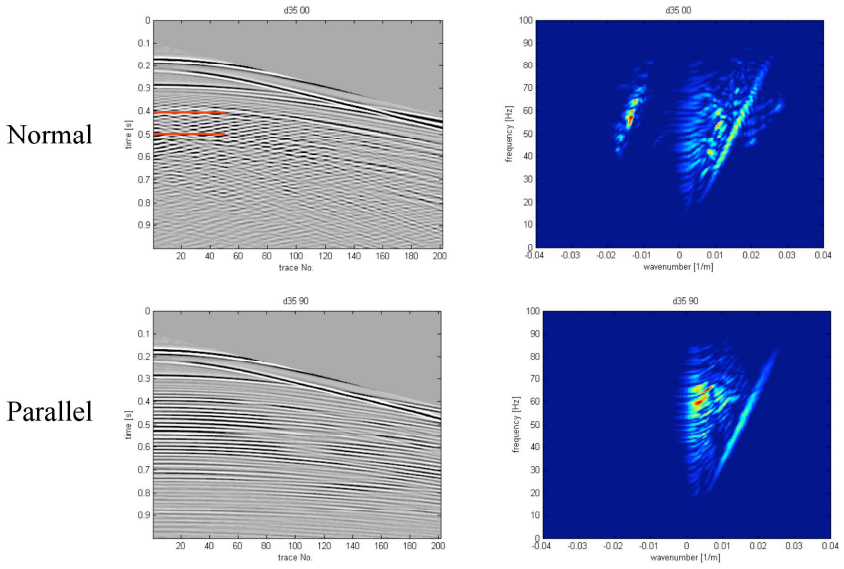

Figure 18. Synthetic shot gathers normal (top left panel) and parallel (bottom left panel) to the fractures with the corresponding FK plot on the right (frequency is on the vertical axis, and wavenumber is on the horizontal axis). Backscattered energy can be seen in the top right panel (normal to fractures) in the negative wavenumber quadrant. None is visible for data parallel to the fractures.

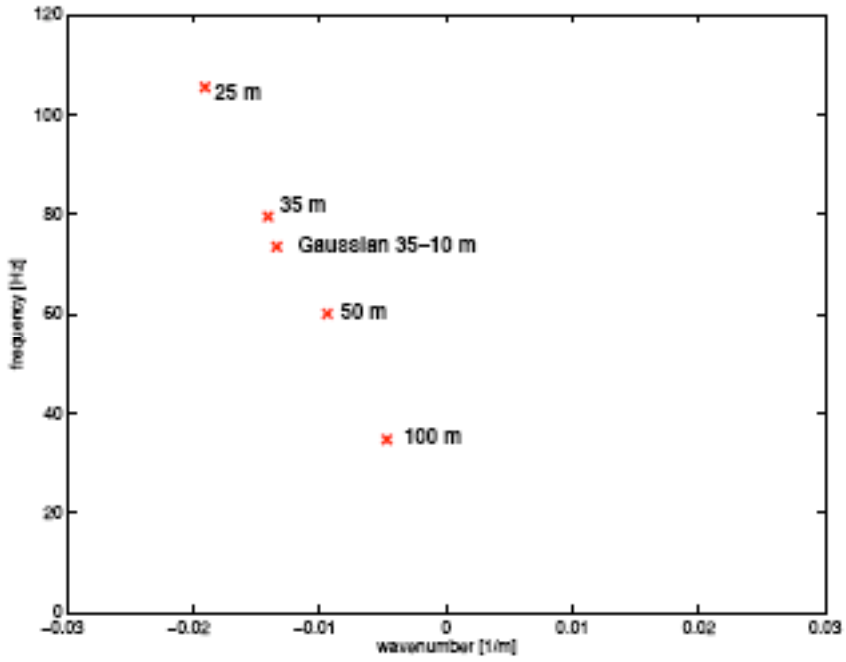

Figure 19. Plot of the Energy maximum in the f-k spectrum as a function of fracture spacing. In all cases, fracture spacing is approximately half of the inverse of the dominant wavenumber: (1/2)(1/0.0047m–1) =106.4m; (1/2)(1/0.0094m–1) =53.2m; (1/2)(1/0.0134m–1) =37.3m; (1/2)(1/0.0.0191m–1) =26.2m.

P and S wave scattered energy can both be analyzed for fracture spacing information. Figure 20 shows an example of the process applied to the numerical model data for a case with fracture spacing of 30m. In this case a window is chosen to analyze the PP scattered energy in the reservoir interval. The resulting spacing estimate is 31.8m. Another option is to analyze the PS energy that arrives later in the section. In Figure 21we extract data from two different time windows and look at the divergence (that is, PP energy) and curl (PS energy) of the wavefield. We can see that PS energy is present at later times. Because S wave arrivals have shorter wavelengths (due to lower propagation velocity) than P waves, these PS arrivals have the added benefit of higher resolution and therefore the ability to provide estimates of finer scale fracture spacing. Figure 22 shows the results of using the PS energy to estimate fracture spacing in such a case (20m fracture spacing). Local wavefield decomposition (LWD) is used to extract the coherent backscattered energy from the data windows (Zhang et al., 2006, Appendix).

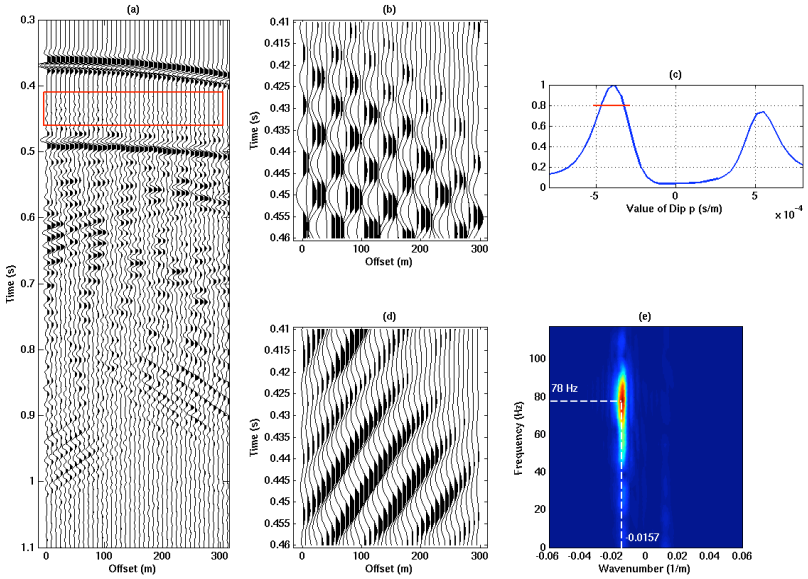

Figure 20. Determination of fracture spacing in f-k domain for model with 30 m spacing. (a) Seismogram of vertical component at near offset for direction perpendicular to fracture strike. Red window contains PP scattered energy between PP reflected at top and bottom interfaces of fractured reservoir; (b) Seismogram of energy in red window after being zoomed in (6 times scale as in (a)). (c) Normalized energy distribution in dip value p after applying LWD method on seismogram in (b); (d) Reconstructed seismic data by using profile with energy above 80% in (c), which is indicated by the red line; (e) Result of f-k transformation of reconstructed data in (d). The value of (k, f) of maximum energy is (-0.0157 1/m, 78 Hz). The estimated spacing is about 31.8 m.

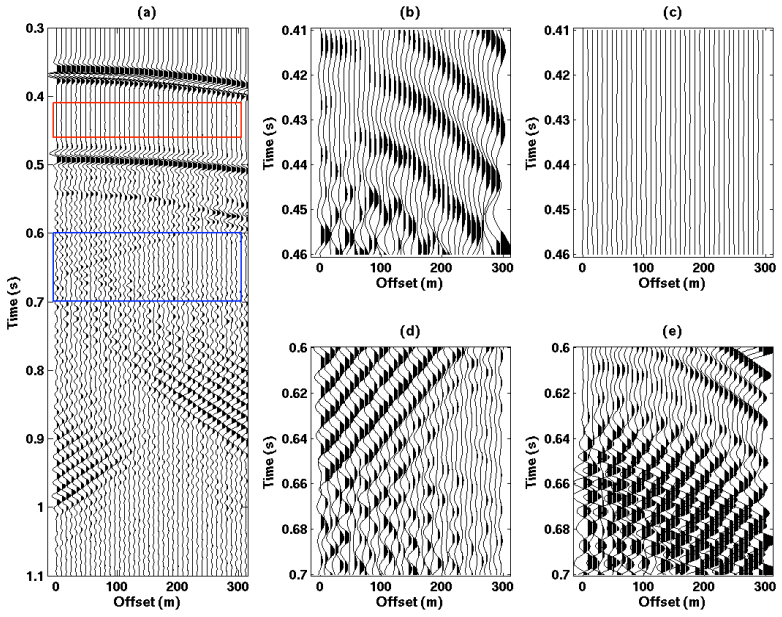

Figure 21. Divergence and curl energy in two successive time windows for model with 20 m fracture spacing. (a) Seismogram of vertical component at near offset in the direction perpendicular to fracture strike. Windows indicated in red and blue are chosen whose divergence and curl energy are compared; (b) Divergence energy contained in the red window; (c) Curl energy contained in the red window at the same scale as in (b); (d) Divergence energy contained in the blue window; (e) Curl energy contained in the blue window at the same scale as in (d).

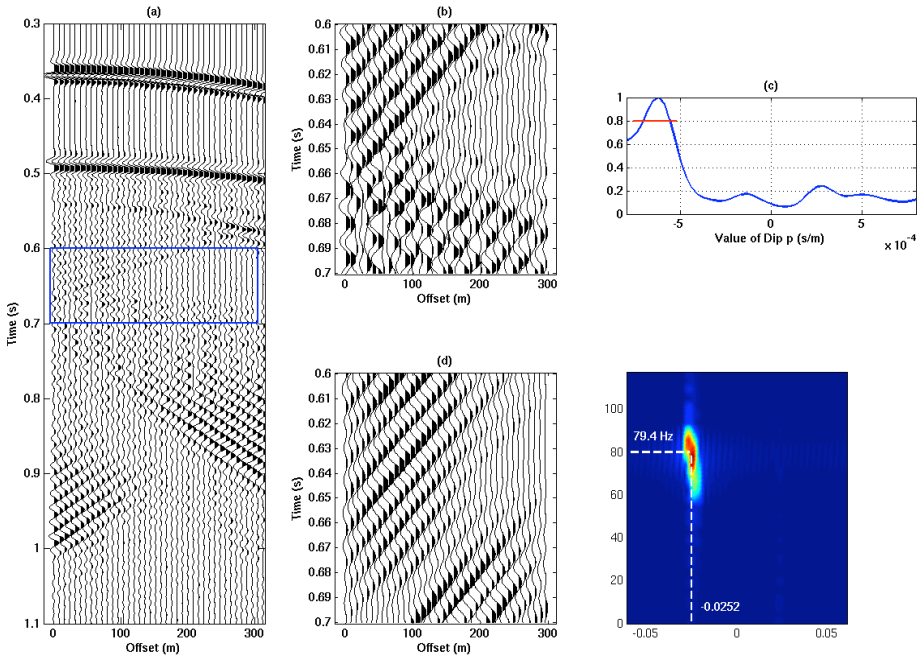

Figure 22. Determination of fracture spacing from the f-k domain for the model with 20 m fracture spacing. (a) Seismogram of vertical component at near offset in the direction perpendicular to fracture strike. Blue window contains PS scattered energy between the PS reflected at top and bottom interfaces of the fractured reservoir; (b) Seismogram of energy in the blue window after being zoomed in (3 times scale as in (a)). (c) Normalized energy distribution in dip value p after applying LWD method on seismogram in (b); (d) Reconstructed seismic data by using profile with energy above 80% in (c), which is indicated by the red line; (e) Result of f-k transformation of reconstructed data in (d). The value of (k, f) of maximum energy is (-0.0252 1/m, 84.7 Hz). The estimated fracture spacing is about 19.8m.

III.C Fracture properties from field data analysis

During the course of this project we had access to two field data sets acquired over fractured carbonate reservoirs for testing our analysis methods—the offshore Emilio Field data (provided by ENI-AGIP), and an onshore reservoir from the Middle East (provided by Shell). The Emilio data was our primary testbed for our methods, with the Middle East data used as a secondary test.

The Emilio Field is a fractured carbonate reservoir located in the Adriatic Sea in about 80m of water. The field is an area of complex folding and faulting at a depth of approximately 2800m. A high quality 3D/4C seismic survey was acquired using ocean bottom cables (OBC). Scattered wave analyses of these data have been presented in previous reports and papers (e.g., Willis et al., 2004a, b, 2005, 2006; Rao et al., 2005;

Grandi et al., 2005; Zhang et al., 2006), while other analyses have been reported elsewhere in the literature (e.g., Vetri et al., 2002; Gaiser et al., 2002).

Orientation estimation results

Our scattering analysis for fracture orientation estimation was applied to the Emilio data using stacks of the near to mid range (< 3500 m) offsets of the preprocessed PP data (Vetri et al, 2003) in eighteen different azimuth orientations from East to West using 20 degree wide overlapping ranges, in 10 degree steps (note that these angle ranges include the corresponding ranges 180 degrees away). This process created eighteen 3D stacked volumes. The transfer functions and scattering indices for the formation zone were computed for each of these stacked volumes (e.g., Willis et al., 2004a, b, Willis et al., 2006). The scattering indices were sorted and directions for those with the highest angular contrast in values were plotted as 'quivers' (i.e., short line segments) giving a map view of the location and direction of possible fractures determined by this method. We then performed a map migration of all the scattering indices to correctly position them in space (Figure 23). The results show a very strong correlation between the spatial distribution and orientation of our fracture results and the fault system in the field. We observe that the zones of high fracture density tend to congregate around the fault zones, particularly near multiple faults and at fault tips. In addition, we see that the quivers tend to align either parallel or perpendicular to the faulting.

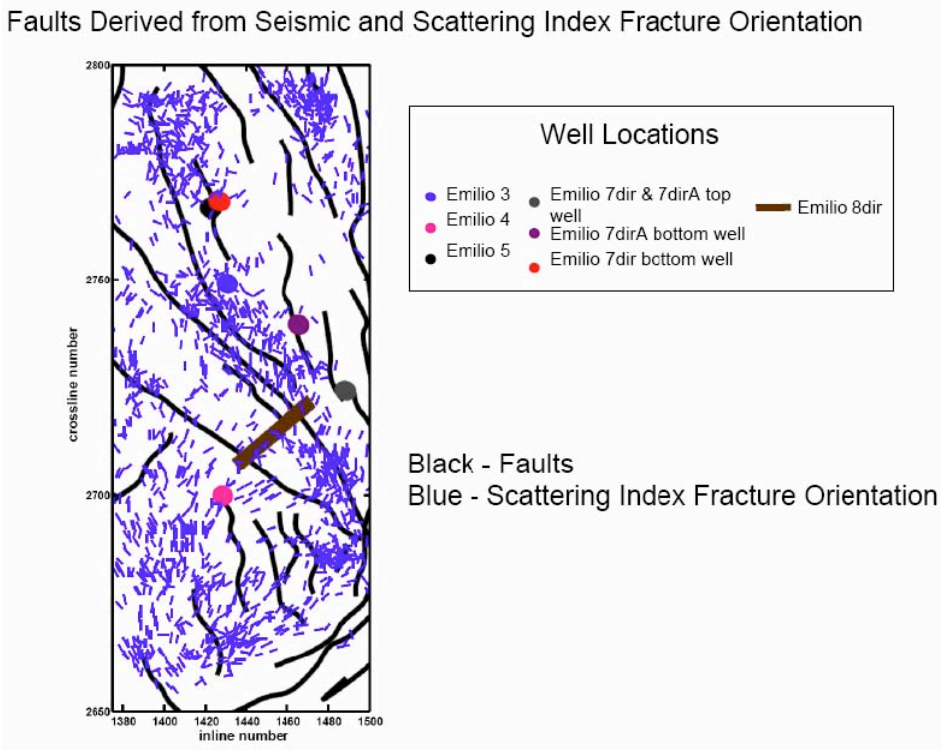

Figure 23. Map-migrated scattering index fracture directions (in blue) for the Emilio field (having angular contrast values >4). The black lines indicate faults derived from seismic data. The well locations are indicated by the round colored circles.

These fracture directions are comparable to those derived by shear wave anisotropy (Vetri et al, 2003) and with available well information (Willis et al., 2006). Figure 24 compares well-derived fracture orientations with those derived by the scattering index analysis. The top row shows the well information (from Vetri et al., 2003) indicating the direction of horizontal stress maximum (SHmax). In general, fractures align subparallel to the SHmax direction. We added a red arrow to the Well 4 results to emphasize the SHmax direction, since break out directions tend to align in the SHmin direction. The middle row shows close-ups from Figure 23 around these three wells. To further clarify the fracture trends, we histogrammed the map migrated scattering directions around each well and plotted them in rose diagram format in the bottom row of Figure 24. There is very good agreement between the scattering index orientations and the well-derived fracture orientations at these three wells. Willis et al. (2006) provides a more complete review of the method and results (see Appendix).

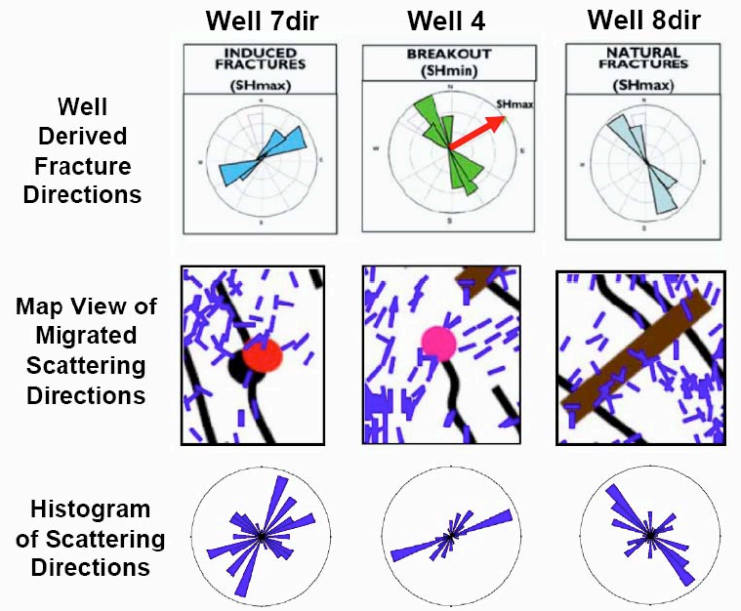

Figure 24. The top set of diagrams show the well derived fracture information (from Vetri et al., 2003) – SHmax is generally the direction of fracture strike. The red arrow indicates the direction of SHmax for well 4. The middle three diagrams are close-ups of Figure 23 around the corresponding well locations showing the agreement of the map migrated scattering directions with the well fracture directions. The bottom three diagrams show the histograms, in rose diagram format, of the map migrated scattering index directions around each of the wells.

The second data set used for testing our method is from an onshore location in the Middle East. The field produces from a gently folded, shallow, fractured carbonate. Production is primarily controlled by fractures oriented in two directions: approximately N50°E (the most important system for fluid flow) and N40°W. The data acquisition used a 'zipper' shot configuration (i.e., a zigzag pattern of shot points between receiver lines), with single component (vertical) receivers. Although this acquisition pattern results in the highest fold along the receiver line direction with lower fold in the other azimuthal directions, the fold was adequate to apply our scattering index methods to the data. The results for a processed swath of data over the center of the field at the reservoir level are shown in Figure 25. The data have been rendered as a color plot of all indices with the intensity of color related to the level of confidence in the presence of fractures, and the color values giving the fracture orientation. Superposed on this plot of the scattering indices are plots of FMI data from several wells in the field. The FMI data provide information on the orientation of the fractures measured from the logs in the reservoir

interval. The FMI results are color coded using the same colors used for the scattering indices—that is, the fracture orientations from the FMI logs and the seismic scattering can be easily compared. The agreement is very good, providing confidence that these methods can be applied to land seismic data that do not have the ideal azimuthal coverage. Figure 26 shows the FMI log data for seven of the wells plotted above the histogram of fracture orientations obtained from the scattering index analysis for a zone around each well. Again, the agreement is quite good for many of the wells.

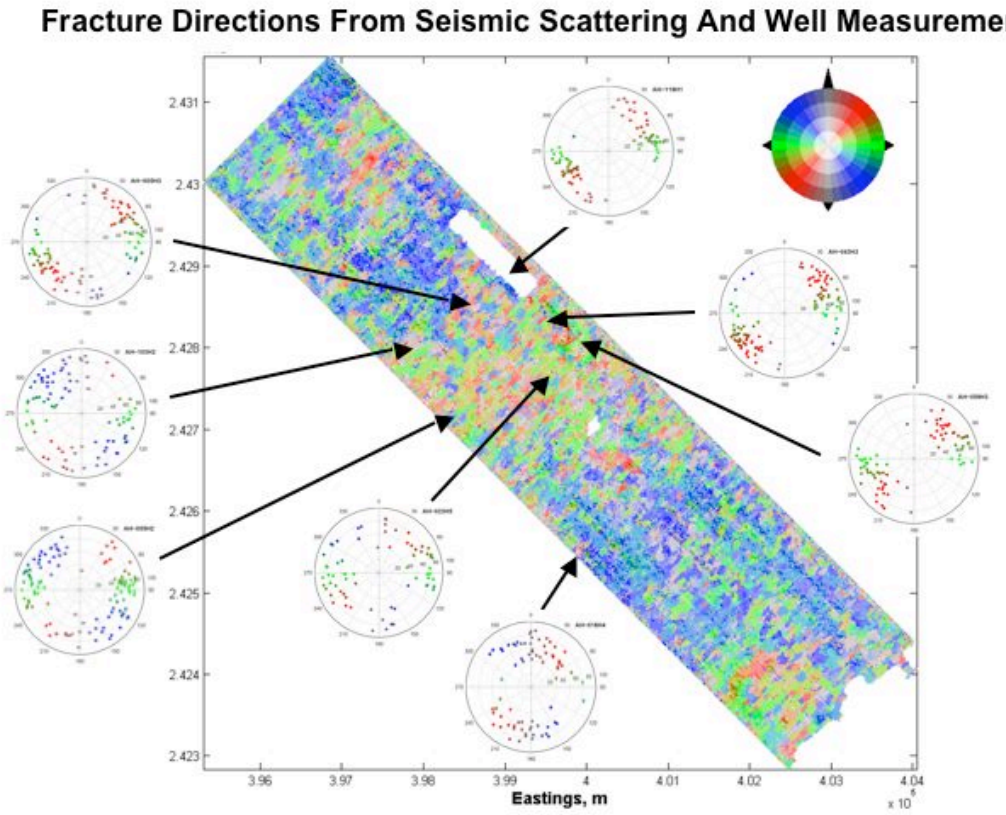

Figure 25. Comparison of scattering indices with FMI well measurements at the reservoir depth. The FMI data from 8 wells in the field are presented as polar plots showing the strike (location of the points on the plot which are also color coded in the same way as the scattering indices) and dip of fractures (radial position of the points, with horizontal fractures lying at the center of the plots and vertical falling on the outer edge of the circle) in the reservoir interval. The scattering index orientations are very consistent with the FMI results. FMI data also show most fractures to be near vertical.

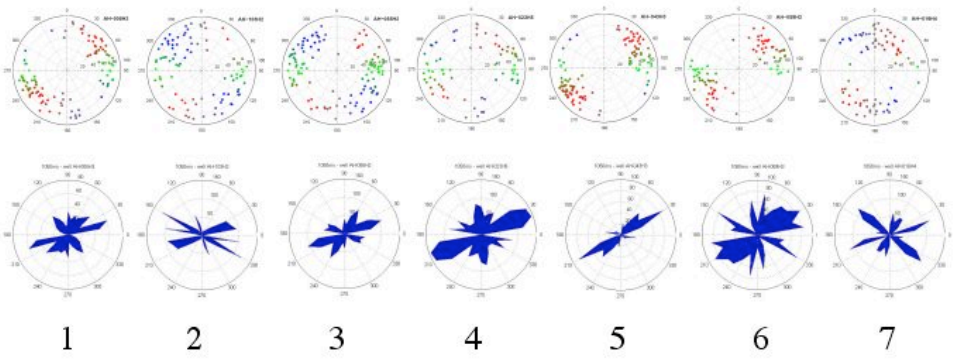

Figure 26. Comparison of scattering index histogram plots with FMI well measurements at the reservoir depth for the onshore carbonate fractured reservoir. The agreement is quite good, particularly for wells 1, 2, 4, 5, and 6.

Spacing estimation results

Both the FK and Spectral Notch methods were applied to the Emilio data to estimate fracture spacing. Both methods resulted in fracture spacing estimates of 25-40m. Validation of these values is difficult since there is no ground truth information for comparison, however the consistency of the estimates from the different methods provides some confidence.

FK method

Sorting of the Emilio data into profiles perpendicular and parallel to the dominant fracture direction shows that the data perpendicular to the fractures display less coherence and more backscattered energy than the data parallel to fractures (Figure 27). In Figure 28 we extract data from four different time windows – two above the fractured reservoir interval and two within or below the fractured interval. Significant backscattered energy is identified from the negative wavenumber portion of the FK plot in the bottom two

windows that are at and below the fractured reservoir. The estimated fracture spacing from the dominant wavenumber values in these windows is 25-40m.

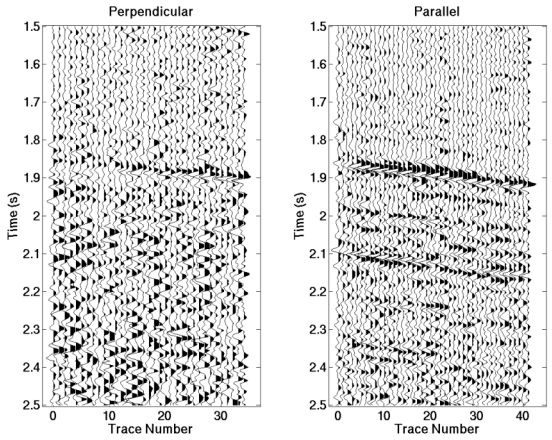

Figure 27 Azimuthal variation of scattered energy from discrete fracture zones in Emilio Field data. (a) Seismic profile in the direction perpendicular to fracture strike; (b) Seismic profile in the direction parallel to fracture strike.

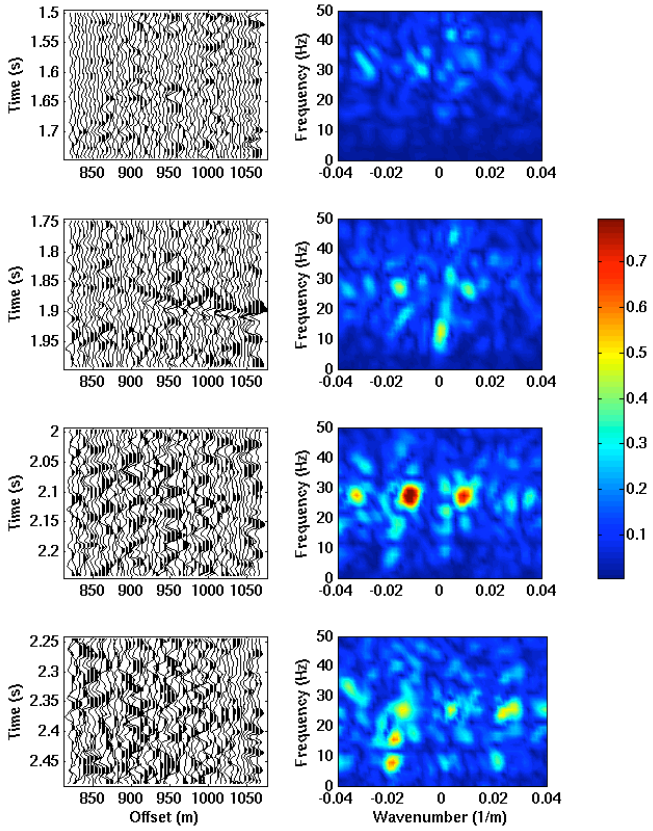

Figure 28. Energy distribution in f-k domain at different time windows for Emilio Field data. Four successive time windows with time duration 0.25 s are used.

Spectral notch method

The spectral notch method (Willis et al., 2005) was also applied to the Emilio data and a fracture spacing estimate was calculated for each CDP point in the field. The results are shown in Figure 29. The range of spacing estimates is 25-50m, with a dominant spacing of about 30-40 m. These values are consistent with the estimates obtained by the FK method.

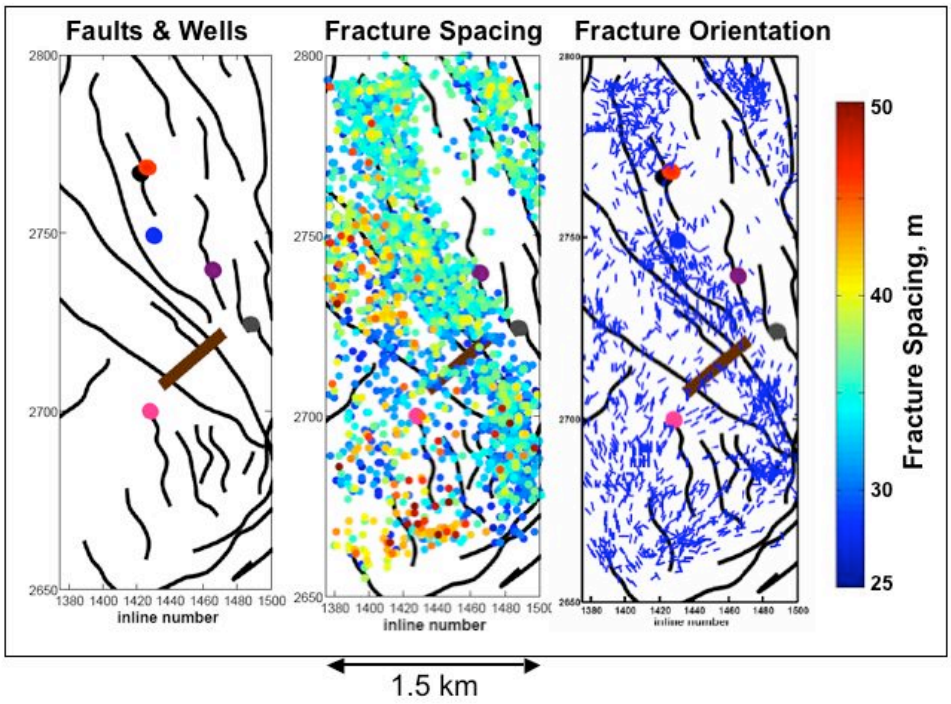

Figure 29. Scattered wavefield analysis of 3-D seismic data volume in a fractured carbonate reservoir (Emilio Field). The left panel shows the seismic faults and well locations. The right panel shows the spatial distribution of fracture density and orientation (the direction of each line segment gives the orientation estimate). The center panel shows the estimated spacing of fracture corridors, with the spacing values given by the color bar on the far right.

III.D Borehole results

Fractures are developed as a result of in-situ stress acting in the subsurface. In some situations the present day stress field is different from the field that created the fractures. In such situations, the current stress field may cause some fractures to be closed and some to be open, and therefore conduits to fluid flow. The methods we have

developed to analyze scattered seismic signals will be most sensitive to fractures with large compliance values, that is fractures that are open. It would be helpful, however, to be able to independently estimate the direction and magnitude of the stress field from borehole measurements. These data could provide additional information for interpreting the orientation directions for open fracture systems, and also be important for any fracture aperture estimation methods. With this in mind, we spent some effort on methods of using cross dipole acoustic logging data (specifically, dispersion crossover behavior), as well as borehole breakout data, to estimate the in-situ stress field. Papers on these methods were provided in earlier reports (Briggs et al., 2004; and Grandi et al., 2004). Briggs et al. (2004) developed a method to jointly invert for azimuthal angle and dispersion relations from cross dipole data. Results for maximum stress angle were compared with borehole breakout data and regional stress maps with good general agreement. Grandi et al. (2004) obtained in-situ stress information based on two methods. The first consists of matching borehole deformations to the modeling of linear poroelasticity equations around a hole in a plate that is subjected to effective compressive horizontal stresses. The second method utilizes the crossover observed in the dispersion of polarized flexural waves to obtain the direction of maximum horizontal stress where the borehole is not deformed (using methods similar to Briggs et al., 2004). The results of these methods agree with independent measures in a general field test.

Neither of these methods was applied to the Emilio of Middle East data sets because cross dipole acoustic log data were not available.

III.E Flow modeling results

The final part of the problem is to go from seismic fracture parameters to flow properties. This is a very difficult problem – flow is controlled by fracture distribution, spacing, aperture, orientation, and connectivity (that is, the network topology). The aperture distribution will be a function of the in-situ stress state as well. We have developed a method to estimate the orientation, spacing, and distribution of fractures from seismic data. Fracture aperture is a very difficult parameter to estimate, although it should be related to the scattering amplitude or energy levels (larger values of fracture

compliance are a function of the fracture aperture, and higher compliance results in higher scattering energy levels). The connectivity of a fracture network is also a difficult parameter to estimate. With some knowledge of the fracture orientations and distribution, we could generate some realizations of the network, assuming some range of fracture lengths and dips (we generally assume vertical fractures, but there may be some variation from this assumption in nature). Such a network can then be used to estimate fractured-interval flow properties in one of two ways – a statistical model to estimate a permeability tensor for an equivalent porous medium, or a direct modeling of flow through the fracture network realization and subsequent permeability estimates. We conducted feasibility tests of both of these methods.

Statistical model – the Oda Model

This method uses the approach of Brown and Bruhn (1998), based on the Oda model (Oda, 1985) of fracture networks, to estimate the permeability tensor from seismically derived fracture parameters. One of the benefits from using this type of approach is that the input to such a model is similar to the format of the data that we can estimate with our seismic methods. Figure 30 shows an example of this from the Emilio Field. In the left panel we see the rose diagrams obtained from the Transfer Function-Scattering Index analysis method applied to the field data set. The right panel shows the permeability tensor estimated from the Oda model (S. Brown, personal communication). In this figure the radial distance represents the permeability value. Key parameters that are needed for this model include fracture aperture, length, and response to applied stress fields. For this example, a uniform fracture aperture of 70 microns was used (based on core measurements from a well in the field) and a constant fracture length of 7m was assumed. This modeling approach is promising, but it is problematic to obtain fracture aperture and length estimates as input values.

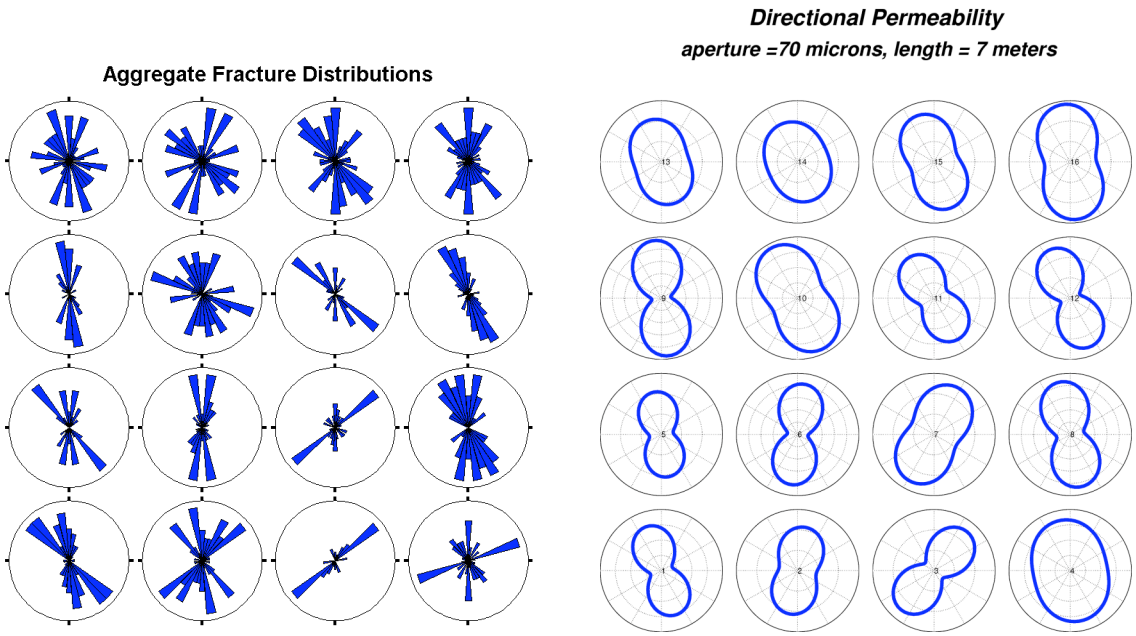

Figure 30. Left panel: angular histograms plots of the fracture distributions estimated from the Emilio Field data. The top of each plot represents fractures aligned north. Right panel: estimated permeability tensor computed from the Oda model as adapted by Brown (personal communication). Fracture apertures and lengths were assumed to be 70 microns and 7 meters respectively. The aperture value was based on mean fracture apertures measured in cores from the field site.

Stoke's flow modeling of fracture networks

As a means of visualizing flow in fracture networks and comparing expressions for equivalent fracture aperture flow to the actual flow, we looked at the numerical solution of the steady-state Navier-Stokes equation using a commercial Computational Fluid Dynamics (CFD) code (FLUENT). We constructed a series of two dimensional models of fractures and fracture networks. The result of this modeling study can be summarized as follows: 1) for fractures connected in series, the equivalent hydraulic aperture is a weighted harmonic mean of cubed apertures of all fractures. 2) For fractures connected in parallel, the equivalent flow is simply the sum of all flows through individual fractures. 3) If a fracture is inclined with respect to the axis of pressure gradient, then the amount of flow will be reduced by the cosine of the inclination angle. 4) Any network of randomly intersecting fractures can be replaced by a single fracture to

give flow equivalence; the aperture of that equivalent fracture will roughly be close to the aperture of the fracture in the network that cuts across the boundaries (inlet and outlet) in the most continuous fashion and has the smallest inclination (with respect to the pressure gradient axis).

IV. Technology Transfer

We have been actively presenting our results to industry through presentations and publications. Presentations have been made to producing companies (Shell, ConocoPhillips, ExxonMobil, BP, Chevron, Total, Eni-Agip, PDO, EnCana, Devon Energy) and contracting companies (Schlumberger, Baker Atlas, Halliburton/Landmark, Pinnacle Technology) at general technology meetings at MIT and as specific presentations at company research and production facilities. Technical papers have been presented at International conferences and industry workshops (SEG, EAGE, SEG-Japan) over the past three years. As a result, the methods developed under this contract have been communicated throughout the industry and have undergone significant peer review. A major summary paper has recently been published in Geophysics (Willis et al., 2006).

V. Conclusions

Major fracture corridors in the subsurface may scatter seismic energy. By analyzing these scattered wave signals (which are often treated as noise and discarded or removed in most processing approaches) the orientation of the fracture corridors can be estimated. Spectral analysis of these signals can also provide information on the fracture spacing or density. Our methods for estimating fracture orientation, fracture spacing, and fracture density from the seismic scattering signals have been tested with numerical modeling data and field data from two different fields. The fracture orientation results have been validated against well log measurements (FMI logs), other seismic analysis methods, and existing geologic models of the fields. The field data tests include offshore and onshore data. Two different fracture spacing estimation methods (FK and Spectral Notch) give similar results at the Emilio Field.

VI. Publications From Project

Burns, D.R., Willis, M.E., Minsley, B.J., and Toksoz, M.N., Characterizing subsurface fractures from reflected and scattered seismic energy, 7th Annual SEG Japan International Symposium on Imaging Technology, 2004.

Minsley, B.J., Willis, M.E., Krasovec, M. Burns, D.R., and Toksoz, M.N., Investigation of a Fractured Reservoir Using P-wave AVOA Analysis: a Case Study of the Emilio Field with Support from Synthetic Examples, expanded Abstract, 74th SEG Annual Meeting, 2004.

Pearce, F., Seismic scattering attributes to estimate reservoir fracture density: a numerical modeling study, M.S. Thesis, Massachusetts Institute of Technology, Cambridge, MA, 2003.

Rao, R., Willis, M., Burns, D., Toksoz, M.N., and Vetri, L, Fracture spacing and orientation estimation from spectral analyses of azimuth stacks, expanded abstract, 75th SEG Annual Meeting, 2005.

Willis, M. E., Burns, D. R., Rao, R., Minsley, B. J., Toksoz, M. N., and Vetri, L., Spatial orientation and distribution of reservoir fractures from scattered seismic energy, Geophysics, v.71, 5,p.043-051, 2006.

Willis, M., Pearce, F., Burns, D.R., Byun, J., and Minsley, B., Reservoir Fracture Orientation and Density from Reflected and Scattered Seismic Energy, expanded abstract, EAGE Meeting, Paris, 2004.

Willis, M., Rao, R., Burns, D., Byun, J., and Vetri, L., Spatial Orientation and Distribution of Reservoir Fractures from Scattered Seismic Energy, expanded abstract, 74th SEG Annual Meeting, 2004.

Willis, M., Rao, R., Burns, D., and Toksoz, M. N., 2005, Fracture spacing and orientation estimation from spectral analyses of azimuth stacks, Expanded abstract, EAGE meeting, Madrid.

Zhang, Y., Campman, X., Grandi, S., Chi, S., Willis, M. E., Toksoz, M. N, Burns, D. R., F-K domain characteristics of the seismic response of a set of parallel discrete fractures, expanded abstract, 76th SEG Annual Meeting, 2006.

VII. References

Briggs, V., 2004, Simultaneous inversion of cross dipole acoustic waveforms in anisotropic media for azimuthal angle and dispersion of fast and slow shear waves, ERL Internal Report.

Brown, S.R. and Bruhn, R.L., 1998, Fluid permeability of deformable fracture networks, *J. Geophys. Res., 103*, 2489-2500.

Gaiser, J., Loinger, E., Lynn, H, and Vetri, L, 2002, Birefringence analysis at the Emilio field for fracture characterization, *First Break* v 20, 505-514.

Grandi, S., Rao, R., Huang, X., and Toksoz, M.N, 2004, An integrated well data analysis for stress estimation, presented at the ERL Industry Consortium Meeting, MIT.

Lynn, H., Simon, K. M., and Bates, C. R., 1996, Correlation between P-wave AVOA and S-wave traveltime anisotropy in a naturally fractured gas reservoir, *The Leading Edge, 15,* 931-935.

Mallick, S., Craft, K.L., Meister, L.J., and Chambers, R.E., 1998, Determination of the principal directions of azimuthal anisotropy from p-wave seismic data. *Geophysics*, v. 63, 692-706.

Minsley, B., Willis, M., Krasovec, M., Burns, D., and Toksoz, M.N., 2004, Fracture detection using amplitude versus offset and azimuth analysis of a 3D P-wave seismic dataset and synthetic examples, *74th Annual SEG Meeting, Expanded Abstracts.*

Nihei, K. T., Nakagawa, S. and Schoenberg, M., 2004, Finite difference modeling of seismic wave interaction with discrete, finite length fractures, 2004 SEG/EAGE Research Workshop, Characterization of Fractured Reservoirs, Vancouver, Canada.

Oda, M., 1985, Permeability tensor for discontinuous rock masses, *Geotechnique, 35*, 483-495.

Rao, R., Willis, M.E., Burns, D.R., Toksoz, M.N., and Vetri, L., 2005, Fracture spacing and orientation estimation from spectral analysis of azimuth stacks, *75th Annual SEG Meeting, Expanded Abstracts.*

Rüger, A., 1998, Variation of P-wave reflectivity with offset and azimuth in anisotropic media: *Geophysics*, 54, 680-688.

Saenger, E. H., Gold, N. and Shapiro, S. A., 2000, Modeling the propagation of elastic waves using a modified finite-difference grid, *Wave Motion*, 31, 77-92

Vetri, L., Loinger, E. Gaiser, J. Grandi, A., Lynn, H, 2003, 3D/4C Emilio: Azimuth processing and anisotropy analysis in a fractured carbonate reservoir, *The Leading Edge*, 675-679.

Willis, M.E., Pearce, F, Burns, D.R, Byun, J. and Minsley, B, 2004a, Reservoir fracture orientation and density from reflected and scattered seismic energy, *EAGE meeting Paris, Expanded Abstracts*.

Willis, M., Rao, R., Burns, D., Byun, J., Vetri, L., 2004b, Spatial orientation and distribution of reservoir fractures from scattered seismic energy, *74th Annual SEG Meeting, Expanded Abstracts.*

Willis, M., Rao, R., Burns, D., and Toksoz, M. N., 2005, Fracture spacing and orientation estimation from spectral analyses of azimuth stacks, Expanded abstract, EAGE meeting, Madrid.

Willis, M., Burns, D. R., Rao, R., Minsley, B., Toksoz, M. N., Vetri, L., 2006, Spatial orientation and distribution of reservoir fractures from scattered seismic energy, *Geophysics, v.71, 5, p 043-051.*

APPENDIX A

GEOPHYSICS, VOL. 71, NO. 5 (SEPTEMBER-OCTOBER 2006); P. O43–O51, 12 FIGS., 1 TABLE.
10.1190/1.2235977

Spatial orientation and distribution of reservoir fractures from scattered seismic energy

Mark E. Willis[1], Daniel R. Burns[1], Rama Rao[1], Burke Minsley[1], M. Nafi Toksöz[1], and Laura Vetri[2]

ABSTRACT

We present the details of a new method for determining the reflection and scattering characteristics of seismic energy from subsurface fractured formations. The method is based upon observations we have made from 3D finite-difference modeling of the reflected and scattered seismic energy over discrete systems of vertical fractures. Regularly spaced, discrete vertical fracture corridors impart a coda signature, which is a ringing tail of scattered energy, to any seismic waves which are transmitted through or reflected off of them. This signature varies in amplitude and coherence as a function of several parameters including: (1) the difference in angle between the orientation of the fractures and the acquisition direction, (2) the fracture spacing, (3) the wavelength of the illuminating seismic energy, and (4) the compliance, or stiffness, of the fractures. This coda energy is most coherent when the acquisition direction is parallel to the strike of the fractures. It has the largest amplitude when the seismic wavelengths are tuned to the fracture spacing, and when the fractures have low stiffness. Our method uses surface seismic reflection traces to derive a transfer function that quantifies the change in an apparent source wavelet before and after propagating through a fractured interval. The transfer function for an interval with no or low amounts of scattering will be more spikelike and temporally compact. The transfer function for an interval with high scattering will ring and be less temporally compact. When a 3D survey is acquired with a full range of azimuths, the variation in the derived transfer functions allows us to identify subsurface areas with high fracturing and to determine the strike of those fractures. We calibrated the method with model data and then applied it to the Emilio field with a fractured reservoir. The method yielded results which agree with known field measurements and previously published fracture orientations derived from PS anisotropy.

INTRODUCTION

Evidence continues to confirm that much of the earth's crust, especially below a critical depth of 500 to 1000 m, contains a predominance of nearly vertical fractured rocks (Crampin and Chastin, 2000) typically aligned subparallel to the regional direction of maximum compression or about 45° to the axis of principal stress (Crampin et al., 1980). These natural fracture systems in an oil and gas reservoir frequently dominate the fluid drainage pattern and turn hydrocarbon saturated rocks with even low matrix permeability into significant commercial assets. In many low permeability oil fields, hydraulic fracturing is undertaken to enhance the natural system of fractures and to increase production rates (e.g., Block et al., 1994; Fehler et al., 1998; Phillips et al., 1998; House et al., 2004). An understanding of these fracture systems is crucial for field development planning to more completely drain the reservoir from the fewest number of wells.

Seismic waves traveling through a rock formation containing aligned fractures are affected by the fractures' mechanical parameters, such as compliance and saturating fluid, and by their geometric properties. If the fracture dimensions and spacing are small relative to the seismic wavelength, then the fractures cause the reservoir rock to behave like an equivalent anisotropic medium with a symmetry axis normal to the strike of the open fractures. Resulting seismic reflections from the top and bottom of a fractured reservoir will display amplitude variations with offset and azimuth (AVOA). In recent years much progress has been made analyzing AVOA effects (e.g.,

Manuscript received by the Editor August 3, 2005; revised manuscript received January 13, 2006; published online August 28, 2006.
[1]Massachusetts Institute of Technology, Department of Earth, Atmospheric, and Planetary Sciences, Earth Resources Laboratory, Cambridge, Massachusetts 02139. E-mail: mewillis@mit.edu; burns@mit.edu; rrao@erl.mit.edu.
[2]ENI E&P, Agip, Milan, Italy.

Lynn et al., 1996; Sayers and Rickett, 1997; Perez et al., 1999; Shen and Toksöz; 2000; Jenner, 2002; Shen et al., 2002; Hall and Kendall, 2003; Lynn and Cox, 2003; Minsley et al., 2004).

If, however, the fracture dimensions and spacing are close in size to the seismic wavelength, then the fractures will scatter the P- and converted S-wave energy to cause a complex, reverberating, seismic signature or coda. This seismic signature will vary as a function of the orientation of the seismic acquisition relative to the fracture orientation. Work by several authors (e.g., Ata and Michelena, 1995; Schultz and Toksöz, 1996; Daley et al., 2002; Nakagawa et al., 2002; Wu et al., 2002; Nakagawa et al., 2003; Willis et al., 2004b) using ultrasonic scale modeling and numeric simulation have demonstrated complicated, azimuthally varying scattering patterns by simulating systems of subsurface aligned fractures. The scattered seismic energy not only provides information about the fracture orientation, but can also be analyzed to provide information about the fracture spacing (Willis et al., 2004a) and fracture density (Pearce, 2003).

In this paper, we describe our recent work (Willis et al., 2003; Willis et al., 2004a, Willis et al., 2004b, Willis et al., 2004c; and Burns et al., 2004) to extract fracture distribution and orientation from scattered coda waves where the fracture systems have a size comparable to the wavelength of the seismic source. We describe our modeling results of vertically fractured reservoirs, our methods to extract the fracture properties from surface reflection seismic acquisition data, and finally, the results on field data.

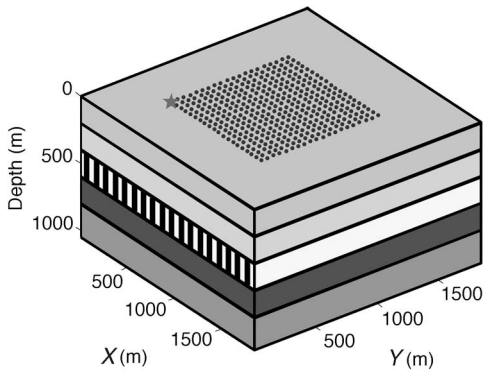

Figure 1. Geometry of the 3D finite-difference model. The layer velocities and densities are shown in Table 1, the source is located in the left front corner (star symbol), and the receivers are spread out in a rectangular area 1000 m in the x-direction and 1000 m in the y-direction. The receiver spacing is 5 m in each direction.

Table 1. Parameters for model.

Layer	Thickness (m)	V_p (m/s)	V_s (m/s)	Density (g/cm^3)	Wavelength of P energy (m)	Wavelength of S energy (m)
1	200	3000	1765	2.20	75	44
2	200	3500	2060	2.25	88	52
3	200	4000	2353	2.30	100	58
4	200	3500	2060	2.25	88	52
5	200	4000	2353	2.30	100	58

MODELING

We model a simple reservoir using the 3D anisotropic, elastic finite-difference code developed by Lawrence Berkeley National Laboratory (Nihei et al., 2002). The code implements the algorithm described by Levander (1988), which uses a staggered grid with an explicit, fourth-order operator in space and a second-order operator in time. The model geometry (Figure 1) and parameters (Table 1) we used consist of five horizontal layers. All layers except the middle layer (third layer) are homogeneous and isotropic elastic media. The background medium for the third layer is isotropic and homogeneous. We want to simulate a periodic series of parallel, vertical fracture corridors inserted into this layer. We use the Coates and Schoenberg (1995) method to represent the fractures by grid cells containing equivalent anisotropic medium. Vlastos et al. (2003) have recently used this same approach in a 2D pseudospectral approach for modeling scattering from fractures.

Following Daley et al. (2002), we use normal and tangential fracture stiffness values of 8×10^8 Pa/m to represent long, compliant, gas-filled fractures. The grid cells containing the fractures are chosen to be vertical planes, a single grid-cell thickness (5 m) and as tall as the layer thickness (200 m), which run the entire width of the model (i.e., parallel to $y = 0$). We generated a series of models with the following regular fracture corridor spacings: no fractures, 10 m, 25 m, 35 m, 50 m, and 100 m. We also generated another model to insure that our results would not be restricted to perfectly regular fracture spacings. The model has a pseudo-Gaussian distribution of vertical, parallel fractures with a mean spacing of 35 m and a standard deviation of 10 m. For each model, we used a Ricker wavelet source with a center frequency of 40 Hz and a causal time delay of 40 ms.

The left side of Figure 2a shows the shot record for the model without fractures. The middle and right side of Figure 2a show the shot records for the 50-m fracture spacing case acquired in directions parallel and normal to the fractures, respectively. The P-wave reflections off the top of layers 2 and 3 arrive at zero offset times of about 170 and 290 ms, respectively. The arrival at 220 ms is the converted S-wave reflected off the top of layer 2. Below these three distinct arrivals on the fractured models is a series of events corresponding to the scattering from the fractures. The other primary events seen on the model with no fractures (at about 400 and 500 ms) can only faintly be seen on the other two shot records; this indicates the large amount of scattered coda energy.

Figure 2b, shows the semblance-based, stacking-velocity analysis for each of the shot records in Figure 2a. Because the model interval P-velocities are all >2900 m/s, it is clear that the shot record normal to the fracture direction has little coherent and stackable P-energy below the top of the fractured zone (290 ms). However, for the parallel case, there are many coherent events below the top fractured zone reflection. In the direction parallel to the fractures, the seismic energy seems to be guided by the aligned fractures, and the resulting scattered energy is more coherent and similar to the direct P-wave reflection. This same pattern of azimuthal variation in the scattered wavefields is observed for all the model results regardless of the fracture spacing.

For shot records acquired parallel to the fractures, the ringing scattered events are seen to be

the most coherent on the near- through midoffset ranges. Figure 3a shows 10 azimuth stacks. The normal moveout (NMO) velocity function applied to all the traces was a single, simple NMO curve that should have done a good job of stacking the primary events. The azimuth stacks were created by applying normal moveout and stack to different azimuth ranges of the model traces starting in the direction normal to the fractures, then rotating by 10° increments until finally parallel to the fractures. Each azimuth stack combined about 80 input traces, which were gathered by collecting the closest set of traces to the nominal azimuth direction from the source location with offsets less than about 400 m. This offset range was chosen because, at offsets greater than 400 m, the scattered energy became less coherent on the shot records acquired parallel to the fractures. The stacked trace labeled *Normal* corresponds to the stack of the traces in the record on the right in Figure 2a. The trace labeled *Parallel* corresponds to the stack of traces in the middle record in Figure 2a. These stacks do not include the far-offset traces to avoid NMO stretch and the complications from the additional converted waves. For comparison, the bottom trace labeled *Control* is the stack of traces from the model without fractures shown in the left record of Figure 2a. For shot records acquired normal to the fracture direction, the observed

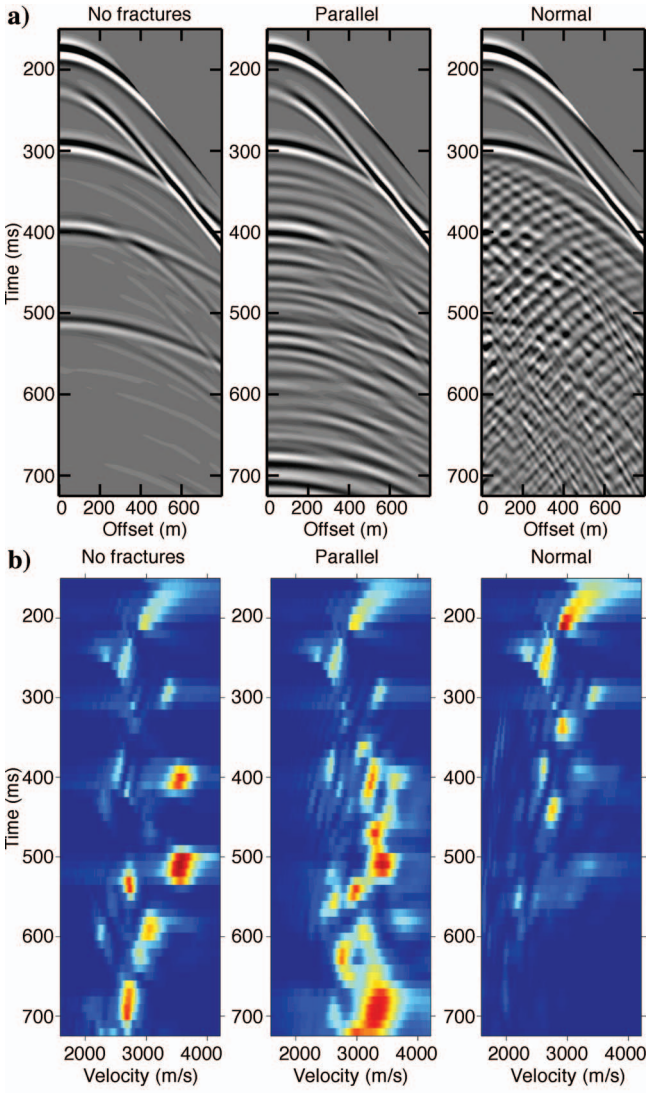

Figure 2. (a) The left shot record is from the model without any fractures. The middle and right shot records are from the model with a 50-m fracture-corridor spacing acquired parallel and normal to the fractures, respectively. (b) Semblance velocity analyses for the corresponding shot records in Figure 2a.

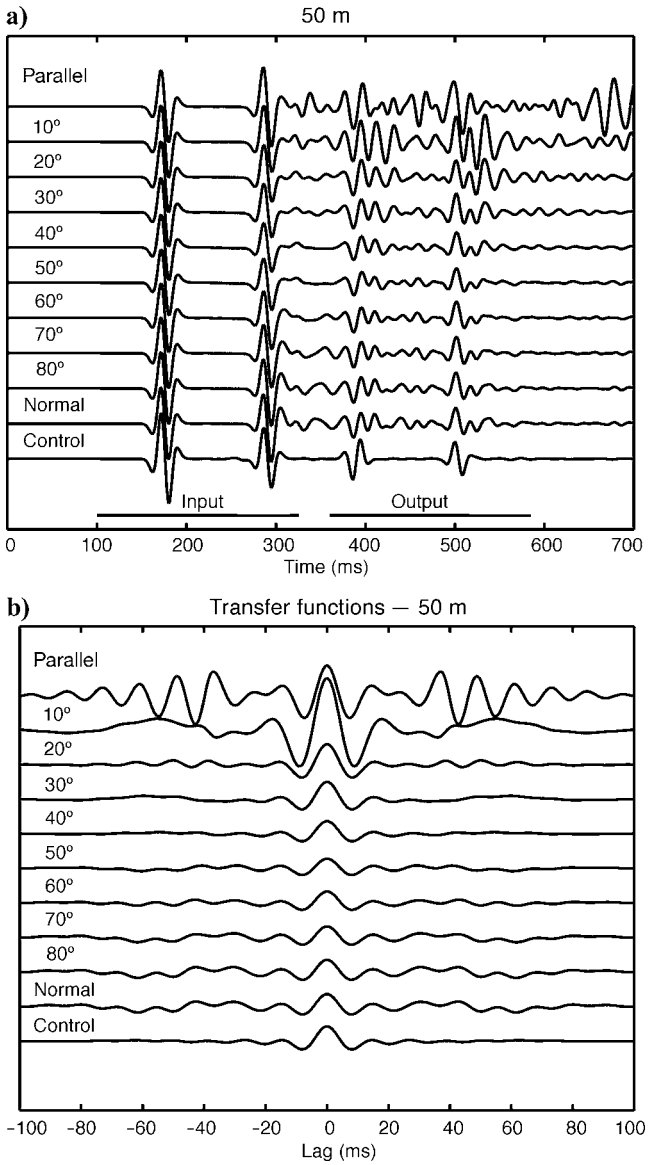

Figure 3. (a) Azimuthal stacks of traces from the 50-m fracture-spacing model. The traces represent azimuth stacks starting in the direction parallel to fracturing (top), and then increasing in 10-degree increments until normal to the fractures. The bottom trace shows the stack for the model without a fractured layer. The lines below the traces show the analysis gates for the input and output windows. (b) Corresponding transfer functions. Relative scaling is preserved within each panel.

scattered wavefield is greatly disruptive with significant backscattered, diffraction-like events. These traces do not stack together well with any NMO velocity. However, the traces acquired parallel to the fractures stack considerably better. On the basis of these observations, the strike of the fracturing may be determined by identifying the acquisition direction with shot records containing coherent, ringing energy which are enhanced the most when stacked. Figure 4a shows the azimuth stacks for all of the models studied. This same trend is present for all models except the 10-m fracture-spacing case. For this model, the fracture spacing is so small that the third layer behaves more like an equivalent anisotropic medium than like one with large-scale fracturing.

EXTRACTING SOURCE WAVELET AND COMPUTING TRANSFER FUNCTION

In the synthetic traces that we generated, it is possible to directly observe the scattered waves and their azimuthally varying trends. This is because there are only a few, isolated reflectors in the model. However, in field data we expect it will be more difficult to clearly observe these scattered wave trains due to the nearly continuously changing nature of subsurface reflectivity and to the potentially lower amplitudes of the scattered energy. Reflections off beds shallower than a fractured zone will not be affected by it. However, reflections below the zone will acquire a ringing coda caused by reverberations in the fractured zone. In addition, if the overburden is fractured, those scattered waves will contaminate or overprint the scattered energy from the zone of interest in the reservoir. Thus, the problem we face is detecting change in the reflection character of an apparent source wavelet as we move to later times on each trace. Specifically, we want to detect the change in the temporal compactness of the apparent source wavelet as it passes through each formation of interest.

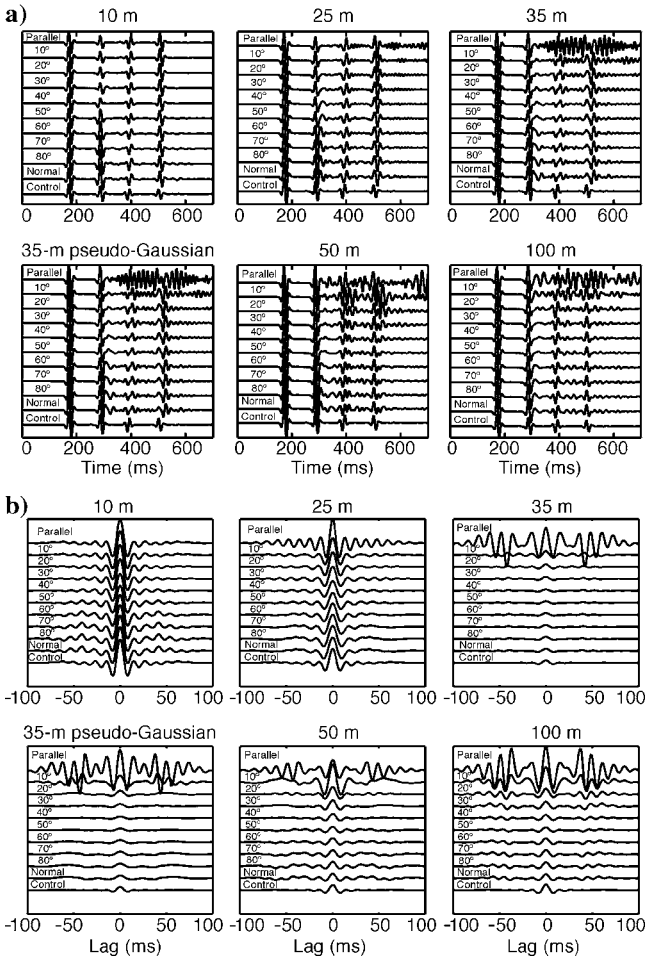

Figure 4. (a) Azimuthal stacks of traces from models with various fracture spacing. (b) Corresponding transfer functions. Relative scaling is preserved within each panel.

Traditional methods of source-wavelet extraction are based upon the notion of the stationarity of the seismic wavelet, which means that the source wavelet does not change as time progresses on the trace. For our purposes, we assume stationarity only within each time window used to estimate the source wavelet. However, because of the mode conversions and reverberation in the fractured interval, the apparent source wavelet does change with time on the trace. So on field data, we extract two apparent source wavelets from the reflection time series — one from above the proposed fractured zone (the input wavelet) and one below it (the output wavelet). These wavelets are represented by their autocorrelations obtained from windowed portions of the reflection time series above and below the fractured zone of interest. We make the standard assumption that the reflectivity series is white. Hence, the autocorrelation of the windowed time series yields the autocorrelation of the source wavelet in that window.

We then compute the time-domain transfer function (sometimes called the impulse response) between the autocorrelations of the two extracted wavelets. The transfer function is computed by deconvolving the autocorrelation of the input wavelet from the autocorrelation of the output wavelet using the Wiener-Levinson algorithm (Robinson and Treitel, 1980). (We have also used spectral division as the deconvolution method, but, in our experience, we find the Wiener-Levinson method produces more time-compact or stable waveforms.) The transfer function characterizes the effect of scattering in the interval of interest between the two windowed portions of the trace. Since both the input and output autocorrelations are zero phase, the resulting transfer function will also be zero phase and symmetric. A simple spike or pulse-shaped transfer function indicates no scattering; however, a long, ringing transfer function reveals that scattering has occurred within the time interval between the analysis windows. This measurement will be insensitive to contamination from an acquisition footprint or from scattering in the overburden. This is because these effects would appear on both the input and the output extracted wavelets and thus will be excluded from the transfer function.

The transfer function can be used to characterize scattering on both prestack and poststack data. On prestack data, it can detect the presence of scattering on a single trace. However, it can also be used to determine the orientation of fracturing by comparing the change in the transfer functions from stacked traces with different acquisition orientations. The transfer functions from traces stacked in the direction parallel to fractures will exhibit more ringing than those in the direction normal to fractures. To show this on the 50-m fracture-spacing model data, we choose the input and output time windows on each of the traces in Figure 3b, as delineated by the labeled bars beneath the traces. We form the autocorrelation of each window and then compute the transfer function between each corresponding pair

of autocorrelations. Figure 3b shows the derived transfer functions. Notice that the transfer function for the control case, the model without fractures, is very impulsive and is similar to a band-limited spike. The transfer function for the stacked normal trace strongly resembles the control case. The transfer functions show very little change in shape until they are within 10° of the fracture strike direction; this indicates a sharp angular resolution. The transfer function for the parallel trace rings for about 100 ms in each direction and is very different from the other functions.

We have applied this analysis to all of the other models, and the results are shown in Figure 4b. In all cases except the 10-m fracture case, the transfer functions ring most prominently in the direction parallel to the fractures. (The 10-m fracture case behaves more like an equivalent anisotropic medium than one that shows discrete fractures.) From these examples, it is clear that the marked ringing behavior of the transfer function for the stacks in the direction parallel to the fractures is a characteristic phenomenon and not an artifact of a random perfect resonance in a particular model. Therefore, the transfer functions can be used to estimate fracture orientation.

METHODOLOGY FOR SCATTERING INDEX

We have shown that stacks made from traces acquired parallel to a prominent fracture system retain the ringing scattered coda energy on the traces. Stacks made in other acquisition directions tend to diminish the scattered coda energy. This same trend is evident on the corresponding transfer functions. By design, a transfer function is symmetric about zero lag; so, we only need to examine its positive time lags. Looking more closely at the transfer functions for orientations parallel to fractures, we clearly see that the ringing coda creates energy in the transfer function at times away from the zero lag. However, in the normal direction, the transfer functions are comparatively compact about the zero lag.

To quantify the amount of ringing or noncompactness in a transfer function, we define a scattering index, SI, with a form given by

$$\mathrm{SI} = \sum_{i=0}^{m} |t_i| i^n,$$

where i is the time lag, t_i is the transfer function (time domain) amplitude at lag i, n is an exponent, typically equal to unity, and m is a lag at which there is no more significant energy in the transfer function. (It is also possible to normalize the scattering index on the basis of its energy and interval-time sample or other such criteria.) This expression weights the large lag times more heavily than the near-zero lag times in the transfer function. The more the transfer function rings, the larger the value of the scattering index. If the transfer function is a simple spike (i.e., it represents no scattering), then the scattering index attains a value of zero.

Figure 5 shows the scattering-index values for the models with 25-, 35-, 50-, and 100-m fracture spacings. The extent of the model does not afford a complete 360° acquisition-direction analysis; so, we have replicated the first-quadrant analysis appropriately for the other three quadrants. These results show that there is a clear maximum of the scattering index in the fracture-parallel direction. It is also clear that in the nonparallel directions, the scattering index is not zero but fluctuates about a smaller but somewhat consistent value. The highest scattering index is for the 35-m fracture spacing case. This fracture spacing corresponds to 0.35 times the P-wavelength and 0.6 times the S-wavelength in the fractured layer. The scattering index formulation allows us to extract the amount of ringing in the transfer functions as a single digit; this makes it easier to analyze, display, and therefore detect the strike of the fracturing.

RESULTS ON FIELD DATA

In early 2000, a 3D/4-C seismic survey was collected over the Emilio Field, located in the central part of the Adriatic Sea, near the eastern coast of Italy. The reservoir unit is a fractured carbonate. Borehole studies by ENI suggest the presence of two orthogonal fracture sets oriented east-northeast and north-northwest in the reservoir. Recent studies have investigated this 3D seismic data using PP- and PS-wave anisotropy to identify fracture characteristics of the reservoir level (Vetri et al., 2003; Gaiser et al., 2002). Figure 6 (modified from Figure 1 of Vetri et al., 2003) shows the interval velocity log and the interpreted seismic section through the field. The most prominent reflector in the section is the Gessoso-Solfifera, highlighted in green, which is a high-velocity chalk formation. The reservoir interval is shown between the cyan and amber lines on the seismic section.

We stacked the near-to mid-range (<3500 m) offsets of the preprocessed PP data (Vetri et al., 2003) in 18 different azimuth orientations from east to west using 20°-wide overlapping ranges, in 10°steps. (Note that these angle ranges included the corresponding ranges 180°away.) This process created 18, 3D-stacked volumes with a CDP spacing of 12.5 m between inlines and 25 m between crosslines. The transfer functions and scattering indices were computed for each of these stacked volumes using 300-ms input and output time windows on either side of a fixed gap of 100 ms containing the formation zone. The 18 stacked traces at each CDP location were

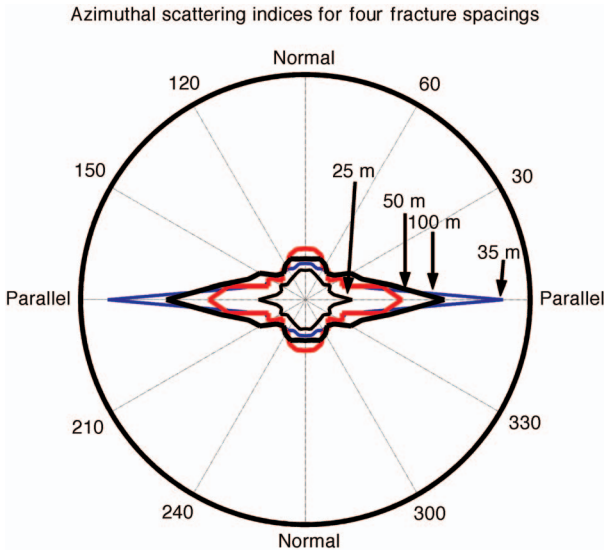

Figure 5. Polar plot of the azimuthal variation of scattering indices derived from the transfer functions of the 25-, 35-, 50-, and 100-m fracture-spacing models. The scattering index is largest in the direction parallel to the fracture orientation. The largest scattering index is for the 35-m fracture spacing; the smallest shown is for the 25-m spacing.

used to compute 18 scattering indices for each of nearly 26,000 CDP locations. The scattering indices were sorted and directions for CDPs with the highest angular contrast in scattering index values (differences > 5) are shown as quivers in Figure 7; this yields a map view of the location and direction of possible fractures determined by this method.

The locations of the fracture measurements are taken from stacked data, and as such, their locations are in the unmigrated positions. To adjust for this potential mispositioning, we performed a map migration of all the scattering indices with angular contrasts >4. These results are shown as blue quivers in Figure 8. Here, we have used the coordinate system of inlines and crosslines (rather than northings and eastings in Figure 7) to plot the seismically derived fault system (in black) and well information on the same diagram. We observe that the clusters of the blue quivers tend to congregate around the fault zones. In addition, we see that the quivers tend to align either parallel or perpendicular to the faulting.

Figure 9 is a plot of the scattering directions for all the CDP locations in the survey, without omitting low angular-contrast values. The scattering index directions have been color coded using the color legend on the top right of the figure. A larger version of this color legend is shown in Figure 10. Small angular contrasts in the scattering indices are denoted by tinting the color of the corresponding CDP cells toward the center of the color legend wheel which is white. Larger angular contrasts are tinted toward brighter colors at the edge of the legend color wheel to indicate greater confidence in the measurement. Green, red, gray, and blue indicate fracture strikes of east, northeast, north, and northwest, respectively.

We next compare our fracture directions with those derived by shear-wave anisotropy. Figure 11b (modified from Figure 10 of Vetri et al., 2003) shows the fracture strike direction derived from the fast direction of the PS waves. We have added a color legend and three black arrows to help interpret their color scale. In Figure 11a we have taken our fracture directions (from Figure 10) and performed modal smoothing of the directions using a 200-m $\times$ 400-m box centered about each CDP. For each CDP location, the direction is chosen as the one which most frequently occurs in the 200-m $\times$ 400-m box of CDPs around it. As before, we plotted arrows to indicate three fracture direction trends. The red large area in the lower part of the right panel is the most obvious feature. This area indicates a northeast fracture direction, which is consistent with the direction indicated by the shear wave data. However, we must keep in mind that these two measurement methods are detecting fractures at two different scales.

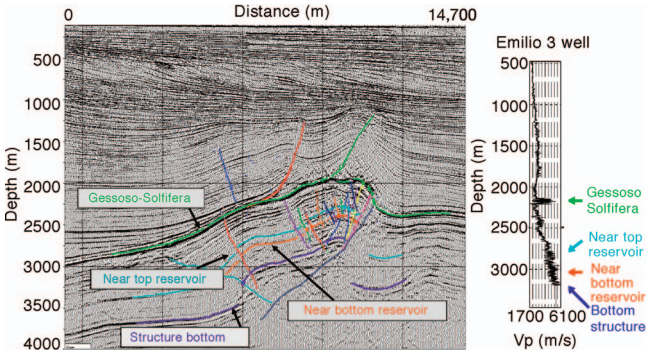

Figure 6. Profile through the Emilio PP data showing the interpreted seismic section (left) and the interval velocity log (right), modified from Vetri et al., 2003.

The velocity anisotropy estimated in Figure 11b detects the effects of subseismic-wavelength fractures; in contrast, the method we describe detects fractured regions that are comparable in size with the seismic wavelength.

The final result is shown in Figure 12, which compares well-derived fracture orientations with those derived by the scattering in-

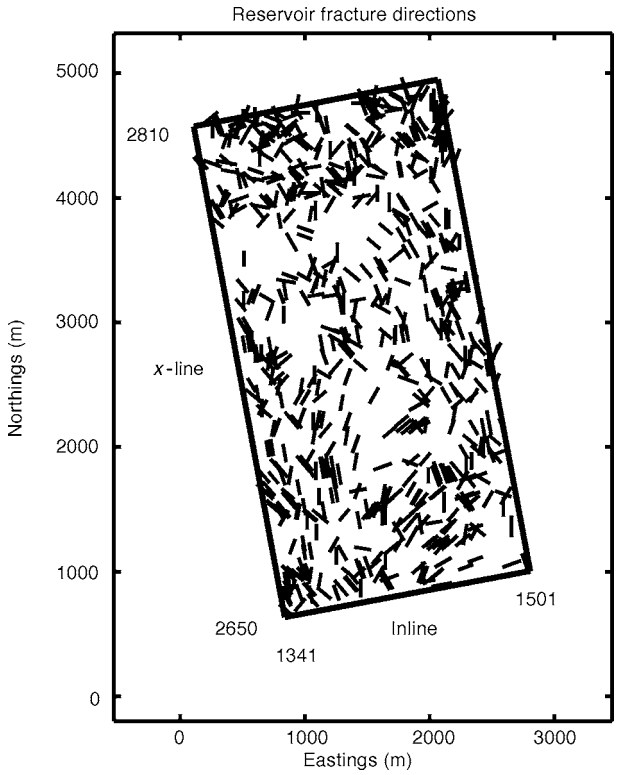

Figure 7. Fracture orientations for the Emilio field from scattering index values showing an angular contrast in values >5.

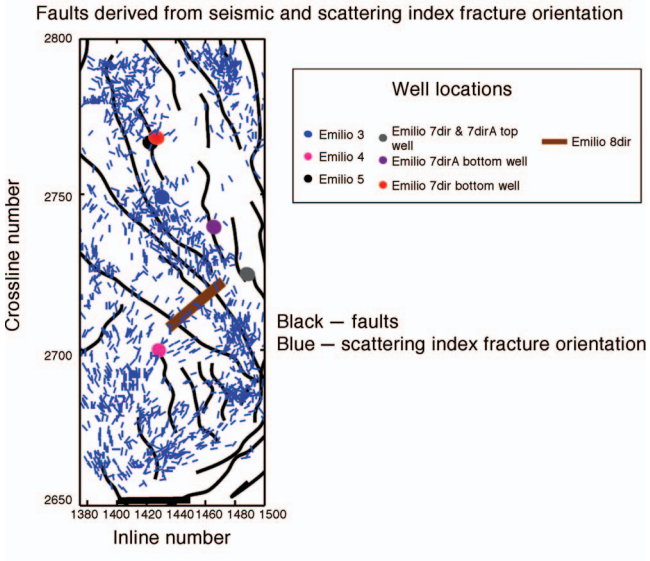

Figure 8. Map-migrated scattering index fracture directions (in blue) for the Emilio field (having angular contrast values >4). The black lines indicate faults derived from seismic data. The well locations are indicated by the colored circles.

dex analysis. The top row shows the well information (from Vetri et al., 2003) that indicates the direction of horizontal stress maximum (SH_{max}). (The FMI log information from the other wells in the field was not available.) In general, fractures align subparallel to the SH_{max} direction. We added a red arrow to the results of Well 4 to emphasize the SH_{max} direction because breakout directions tend to align in the SH_{min} direction. The middle row shows close-ups from Figure 8 around these three wells. To further clarify the fracture trends, we compiled a histogram of the map-migrated scattering directions in a 600-m box around each well in Figure 9 and plotted them in a rose-diagram format; the plots are displayed in the bottom row of Figure 12. There is good agreement between the scattering-index-derived orientations and the well-derived fracture orientations at these three wells.

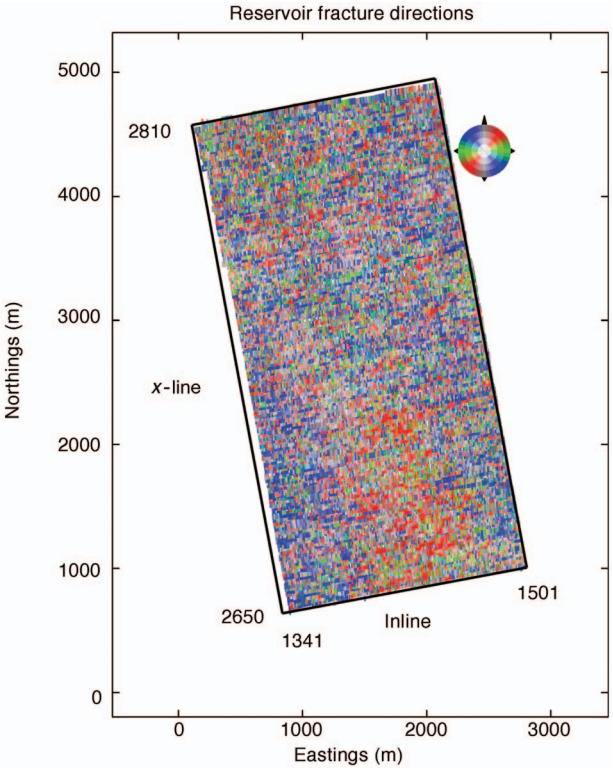

Figure 9. Analysis of fracture orientations for all CDP locations in the field. The color legend at the top right indicates the fracture direction in hue and the increasing angular contrast with intensity.

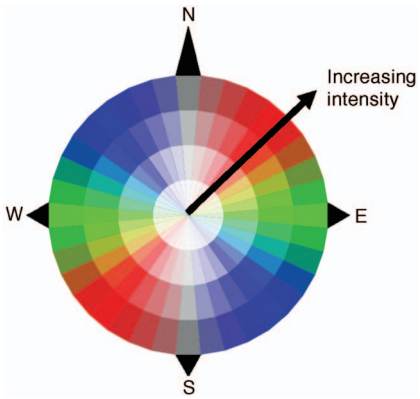

Figure 10. Enlarged view of color legend used to plot fracture orientation directions in Figures 9 and 11a. The color hue indicates the direction of detected fractures. The intensity or saturation of the color indicates the relative magnitude of the azimuthal difference in the detected scattering index: center (whiter) colors indicate less difference; outer (more intense) colors in indicate larger difference.

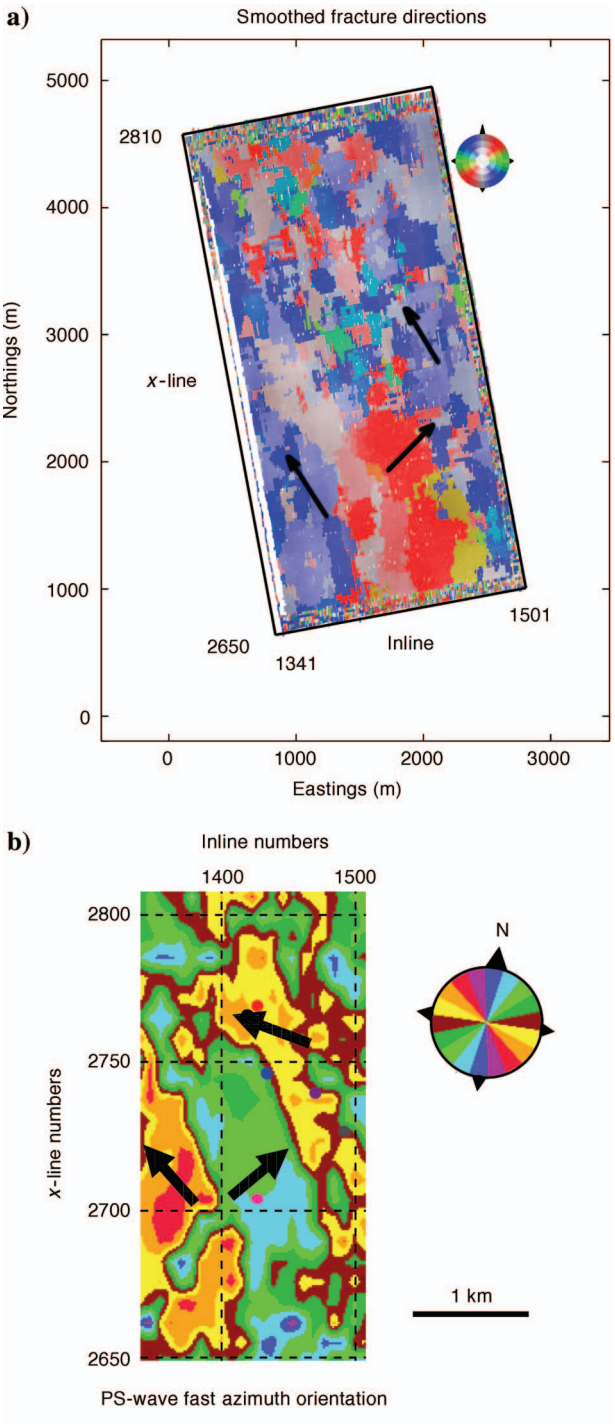

Figure 11. (a) Modally smoothed fracture orientations derived from the scattering index analysis in Figure 9 with its corresponding color-coded legend at the top right. (b) Fracture strike directions derived from PS anisotropy (Vetri et al., 2003) with its corresponding color-coded direction legend. The black arrows indicate three fracture orientation trends.

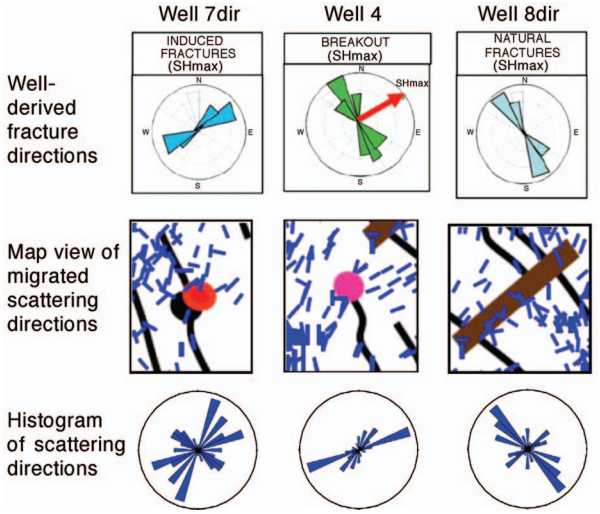

Figure 12. The upper set of diagrams show the well-derived fracture information (from Vetri et al., 2003). SH_{max} is generally the direction of fracture strike. The red arrow indicates the direction of SH_{max} for Well 4. The middle three diagrams are close-ups of Figure 8 around the corresponding well locations that show the agreement of the map-migrated scattering directions with the well fracture directions. The bottom three diagrams show the histograms, in rose-diagram format, of the map-migrated scattering index directions around each of the wells.

CONCLUSIONS

Large-scale zones of fracturing control fluid flow in certain reservoirs, and such zones can scatter seismic energy, depending on the fracture density and compliance as well as on the fracture spacing relative to the seismic-source wavelength. This scattered wave energy contains information about the fracture properties. Using numerical modeling data, we developed a method for analyzing scattered wave energy from fractured reservoirs. A deconvolutional process that measures the ringiness of the transfer function can be used to estimate fracture orientation from azimuthally stacked data. The application of this method on field data provides fracture orientation estimates which agree very closely with previous borehole studies in the Emilio field. It also agrees, at least over part of the survey area, with the general trends of previous PS anisotropy studies in the field. The anisotropy measurements contain information about the fine-scale (with respect to the seismic wavelengths) fracturing in the formation. However, the fracture measurements obtained by this study describe discrete fracture properties that are on the order of the seismic wavelength. As such, we can expect the kind of differences we observe between the anisotropic (fine scale), well-based (intermediate scale), and scattering index (seismic-wavelength scale) fracture direction estimates. The value of the scattering index methodology is that it is a very simple, easy-to-parameterize algorithm that should not be prone to overburden effects. Its application on both model and field data show that it is both robust and accurate at the wells.

ACKNOWLEDGMENTS

We thank Joongmoo Byung, Fred Pearce, Yang Zhang, and Shihong Chi who ran the finite-difference models used in this paper. We thank the Lawrence Berkeley National Laboratory for use of their 3D finite-difference modeling code. We would especially like to thank ENI S.p.A. AGIP for allowing us to show the Emilio data and for providing financial and technical support. We also thank the U. S. Department of Energy (grant DE-FC26-02NT15346) and the Earth Resources Laboratory Founding Member Consortium for funding this work. We thank the three reviewers with GEOPHYSICS, including Daniel Ebrom and Andreas Ehinger, for helpful suggestions to make this paper more complete and easier to read.

REFERENCES

Ata, E., and R. J. Michelena, 1995, Mapping distribution of fractures in a reservoir with P-S converted waves: The Leading Edge, **12**, 664–676.
Block, L., C. H. Cheng, M. Fehler, and W. S. Phillips, 1994, Seismic imaging using microearthquakes induced by hydraulic fracturing: Geophysics, **59**, 102–112.
Burns, D., M. E. Willis, B. Minsley, and M. N. Toksöz, 2004, Characterizing subsurface fractures from reflected and scattered seismic energy: Presented at the 112th SEGJ Conference.
Coates, R. T., and M. Schoenberg, 1995, Finite-difference modeling of faults and fractures: Geophysics, **60**, 1514–1525.
Crampin, S., and S. Chastin, 2000, Shear-wave splitting in a critical crust: II — compliant, calculable, fluid-rock interactions, in Anisotropy 2000: Fractures, converted waves and case studies: SEG.
Crampin, S., R. McGonigle, and D. Bamford, 1980, Estimating crack parameters from observations of P-wave velocity anisotropy: Geophysics, **45**, 345–360.
Daley, T. M., K. Nihei, E. Myer, J. Queen, M. Fortuna, J. Murphy, and R. Coates, 2002, Numerical modeling of scattering from discrete fracture zones in a San Juan Basin gas reservoir: 72nd Annual International Meeting, SEG, Expanded Abstracts, 109–112.
Fehler, M., L. House, W. S. Phillips, and R. Potter, 1998, A method to allow temporal variation in travel-time tomography using microearthquakes induced during hydraulic fracturing: Tectonophysics, **289**, 189–201.
Gaiser, J., E. Loinger, H. Lynn, and L. Vetri, 2002, Birefringence analysis at the Emilio field for fracture characterization: First Break, **20**, 505–514.
Hall, S., and J.-M. Kendall, 2003, Fracture characterization at Valhall: Application of P-wave amplitude variation with offset and azimuth (AVOA) analysis to a 3D ocean-bottom data set: Geophysics, **68**, 1150–1160.
House, N., B. Fuller, and J. Shemeta, 2004, Integration of surface seismic, 3D VSP, and microseismic hydraulic fracture mapping to improve gas production in a tight complex reservoir: 74th Annual International Meeting, SEG, Expanded Abstracts, 414–416.
Jenner, E., 2002, Azimuthal AVO: Methodology and data examples: The Leading Edge, **21**, 782–786.
Levander, A. R., 1988, Fourth-order finite-difference P-SV seismograms: Geophysics, **53**, 1425–1436.
Lynn, H., and D. Cox, 2003, P-wave AVOA interpretation needs the input of additional information: 73rd Annual International Meeting, SEG, Expanded Abstracts, 124–126.
Lynn, H., K. M. Simon, and C. R. Bates, 1996, Correlation between P-wave AVOA and S-wave traveltime anisotropy in a naturally fractured gas reservoir: The Leading Edge, **15**, 931–935.
Minsley, B., M. E. Willis, M. Krasovec, D. Burns, and M. N. Toksöz, 2004, Investigation of a fractured reservoir using P-wave AVOA analysis: A case study of the Emilio Field with support from synthetic examples: 74th Annual International Meeting, SEG, Expanded Abstracts, 248–251.
Nakagawa, S., K. Nihei, and L. Myer, 2002, Numerical simulation of 3D elastic wave scattering off a layer containing parallel periodic fractures: 72nd Annual International Meeting, SEG, Expanded Abstracts, 1967–1970.
———, 2003, Three-dimensional elastic wave scattering by a layer containing vertical periodic fractures: Journal of the Acoustical Society of America, **13**, 3012–3023.
Nihei, K., S. Nakagawa, L. Myer, and E. Majer, 2002, Finite difference modeling of seismic wave interactions with discrete, finite length fractures: 72nd Annual International Meeting, SEG, Expanded Abstracts, 1963–1966.
Pearce, F., 2003, Seismic scattering attributes to estimate reservoir fracture density: a numerical modeling study: M.S. thesis, Massachusetts Institute of Technology.
Perez, M., R. Gibson, and M. N. Toksöz, 1999, Detection of fracture orientation using azimuthal variation of P-wave AVO response: Geophysics, **64**, 1253–1265.
Phillips, W., T. Fairbanks, J. Rutledge, and D. Anderson, 1998, Induced microearthquake patterns and oil-producing fracture systems in the Austin chalk: Tectonophysics, **298**, 153–169.
Robinson, E., and S. Treitel, 1980, Geophysical signal analysis: Prentice Hall Inc.

Sayers, C. M., and J. Rickett, 1997, Azimuthal variation in AVO response for fractured gas sands: Geophysical Prospecting, **45**, 165.
Schultz, C., and M. N. Toksöz, 1996, Experimental study of enhanced backscattering from a highly irregular, acoustic-elastic interface: Journal of the Acoustical Society of America, **99**, 880–892.
Shen, F., J. Sierra, D. R. Burns, and M. N. Toksöz, 2002, Azimuthal offset-dependent attributes applied to fracture detection in a carbonate reservoir: Geophysics, **67**, 355–364.
Shen, F., and M. N. Toksöz, 2000, Scattering characteristics in heterogeneously fractured reservoirs from waveform estimations: Geophysical Journal International, **140**, 251–266.
Vetri, L., E. Loinger, J. Gaiser, A. Grandi, and H. Lynn, 2003, 3D/4C Emilio: Azimuth processing and anisotropy analysis in a fractured carbonate reservoir: The Leading Edge, 675–679.
Vlastos, S., E. Liu, I. G. Main, and X.-Y. Li, 2003, Numerical simulation of wave propagation in media with discrete distributions of fractures: Effects of fracture sizes and spatial distributions: Geophysical Journal International, **152**, 649–668.
Willis, M. E., D. R. Burns, R. Rao, and B. Minsley, 2003, Characterization of scattering waves from fractures by estimating the transfer function between reflected events above and below each interval: Annual Sponsors' Meeting of the Massachusetts Institute of Technology Earth Resources Laboratory.
Willis, M. E., D. Burns, R. Rao, B. Minsley, and Y. Zhang, 2004a, Characterizing seismic scattering from discrete fracture systems: Presented at the SEG Research Workshop on Fractured Reservoirs.
Willis, M. E., F. Pearce, D. R. Burns, J. Byun, and B. Minsley, 2004b, Reservoir fracture orientation and density from reflected and scattered seismic energy: 66th Annual International Meeting, EAGE, Extended Abstracts.
Willis, M. E., R. Rao, D. Burns, J. Byun, and L. Vetri, 2004c, Spatial orientation and distribution of reservoir fractures from scattered seismic energy: 72nd Annual International Meeting, SEG, Expanded Abstracts, 1535–1538.
Wu, C., J. Harris, and K. Nihei, 2002, 2-D finite-difference seismic modeling of an open fluid-filled fracture: Comparison of thin-layer and linear-slip models: 72nd Annual International Meeting, SEG, Expanded Abstracts, 1959–1962.

APPENDIX B

F-K Domain Characteristics of the Seismic Response of a Set of Parallel Discrete Fractures

Yang Zhang, Xander Campman, Samantha Grandi, Shihong Chi, Mark E. Willis, M. Nafi Toksöz and Daniel R. Burns, Earth Resources Laboratory, Massachusetts Institute of Technology.*

Summary

We model seismic wave propagation in a reservoir with discrete fracture zones using a finite difference program, which implements the Coates-Schoenberg formulation for fractured media. We study the behavior of scattered energy in the direction perpendicular and parallel to fracture strike. In the modeled data, we observe variations in the coherence of seismic energy and interference between backward and forward scattered energy. The observed scattered energy contains information about the fracture zones. We develop a method to extract the dominant coherent back sctattered energy. The fracture spacing is then estimated from the frequency wave-number spectrum of this back scattered energy. Results show that our method gives quite accurate estimates for several different spacings.

Introduction

Fractures impact the mechanical properties of a solid, affect seismic wave propagation and control fluid flow and production of oil and gas in a reservoir. Knowledge of their distribution, orientation and physical properties are therefore of great importance for developing production and stimulation programs.

Several studies explain fracture-induced anisotropy using effective-media theory (e.g., Schoenberg and Sayers, 1995), which assumed that fractures or cracks with scales much smaller than the seismic wavelength, are isolated and sparsely distributed in the media. Such fractured media imparts a particular signature to 3D seismic data, an AVOaz – amplitude variation with offset in azimuth effect. Vetri, et al. (2003) analyzed the AVOaz of PP and PS reflected energy to obtain information about fracture orientation, density and other properties. PS (converted) energy can also be used as a tool for fractured-reservoir characterization by analyzing the splitting of shear waves (Gaiser, et al., 2002).

However, the magnitude of seismic anisotropy in field data cannot always be well explained by effective media theory (Lynn, 2004; Zhang, et al., 2005). In some geological situations, small cracks cluster into large-scale fracture corridors or fault zones (Liu, et al., 2000), thereby causing a different seismic signature than do individual small cracks. In such cases, discrete fracture models need to be considered in order to better explain field data observations. Scattering is characteristic on the seismic response of media with large discrete fractures.

In this paper, we analyze data obtained by modeling seismic wave propagation through a medium with discrete fractures. We compare the results from receiver lines perpendicular and parallel to fracture strike. Similar experiments were done by Willis et al. (2004) and Willis et al. (2006), to validate a method that estimates dominant fracture orientation at the reservoir level. Given the fracture strike, fracture spacing can be estimated from the scattered field. In this abstract we describe a method to extract coherent back scattered energy and estimate fracture spacing from its frequency wave-number spectrum.

Modeling Method

A system of aligned cracks, or fractures, can be described as an effective anisotropic medium when the dominant wavelength is long compared to the fracture scales (like width and spacing). Schoenberg and Muir (1989) derived the effective properties of a finely layered medium based on this long-wavelength equivalent medium theory. In order to accurately model wave propagation through boundaries in an elastic solid with a Finite-Difference (FD) scheme, Muir et al. (1992) extended Schoenberg and Muir's derivation to represent the stiffness coefficient of a grid cell traversed by a boundary. Coates and Schoenberg (1995) developed this idea further to represent fractures with linear slip behavior in a FD scheme. We use this method to represent discrete fractures in our model. Our finite difference code is 2nd order accuracy in both space and time, and uses a rotated-staggered-grid scheme.

Description of the model

We implement fractures as compliant zones of thickness equal to a single cell in the finite difference grid, and we represent their properties assigning anisotropic elastic constants to this grid cell. The lateral extent of the fractures is large compared to the wavelength. We consider a 3-layered model; the fractured layer is sandwiched between two homogeneous, isotropic layers. The source and receiver arrays are located at the surface. Figure 1 shows the schematics of the model. Detailed model parameters are listed in Table 1.

Scattering characteristics

Because of the scale of the fractures, waves traveling through the fractured reservoir are strongly scattered. Figure 2 shows the vertical component acquired over the 3-layered model. In each of the panels, the direct wave has been muted. As a reference, Figure 2a shows the result for

the layered model without fractures. We can identify reflected and converted energy from the top and bottom of the reservoir. Between 0.55 and 0.6 s, we observe a *P* wave that is reflected as an *S* wave at the bottom of the reservoir and transmitted as a *P* wave (denoted by *PSP* in Figure 2a).

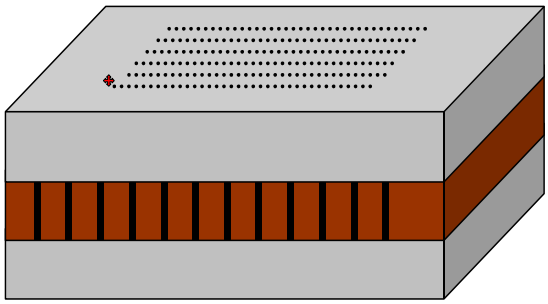

Figure 1: A fractured reservoir embedded in a three-layered model.

Figure 2b shows a line collected over the fractured reservoir, perpendicular to the fracture strike. Scattered energy from the fracture zones contaminates the events arriving at later times, especially the P to S converted energy at the top and bottom of the reservoir. Strong scattered waves are the dominant energy in this case. Frequency-wavenumber spectra of these data show both forward and backward scattered energy and further analysis reveals that most of this energy is composed of S-waves. Interference between forward and backward scattered waves causes the coda to appear incoherent. Figure 2c shows a line collected parallel to the fractures. Scattered coda is more coherent when the line is parallel to the fractures suggesting that energy is scattered from out-of-the-plane fractures parallel to the acquisition line. Even though this energy is coherent, it obscures the *S*-reflection from the bottom of the reservoir.

Spacing estimation

Like fracture orientation, spacing between fracture corridors is an important parameter impacting fluid mobility. Grandi, et al. (2005) analyzed backscattered energy at near offsets in shot-gathers sorted in the normal to fracture orientation to estimate fracture spacing in the f-k domain. Figure 3 shows the results of using the same method on modeled data generated from a 30 m fracture spacing model. As an improvement over regular f-k filtering, backscattered energy is extracted using the Local Wavefield Decomposition (LWD) method (Sacchi, 2004). Figure 3a shows a near offset shot gather perpendicular to fracture strike. Data are windowed between the PP reflected energy from the top and bottom interfaces of the reservoir. The scattered energy in this window is magnified and shown in Figure 3b. LWD is then applied to isolate the locally coherent scattered energy. Figure 3c shows the normalized energy distribution of the decomposed seismic data at each dip value p. We can see that there are two main parts of the scattered energy corresponding to back scattered (negative dip values) and forward scattered (positive dip values) energy. Energy above 80% at negative values of p is used to reconstruct a new seismic section as shown in Figure 3d. This new section represents the dominant part of the backscattered energy from the fractures.

The f-k content of the backscattered energy may be used to estimate fracture spacing:

$$d = \frac{\lambda_a}{2} = \frac{v_a}{2f} = \frac{1}{2\,|\,k_a\,|}\,.$$

where d is the estimated fracture spacing, k_a and f are the wave number and frequency of the dominant back scatteerd energy, v_a is an apparent velocity and λ_a is an apparent wavelength.The idea of this formulation is that the repeat pattern observed in the back scattered energy has wave number information which is related to fracture spacing. Inspection of snapshots of the wave field gathered during modeling reveals that seismic waves bouncing between fractures leads to resonance and modes propagation. The repeat pattern of back scattered waves received at surface referred to in this paper, might be different from the modes in the fracture zone.

As indicated in Figure 3e, the (k, f) values of the maximum energy in the spectrum are (-0.0157 1/m, 78 Hz), hence the estimated fracture spacing with our equation is 31.8 m. The actual spacing between fractures zones in this model is 30 m. We have repeated this for various (larger) fracture spacings and each time the spacing estimated with our methodology was very close to the actual spacing.

We also applied the same process to data from a model with smaller -- 20 m -- fracture spacing. In this case there is almost no backscattered energy in the window within the reservoir P reflectors because the frequency content of the seismic source is too low to effectively discriminate fractures. Most energy locates at positive values of p. To overcome this limitation in resolution, we move the window to later times to capture scattering containing PS converted energy from the fractured zone. Shear waves have shorter wavelengths and therefore, a higher resolving power than P waves. Figures 4b-e compare the divergence and curl energy computed in two windows, the shallow (PP) window and a deeper (PS) window. We can see that in the shallow (red) window there is strong divergent energy (Figure 4b) but almost no curl energy (Figure 4c). In the deeper (blue) window, both divergent (Figure 4d) and curl (Figure 4e) energies are strong, the curl energy is especially

Table 1: Modeling parameters for the 3D layered fractured reservoir.

	Vp (m/s)	Vs (m/s)	Density (kg/m^3)	Nominal Wavelength (m)	
				P	S
Top Layer	2460	1230	2300	60	30
Fractured Layer*	3300	1800	2200	80	45
Bottom Layer	2460	1230	2300	60	30
Fracture Compliance	$Z_N = Z_T = 2\times10^{-10}$ (m/Pa)				
Source	Point Source, Ricker Wavelet, center frequency $f_0 = 40$ (Hz)				
Fracture spacing	30m				

large at these later times. In addition, the coherent back scattered energy in the deeper (blue) window is higher than that in the shallow (red) window. Strong PS converted waves can be generated at interfaces with high contrast (Toksöz et al., 2005), such as fracture zones, and it may therefore be more advantageous to choose scattered energy arriving later in time. By doing so, we may be able to resolve the finer structure of the reservoir.

Conclusion

We have modeled seismic-wave propagation in a medium with discrete vertical fractures in order to explain observations made in field data. The wave field is scattered by such fractures. We observe that scattering appears differently in different directions. In the direction perpendicular to the fractures, scattered waves in the forward and backward direction interfere, causing the scattered wave field to appear incoherent. In the parallel direction the scattered wave field is more coherent. We analyzed the scattered energy to ultimately obtain an estimation of fracture spacing. First, we separated the dominant back scattered energy from the data. Then, we estimated the fracture spacing from the f-k spectrum of this backscattered wave field. We also observed that following the reflection off the top of the reservoir, the scattered energy contains progressively more P-S converted energy. This energy may be used to extract information from finer structures. Application of this method to a field data set is in progress.

References

Coates, R. T. and Schoenberg, M., 1995. *Finite-difference modeling of faults and fractures*, Geophysics, 60(5), pp. 1514-1526.

Gaiser, J., Loinger, E., Lynn, H. and Vetri, L., 2002, *Birefringence analysis at Emilio Field for fracture characterization,* First Break, 20, 505-514

Grandi, S., Willis, M. E., Burns, D. R. and Toksöz, M. N., 2005, F-K analysis of backscattered signal to estimate fracture orientation and spacing, ERL Consortium Meeting Report

Liu, E., Hudson, J. A. and Pointer, T., 2000, *Equivalent medium representation of fractured rock*, J. Geophysical Research, 105, 2981-3000

Lynn, H. B., 2004, *The winds of change*, The Leading Edge, 23, 11, 1156-1268

Muir, F., Dellinger, J., Etgen, J. and Nichols, D., 1992. *Modeling elastic fields across irregular boundaries*, Geophysics, 57(9), pp.1189-1193.

Sacchi, M. D., Data reconstruction by generalized deconvolution, 2004, 74th SEG Expanded Abstracts

Schoenberg, M. and Muir, F., 1989. *A calculus for finely layered anisotropic media,* Geophysics, 54(5), pp. 581-589.

Schoenberg, M. and Sayers, C. M., 1995, *Seismic anisotropy of fractured rock*, Geophysics, 60, 1, 204-211

Toksöz, M., Chi, S., Zhang, Y., Sze, E. and Lu, R., 2005, Characterization of an explosion source in a complex medium by modeling and wavelet domain inversion, 27th Seismic Research Review Proceeding.

Vetri, L., Loinger, E., Gaiser, J., Grandi, A. and Lynn, H., 2003, 3D/4C Emillio: *Azimuth processing and anisotropy analysis in a fractured carbonate reservoir*, The Leading Edge, 22, 675-679

Willis, M.E., Pearce, F, Burns, D.R, Byun, J. and Minsley, B, 2004, Reservoir fracture orientation and density from reflected and scattered seismic energy, *EAGE meeting Paris.*

Willis, M., Burns, D. R., Rao, R., Minsley, B., Toksoz, M. N., Vetri, L., 2006, Spatial orientation and distribution of reservoir fractures from scattered seismic energy, *Geophysics, in press.*

Zhang, Y., Chi, S., Willis, M. E., Burns D. R. and Toksöz, M. N., 2005, *Comparison of discrete fracture and effective media representation of fractures on azimuthal AVO*, Expanded Abstracts, 75th SEG Ann. Mtg.

Acknowledgements

This work was funded by the ERL Industrial and Founding Members Consortium and a grant from the DOE award number DE-FC26-02NT15346. Additional support came from Shell Gamechanger.

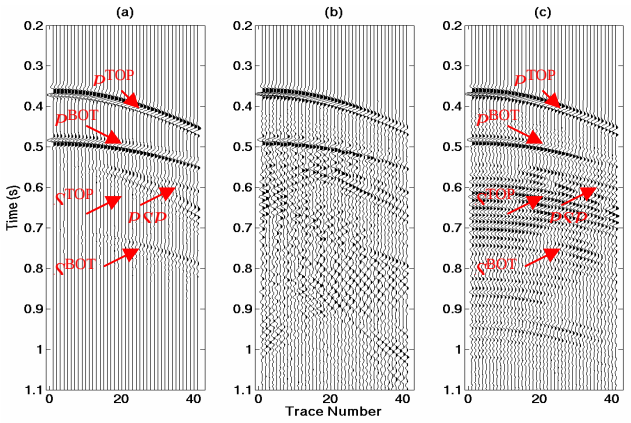

Figure 2: (a) Vertical velocity recorded in a line over the medium without fractures. (b) Vertical velocity measured in a line over the medium with fractures, perpendicular to the fractures. (c) as (b), but parallel to the fractures..

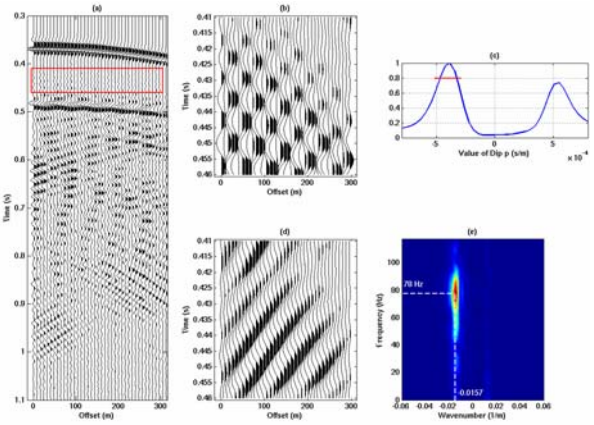

Figure 3: Determination of fracture spacing in f-k domain for model with 30 m spacing. (a) Seismogram of vertical component at near offset for direction perpendicular to fracture strike. Red window contains PP scattered energy between PP reflected at top and bottom interfaces of fractured reservoir; (b) Seismogram of energy in red window after being zoomed in (6 times scale as in (a)). (c) Normalized energy distribution in dip value p after applying LWD method on seismogram in (b); (d) Reconstructed seismic data by using profile with energy above 80% in (c), which is indicated by the red line; (e) Result of f-k transformation of reconstructed data in (d). The value of (k, f) of maximum energy is (-0.0157 1/m, 78 Hz). The estimated spacing is about 31.8 m.

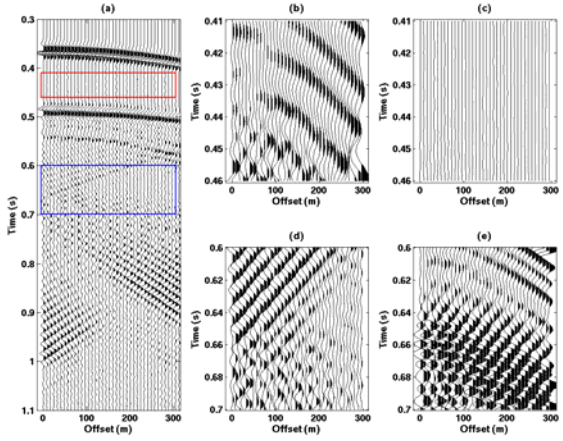

Figure 4: Divergence and curl energy in two successive time windows for model with 20 m fracture spacing. (a) Seismogram of vertical component at near offset in the direction perpendicular to fracture strike. Windows indicated in red and blue are chosen whose divergence and curl energy are compared; (b) Divergence energy contained in the red window; (c) Curl energy contained in the red window at the same scale as in (b); (d) Divergence energy contained in the blue window; (e) Curl energy contained in the blue window at the same scale as in (d).

EDITED REFERENCES

Note: This reference list is a copy-edited version of the reference list submitted by the author. Reference lists for the 2006 SEG Technical Program Expanded Abstracts have been copy edited so that references provided with the online metadata for each paper will achieve a high degree of linking to cited sources that appear on the Web.

REFERENCES

Coates, R. T., and M. Schoenberg, 1995, Finite difference modeling of faults and fractures: Geophysics, **60**, 1514–1526.

Gaiser, J., E. Loinger, H. Lynn, and L. Vetri, 2002, Birefringence analysis at Emilio Field for fracture characterization: First Break, **20**, 505–514.

Grandi, S., M. E. Willis, D. R. Burns, and M. N. Toksöz, 2005, F-K analysis of backscattered signal to estimate fracture orientation and spacing: ERL Consortium Meeting Report.

Liu, E., J. A. Hudson, and T. Pointer, 2000, Equivalent medium representation of fractured rock: Journal of Geophysical Research, **105**, 2981–3000.

Lynn, H. B., 2004, The winds of change: The Leading Edge, **23**, 1156–1268.

Muir, F., J. Dellinger, J. Etgen, and D. Nichols, 1992, Modeling elastic fields across irregular boundaries: Geophysics, **57**, 1189–1193.

Sacchi, M. D., 2004, Data reconstruction by generalized deconvolution: 74th Annual International Meeting, SEG, Expanded Abstracts, 1989–1992.

Schoenberg, M., and F. Muir, 1989, A calculus for finely layered anisotropic media: Geophysics, **54**, 581–589.

Schoenberg, M., and C. M. Sayers, 1995, Seismic anisotropy of fractured rock: Geophysics, **60**, 1, 204–211.

Toksöz, M., S. Chi, Y. Zhang, E. Sze, and R. Lu, 2005, Characterization of an explosion source in a complex medium by modeling and wavelet domain inversion: 27th Seismic Research Review Proceeding.

Vetri, L., E. Loinger, J. Gaiser, A. Grandi, and H. Lynn, 2003, 3D/4C Emillio: Azimuth processing and anisotropy analysis in a fractured carbonate reservoir: The Leading Edge, **22**, 675–679

Willis, M., D. R. Burns, R. Rao, B. Minsley, M. N. Toksoz, and L. Vetri, 2006, Spatial orientation and distribution of reservoir fractures from scattered seismic energy: Geophysics, in press.

Willis, M. E., F. Pearce, D. R. Burns, J. Byun, and B. Minsley, 2004, Reservoir fracture orientation and density from reflected and scattered seismic energy: Presented at the 66th Annual Conference and Exhibition, EAGE.

Zhang, Y., S. Chi, M. E. Willis, D. R. Burns, and M. N. Toksöz, 2005, Comparison of discrete fracture and effective media representation of fractures on azimuthal AVO: 75th Annual International Meeting, SEG, Expanded Abstracts, 305–307.

APPENDIX C

Finite Difference Modeling of Seismic Responses to Intersecting Fracture Sets

Shihong Chi, Yang Zhang, Xander Campman and M. Nafi Toksöz
Earth Resources Laboratory
Dept. of Earth, Atmospheric, and Planetary Sciences
Massachusetts Institute of Technology
Cambridge, MA 02139

May 27, 2006

Abstract

Fractured reservoir characterization is becoming increasingly important for the petroleum industry. Current methods for this task are developed based on effective media theory, which assumes the cracks or fractures in a reservoir are much smaller than the seismic wavelength. A discrete fracture model has to be used for large-scale fractures. We describe an approach of using a finite difference method for modeling seismic wave propagation in rock formations with intersecting fracture sets. We then use the code to study the behavior of seismic waves, particularly scattering due to such fracture sets with various spacing and compliances. The scattering pattern due to fractures varies azimuthally. We find that converted PS and PSP waves from the bottom of the fractured layers show strong interference by the scattered waves. We observe coherent scattered waves in shot gathers parallel to the fracture orientation and significant backscattering at near offsets and forward scattering at far offsets in the gathers normal to the fracture orientation. When two sets of fractures are present, scattering becomes stronger and more complex scattered waves appear in the gathers. The scattering becomes stronger with increasing the fracture compliances and decreasing spacing (still on the order of seismic wave length). When the fracture sets are not orthogonal to each other, the gathers still show coherent scattering in the fracture orientations. Azimuthal characteristics of the scattered waves may be used to analyze fracture orientations, spacing, and relative compliance of intersecting fracture sets.

1 Introduction

The purpose of this paper is to describe a finite difference method for modeling seismic wave propagation in rock formations with intersecting fracture sets with spacing on the order of the wavelength or larger. We intend to provide a widely usable tool for aiding developments of methods for extracting orientation, spacing, and compliance of such fracture sets. We study the behavior of seismic waves, particularly scattering due to such fracture sets. Fractured reservoir characterization has drawn increasing attention in the petroleum industry. Many people have studied seismic responses to fractures and characterized fractures using seismic data based on effective media theory, which assumes the fractures are penny shaped cracks (Hudson, 1986; Liu et al., 2000) or the spacing of the fractures sets are much smaller than the seismic wavelength (Schoenberg and Sayers, 1995). Using effective media theory, the fractured rocks can be approximated as homogeneous anisotropic media of lower symmetries. Based on this theory, azimuthal AVO of reflected PP and converted PS waves are commonly used for determining fracture orientation and other parameters

(Vetri et al., 2003; Shen et al., 2002). Schoenberg and Helbig (1997) discussed a geophysically important subset of orthorhombic media consisting of vertically fractured transversely isotropic media with a vertical symmetry axis (VTI) in great detail. They evaluated possible methods to quantify fracture orientation and compliance and background elastic parameters using multi-azimuth surface seismic, VSP and cross-well data. Natural fractures in reservoirs often contain two or more intersecting sets. They can be orthogonal or non-orthogonal depending on the stress history (Reiss, 1980; Nelson, 1985). Nichols et al. (1989) described the problem of modeling rocks with multiple sets of fractures based on the compliance addition theory outlined by Schoenberg and Muir (1989). They also showed explicitly how to obtain the resultant compliance tensor for an orthogonal fracture set embedded in an isotropic medium and that such a fracture set renders the medium orthorhombic. Grechka and Kachanov (2005) studied the effective anisotropy of multiple fractures in rocks, where networks of small fractures control the fluid flow. They concluded that regardless of the number of fracture sets embedded in otherwise isotropic host rock, their orientations, or types of fluid infill, the symmetry of the effective medium is approximately orthorhombic. They also showed that both theories of Schoenberg and Kachanov describe the effective media well. For the long wavelength effect of realistic fractures on seismic responses, i.e., when wavelengths are much larger than the fracture spacing, we use Schoenberg's formulation for the equivalent anisotropic medium in terms of elastic compliance.

The effective media theory has been widely used in various seismic applications.Sayers (1998) analytically determined the misalignment of the orientation of fractures and the principal axes for P and S waves in rocks containing multiple non-orthogonal fracture sets. Schoenberg et al. (1999) showed the azimuth-dependent tuning of seismic waves reflected from a thin reservoir layer containing one or more sets of fractures. Bakulin et al. (2000a,b) and Bakulin et al. (2000c) attempted to invert various seismic signatures for formation parameters.

However, when the fracture spacing is on the order of the seismic wavelength, the effective medium theory cannot capture the effect of fractures. Recent works (Nihei et al., 2002; Lynn, 2004; Willis et al., 2004b,a, 2006) have studied the effect of discrete parallel fractures because geological evidence shows that fractures with spacing on the order of the seismic wavelength commonly exist in reservoirs. Zhang et al. (2005) showed on synthetic seismic data that the azimuthal AVO properties are very different for penny shaped cracks and discrete parallel fractures. In the field, many fractures are not parallel, but intersecting. In modeling seismic responses to small fracture networks and large discrete fractures, it is important to be able to represent the fractures at various scales properly.

Coates and Schoenberg (1995) developed a general formulation for modeling multiple intersecting sets of fractures with arbitrary orientations using a finite difference method. To model a linear-slip fracture when the fracture is at an angle to the finite difference grid, they used a suitable equivalent anisotropic medium to replace the elastic medium within each finite difference cell intersected by the fracture, together with the embedded segment of the fracture. Nihei et al. (2002) and Vlastos et al. (2003) modeled the seismic responses of discrete sets of parallel fractures. We extend their approach to model multiple intersecting sets of fractures. We represent them discretely in our modeling. We present details on how to represent orthogonally and non-orthogonally intersecting fractures in finite difference modeling. We further simplify the model building process, particularly on how to represent the areas near the fracture intersections. Then we study the characteristics of seismic scattering due to intersecting fracture sets.

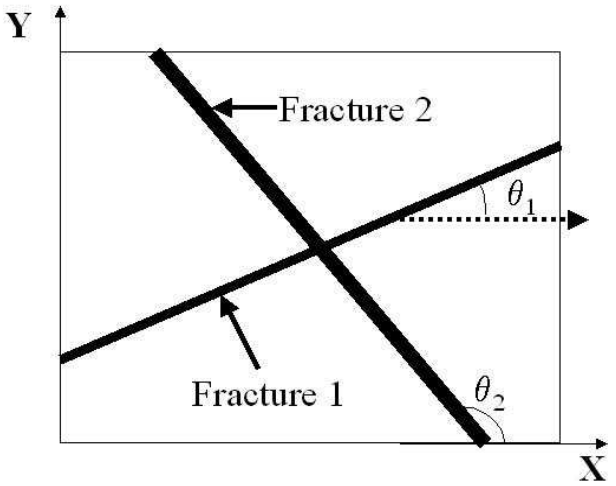

Figure 1: Two intersecting vertical fractures passing through the map view of a 3-D finite-difference cell. Each fracture normal forms an angle θ_i to the finite difference grid direction.

2 Effective Media Theory of Multiple Sets of Fractures

For multiple sets of vertical fractures, Nichols et al. (1989) show that the compliance matrix for the equivalent medium is

$$S = S_b + \sum_{i=q}^{m} \Delta S_i, \tag{1}$$

where m is the number of fracture sets, S_b and ΔS_i are the compliance of background medium and contribution from the i-th fracture set (see Figure 1). It is obvious that the order in which the fractures are included does not affect the final compliance. Assuming the i-th fracture strike forms an angle θ_i to the finite difference grid direction, the Bond transformation matrix can be written as (Auld, 1990)

$$B = \begin{bmatrix} \frac{1+\cos 2\theta_i}{2} & \frac{1+\cos 2\theta_i}{2} & 0 & 0 & 0 & \sin 2\theta_i \\ -\frac{\sin 2\theta_i}{2} & \frac{\sin 2\theta_i}{2} & 0 & 0 & 0 & \cos 2\theta_i \\ 0 & 0 & 0 & \sin 2\theta_i & -\cos\theta_i & 0 \end{bmatrix} \tag{2}$$

and

$$\Delta S_i = B^T Z_i B, \tag{3}$$

where in the fracture coordinate system, the compliance of each fracture set can be written as

$$Z_i = \begin{bmatrix} Z_i^N & 0 & 0 \\ 0 & Z_i^V & 0 \\ 0 & 0 & Z_i^H \end{bmatrix} \tag{4}$$

where Z_i^N, Z_i^V, and Z_i^H represent the normal, vertical and horizontal compliance of the i-th fracture, respectively. A rotationally symmetric fracture has equal vertical and horizontal compliance. Inversion of the compliance matrix yields thpe elastic stiffness matrix. Schoenberg and Sayers (1995) showed that the equivalent media of isotropic host media embedding non-orthogonally and orthogonally intersecting fractures is monoclinic and orthorhombic, respectively. If the formation shows horizontal stratification, we generally represent it as transversely isotropic with a vertical rotation symmetry axis (VTI). If only a set of vertical

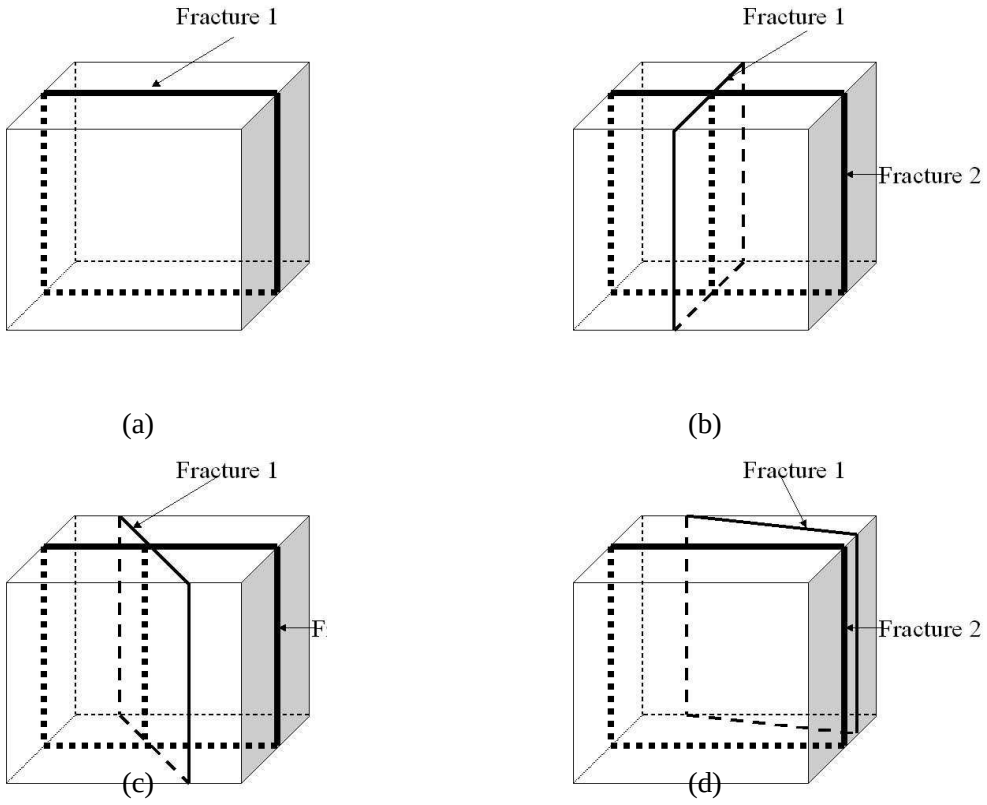

Figure 2: A 3-D finite difference cube containing fracture(s). a. Fracture strike is parallel to one axis; b. Strikes of two orthogonally intersecting fractures are parallel to two axes; c. Only the strike of one of the two orthogonally intersecting fractures is parallel to one axis; d. Only the strike of one of the two non-intersecting fractures is parallel to one axis.

fractures embeds in it, the effective medium property of the fractured formation is orthorhombic (Schoenberg and Helbig, 1997). If two sets of orthogonally intersecting fractures exist in the VTI formation, the effective medium property of the fractured formation should still be orthorhombic. If the two sets are non-orthogonal in the VTI formation, the effective medium property of the fractured formation has been shown to be monoclinic (Winterstein, 1990).

3 Representing Discrete Intersecting Fractures in Finite-Difference Modeling

To model seismic responses due to orthogonally intersecting fracture sets using the finite difference method in a Cartesian coordinate system, we can choose one of the coordinate axes parallel to the fracture strike.

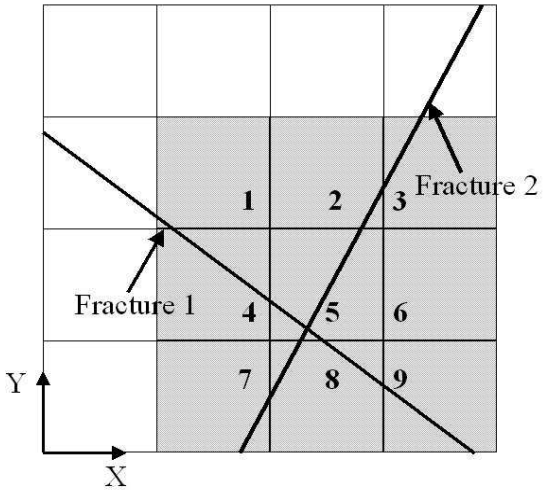

Figure 3: Top view of a set of intersecting fractures overlaying on the finite difference grid. Cells 1 to 9 can use the same property based on effective media theory to reduce the modeling complexity.

We assign the finite difference cells containing only one fracture the equivalent transversely isotropic (with a horizontal rotation symmetry axis) (HTI) elastic property (Figure 2a) and assign the cells containing the intersections the equivalent orthorhombic elastic property (Figure 2b). For non-orthogonally intersecting fracture sets, we can choose one set whose strike will be parallel or normal to the axes (Figure 2c). The finite-difference cells containing intersection(s) of fractures (Figure 2c) possess the properties of monoclinic media (Figure 2d), because the dimension of the grids is much smaller than seismic wavelength and elastic properties of these cells can be approximated using the effective media theory (Schoenberg and Sayers, 1995). For cells containing only fractures normal or parallel to the coordinate axes, we can assign the cell HTI properties. Otherwise, cells only contain the fractures intersecting the axes with an angle other than 0 or 90 degrees. For these cells, we find the elastic stiffness in the current coordinate system using equation 6 and assign them to the respective cells. The properties of these cells show the characteristics of monoclinic media.

To simplify the model building process, we can assign the same parameters to a small region surrounding the intersections based on long wave equivalent media theory. For example, finite difference cells 1 through 9 enclosing the intersection shown in Figure 3 can use the same property if the cell size is much smaller than the seismic wavelength. In some reservoirs, fractures in production zones at different depth show different orientation (Figure 4). In modeling the seismic response using the finite-difference technique, we can choose fractures in one hydrocarbon zone with strike parallel or normal to the axes, while fractures in another zone make an angle with the axes other than 0 or 90 degrees. The apparent elastic stiffness matrix of the other zone resembles that of monoclinic media because of matrix rotation. To simulate the effects of all fractures from the whole field, the finite-difference program has to be able to simulate wave propagation in a monoclinic formation. This situation further shows the need for this study.

4 Finite Difference Implementation

In our finite difference implementation, we use a rotated staggered grid scheme, which allows strong contrasts in the medium and leads to less dispersion errors and a higher computational efficiency (Saenger et al.,

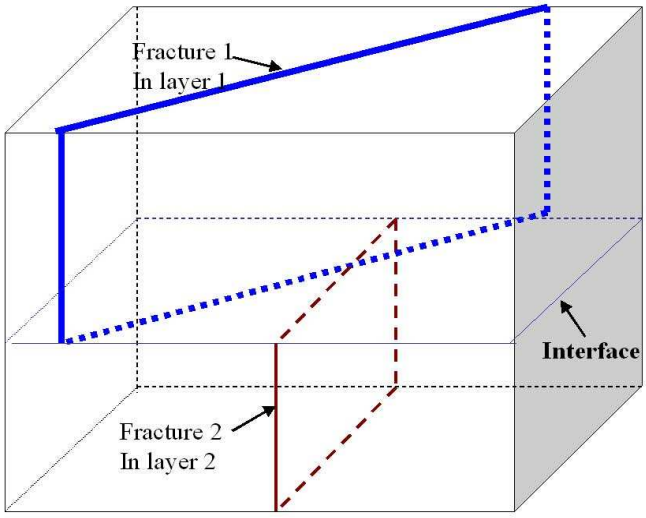

Figure 4: Fractures in different reservoir layers showing different strikes.

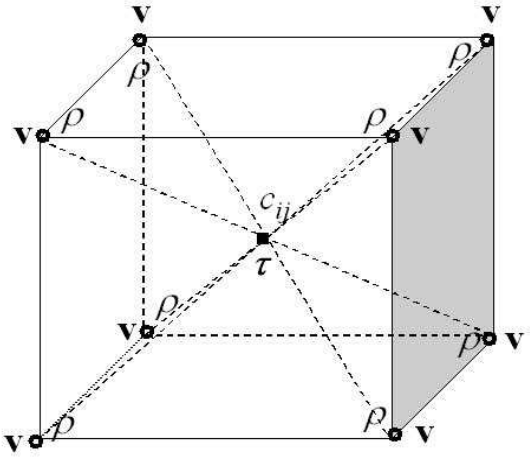

Figure 5: The locations of velocity, stress, and elastic properties in an elementary finite difference cell using rotated staggered grid scheme.

2000). In such a scheme, all components of one physical property (e.g., stress, velocity, elastic stiffness, and density) are placed at one single location as shown in Figure 5. It is not necessary to average any elastic stiffness values as in the standard staggered method (Virieux, 1986). Therefore, this scheme can incorporate the high contrasts existing in fractured media without smoothing the elastic stiffnesses, resulting in a more accurate representation of the fractures.

To effectively absorb wave reflections from the model boundaries, we apply a perfectly matched layer boundary condition (Marcinkovich and Olsen, 2003). We use the first order velocity-stress equations for orthorhombic media. Starting from Hooke's law, we can write:

$$\partial_t \tau_{ij} = \frac{1}{2} c_{ijkl}(v_{k,l} + v_{l,k}). \tag{5}$$

Using the Voigt notation, for orthorombic media, the stiffness tensor c_{ijkl} is given by

$$\boldsymbol{c} = \begin{bmatrix} c_{11} & c_{12} & c_{13} & 0 & 0 & 0 \\ 0 & c_{22} & c_{23} & 0 & 0 & 0 \\ 0 & 0 & c_{33} & 0 & 0 & 0 \\ 0 & 0 & 0 & c_{44} & 0 & 0 \\ 0 & 0 & 0 & 0 & c_{55} & 0 \\ 0 & 0 & 0 & 0 & 0 & c_{66} \end{bmatrix} \tag{6}$$

where τ_{ij} and v_i are elements of the stress tensor and velocity, respectively, and $i, j = x, y, z$. To model wave propagation in non-orthogonal sets of fractures or equivalent monoclinic media, we need to extend equation 6

$$\boldsymbol{c} = \begin{bmatrix} c_{11} & c_{12} & c_{13} & 0 & 0 & c_{16} \\ 0 & c_{22} & c_{23} & 0 & 0 & c_{26} \\ 0 & 0 & c_{33} & 0 & 0 & c_{36} \\ 0 & 0 & 0 & c_{44} & c_{45} & 0 \\ 0 & 0 & 0 & 0 & c_{55} & 0 \\ 0 & 0 & 0 & 0 & 0 & c_{66} \end{bmatrix} \tag{7}$$

Comparing equations 6 and 7, we find that modeling wave propagation in reservoirs containing non-orthogonal fracture systems using the finite difference method demands extra computation cost and memory storage. Otherwise, no additional difficulty occurs.

5 Seismic Scattering due to Intersecting Fractures

In this section, we study the characteristics of the seismic responses from fractured reservoirs. We assume the background formation is isotropic. The fluid filling the fractures is gas. The fractures are 1) orthogonal or 2) non-orthogonal. In both cases, we consider a three-layered model and fractures penetrate through the second layer. Table 1 shows the elastic properties of the background layers. The receiver arrays and the source are located at the earth surface. Figure 6 shows the generic, schematic diagram of the model. In this three-layer reservoir model, the second layer contains the fractures. We first assume the fractures are rotationally invariant and the normal and transverse compliance of the fractures are equal to 2×10^{-10} m/Pa. Therefore, each set of fractures contributes equally to receiver responses. The source and receiver arrays are located at the surface. We use Ricker wavelet as our point source with center frequency at 40 Hz.

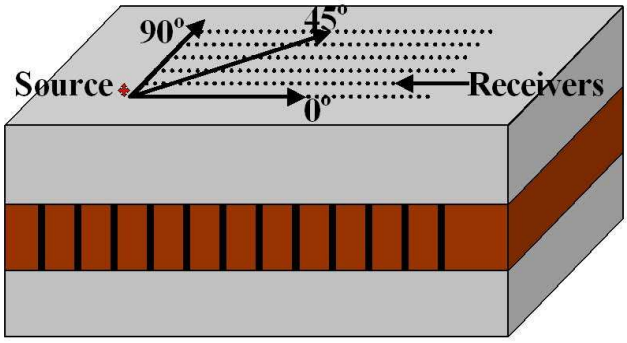

Figure 6: A fractured three-layered reservoir model. Two sets of fractures penetrate through the second layer.

Table 1: The elastic properties of background media for the three-layer model.

	v_p (m/s)	v_s (m/s)	ρ (kg/m^3)	λ_P (m)	λ_S (m)
Top layer	2460	1230	2300	60	30
Middle layer	3300	1800	2200	80	45
Bottom layer	2460	1230	2300	60	30

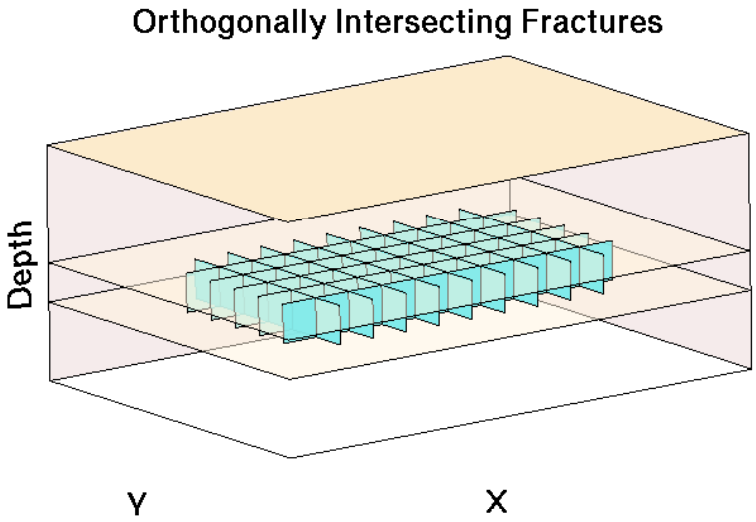

Figure 7: A 3D schematic of the reservoir model with two sets of orthogonally intersecting fractures.

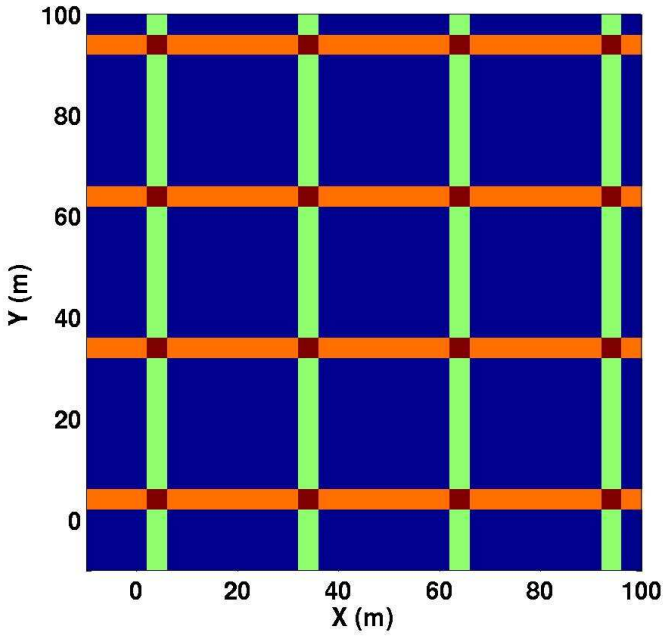

Figure 8: Elastic property distribution of two sets of orthogonally intersecting fractures as indicated by different colors.

5.1 Case 1: Two sets of orthogonally intersecting fractures

We first use the finite difference program to model seismic wave propagation in a medium containing two sets of orthogonally intersecting fractures. Each set of fractures has a regular 30 m spacing. Figure 7 is a 3D schematic of the model. Figure 8 is a zoom-in view of a horizontal slice of the fractured second layer. Different colors represent the background, the two sets of fractures and their intersections.

To understand seismic scattering due to fractures, we also conduct modeling of seismic wave propagation in the same layered background model without fractures and in a model with only one set of parallel vertical fractures of 30 m spacing as references. Figures 9 shows the vertical component of velocity acquired over the 3-layered model without fractures in the middle layer. Figures 10 and 11 show the vertical component of velocity acquired over the model with one set of parallel fracture. Figure 12 and 13 show the vertical component of velocity acquired over the 3-layered model with the orthogonal fractures in the middle layer. In each of the panels, the direct wave has been muted. We have identified reflected and converted waves from the top and bottom of the reservoir.

To identify the events shown in Figure 9, we estimate the arrival times of the P, S, and converted waves from the top and bottom of the middle layer at near offsets. Using these estimated arrival times, we identify the reflected P and P to S waves from the top and bottom of the middle layer. At near offsets, the reflected P wave is very strong and the reflected P to S waves become stronger when the offsets get larger. At intermediate to far offsets, immediately following the reflected P wave from the bottom of the middle layer, a converted PSP wave appears. The shot gathers do not show any azimuthal difference.

Figure 10a shows a line collected over the fractured reservoir perpendicular to the fracture strike. Scattered energy from the fracture zones contaminates the events arriving in later time, especially for PS energy converted at the top and bottom of the reservoir. Strong scattered waves are the dominant energy in this case. Frequency-wavenumber spectra of these data show both forward and backward scattered energy and

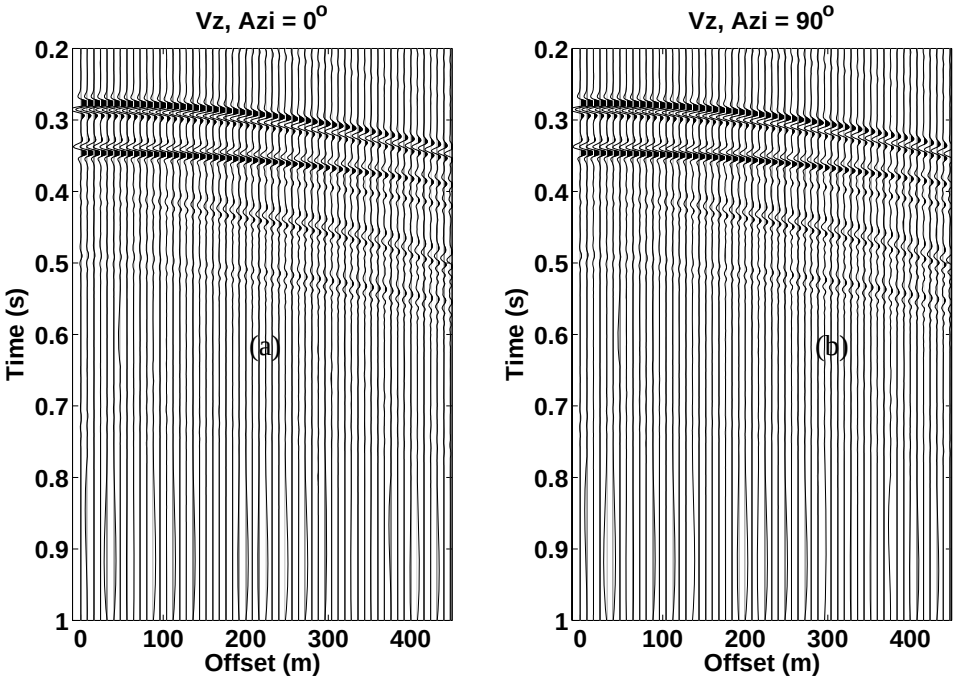

Figure 9: Shot gathers for the three layer base model.

further analysis reveals that most of this energy is composed of S-waves. To compare seismograms for different fractured reservoir models, all the amplitudes of the seismograms are amplified 15 times. Comparing the shot gather at zero azimuth relative to x coordinate axis in Figures 9a and 10a, we easily identify the reflected and converted modes at the top and bottom of the reservoir. At near offsets of Figure 10a for zero azimuth, we see backscattered waves with almost the same slowness arrive as late as 0.7 s. The early arrivals of the backscattered waves interfere the PP wave reflected from the reservoir bottom, so they arrive at the receivers as P wave. However, the moveout velocity is slower than that of the P wave and the wavefront is almost linear, which indicates the wavefront of the backscattered waves due to the set of vertical fractures is similar to a plane wave. At far offsets, we observe that the converted PS and PSP waves from the reservoir bottom show strong interference by the scattered waves, while the PS reflection from the reservoir top can still be seen clearly. We also see strong coherent forward scattered waves following the PS reflection from the bottom of the second layer. These events appear to have velocities slower than that of the shear waves and form two plane wave packs. The dominance of backward scattering at near offsets and forward scattering at far offsets indicates seismic waves transmitted to the fractured layer are mainly reflected by and transmitted through the fracture sets at near and far offsets, respectively. In the middle range of offsets, the back scattered and forward scattered waves interfere and cause some cancellation. With the increase of azimuth, the backward scattered waves seem to become somewhat stronger and the wavefronts become flatter; the forward scattered waves become weaker.

At the 90 degree azimuth, where the receiver line is parallel to the fracture strike, the scattered waves appear to form coherent wavefronts from 0.5 s and later, parallel to that of the PS wave reflected off the bottom of the reservoir layer. The scattered waves also interfere with the PS wave from reservoir top and

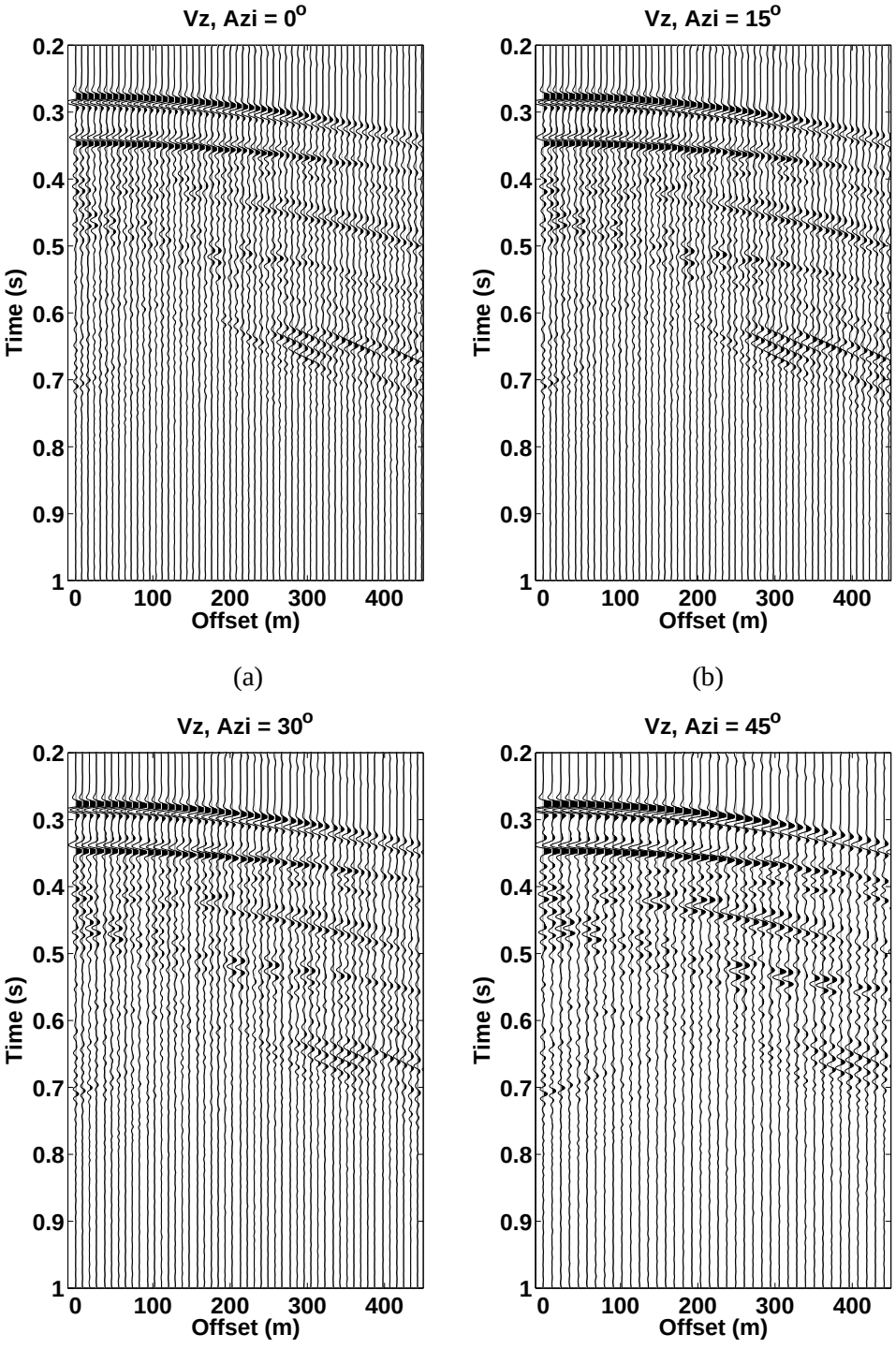

(a) (b)

(c) (d)

Figure 10: Shot gathers for a set of parallel fractures embedded in the middle layer

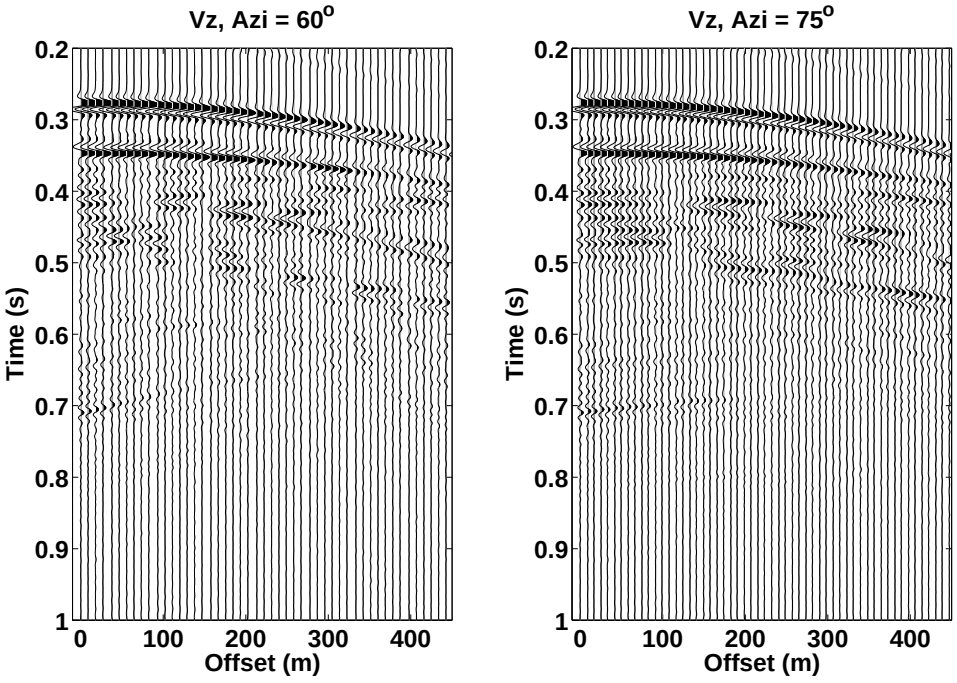

(a) (b)

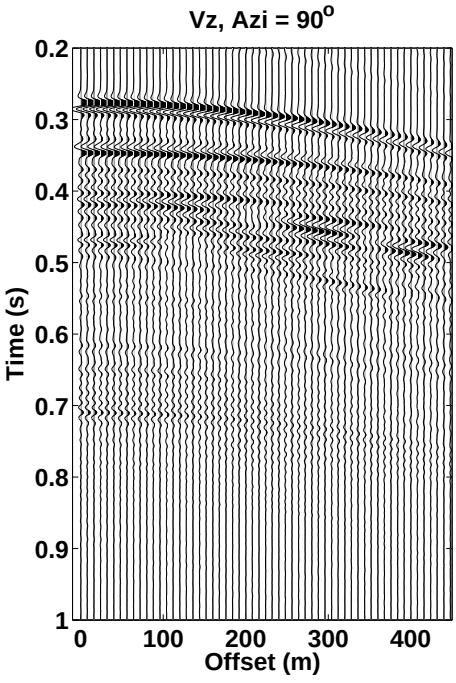

(c)

Figure 11: Shot gathers for a set of parallel fractures embedded in the middle layer

PSP from reservoir bottom and cause amplitude variations with offset.

In summary, we observe the following from the azimuthal shot gathers for the single set fracture model:

1. Seismic responses show azimuthal dependence;

2. Backscattering becomes stronger with increase of azimuth (less than 60 degrees). Forward scattering exists at all azimuths at far offsets. At 90° azimuth, the scattering forms coherent wavefronts, though tuning with offset appears.

3. The reflected PP from the top and bottom of the fractured layers are almost not affected and converted PS waves can be clearly seen up to 75 degree azimuth. At 90-degree azimuth, the scattering waves completely overwhelm the PS waves, but the scattered wavefronts seem to have the same moveout velocity as the converted PS wave from the bottom of the fractured layer.

Figure 12 and 13 show shot gathers for two sets of orthogonally intersecting fractures embedded in the middle layer. Because the model is completely symmetric relative to the 45-degree azimuth, and the two sets of fractures are of the same compliance, the gathers at 0 and 90 degrees are the same. They show the combination of characteristics of the scattering waves due to the single set of fractures at 0 and 90 degrees as shown in Figure 10a and 11c. In other words, we observe both back and forward scattering at near and far offsets, respectively imposed upon the coherent scattered waves, though the scattering seems stronger than that in the single fracture case. The reflected PP arrival from the bottom also shows strong interference by the scattered waves. At the 45-degree azimuth, the scattered waves become strong and appear at all offsets. Figure 14 shows the snapshots (a) in a horizontal plane crossing the fractured layer and (b) in a vertical plane including the source position parallel to the x axis. In the horizontal plane, the incident wave keeps the circular shape of its wavefront, but the wavefield within the fractured medium mirrors the fracture distribution. The snapshot in the vertical plane (Figure 14b) shows the incident wavefront is separated by the vertical fractures. The reflected P wave from the top of the reservoir is not affected, but the waves that follow it show considerable interference. At far offsets, the effects of the elastic property distribution on wave propagation are more complicated than those at the near offsets.

5.2 Orthogonally intersecting sets of different spacing

To study the sensitivity of the scattered wavefield to the spacing of the orthogonal fracture sets, we choose the spacing of the fracture set with orientation at 90 degree and 0 degree azimuths to be 30 m and 42 m, respectively. Figures 15 and 16 show the shot gathers. The gathers at 0 and 90 degree azimuths also show the combination of characteristics of the scattering waves due to the single set of fractures at 0 and 90 degrees as shown in Figure 10. However, the coherent scattering due to the fracture set of 42 m spacing is less pronounced than the 30 m one. The converted PS and PSP waves from the top and bottom of the fractured layer are still recognizable from the 0 azimuth shot gather. At the 90-degree azimuth, the reflected PP arrival from the bottom also shows strong interference by the scattered waves and the converted waves are difficult to identify. Therefore, the spacing of a fracture set significantly affects the scattering pattern.

5.3 Orthogonally intersecting sets of different compliances

If the two principal horizontal stresses are of different magnitudes, it will cause the fracture sets to have different compliances. To investigate the scattering of seismic waves due to two sets of intersecting fractures of different compliances, we choose the same 30 m spacing for the orthogonal sets of fractures, but the compliance of the set parallel to x axis is four times of that of the set normal to the x axis. The less

compliant fracture has the same compliance as those for the model with equal strength fracture sets. Figure 17 shows shot gathers at 0 and 90 degree azimuths. Comparing them with the gathers at the same azimuths in Figure 12a (the gathers at 0 and 90 degree azimuths are the same due to geometric symmetry of the model used for generating Figure 14), we see at 0 degree azimuth, parallel to the more compliant fracture set, the coherent scattered waves are much stronger than that from the more rigid fracture set whose orientation is at 90 degree azimuth. Strong forward and backward scattering appears at almost all offsets in the gather at 90 degree azimuth besides the coherent scattering due to fracture set oriented at 90 degree azimuth. The scattered waves due to the more compliant set also last much longer to around 0.9 s.

6 Case 2: Two 45-degree intersecting fracture sets

Figure 18 shows the model for non-orthogonally intersecting fracture sets, which make a 45-degree angle. As in Figure 8, the different colors in Figure 19 represent the background, the two sets of fractures and their intersections. The spacing of the set normal to the x axis is 30 m, and the spacing of the other set at 45-degree azimuth is 42 m. Both sets of fractures have the same compliance. The finite difference cells neighboring the intersections of the fractures can be assigned the same anisotropic properties computed using effective media theory, since the cell size is much smaller than the seismic wavelength. Here we choose 9 cells surrounding an intersection including the intersection itself. Average properties of the neighboring cells can also be considered when assigning properties to each cell. This will be a bit more complicated, but we do not expect it will make much difference since the size of the intersection area is about one order of magnitude smaller than the seismic wavelength.

The gathers in Figure 20 are best compared with those for the orthogonal intersecting fracture sets in Figures 12 and 13 and those for a single fracture set in Figures 10 and 11. At the 0-degree azimuth, the shot gather is similar to that for the single set of fractures. The 45 degree oriented fracture set apparently increases the forward scattering at far offsets. Otherwise, this gather does not show much sensitivity to the fracture set at the 45-degree azimuth. At the 90 degree azimuth, the gather shows significant forward scattering coming from the 45 degree oriented fracture and weak backward scattering. The coherent scattered waves are still clear around 0.4 – 0.5 s, but they show significant interference at later time from 0.6 and afterward. The shot gather at 45-degree azimuth shows coherent scattering mimicking those of 90-degree azimuth, since the receiver line is parallel to the orientation of one fracture set. Comparing to the gather at 90-degree azimuth, we see the scattering coming from the fracture set of shorter spacing is stronger and interferes with the coherent scattering.

Figure 21 shows the snapshots (a) in a horizontal plane crossing the fractured layer and (b) in a vertical plane including the source position parallel to the horizontal axis for the model including the two sets of non-orthogonally intersecting fractures. In the horizontal plane, the wavefront of the point source is still circular, but the wavefield within the fractured medium mirrors the fracture distribution, particularly at near offsets. The snapshot in the vertical plane Figure 21b shows the incident wavefront is divided by the vertical fractures in both azimuths. The reflected P wave from the top of the fractured layer is not affected. The waves that follow it show stronger interference than those in Figure 14 and the wavefield becomes more complex.

7 Conclusions

We describe a novel method for using a finite difference scheme to simulate wave propagation in media with intersecting fracture sets. We use effective media theory to compute the anisotropic elastic stiffness

for finite difference cells containing any segments of a fracture and assign the properties to those cells. Surrounding the intersections of the fracture sets, we use the long wavelength approximation and treat the cells as homogeneous to simplify the elastic stiffness calculation. Our implementation uses the rotated staggered grid and perfectly matched layer absorbing boundary condition to achieve good accuracy for scattered wave study.

We then use the finite difference program to model the wave propagation in layered formations with one set of parallel fractures, two sets of orthogonally intersecting fractures with the same spacing, different spacing, and different compliances, and two sets of non-orthogonally intersecting fractures. The reflected P waves from the top and bottom of the fractured layer are not significantly affected by the presence of the fracture sets. The converted PS and PSP waves from the bottom of the fractured layers show strong interference except at small azimuths. We observe coherent scattered waves in shot gathers parallel to the fracture orientation and significant backscattering at near offsets and forward scattering at far offsets. The scattering pattern varies azimuthally. When two sets of fractures are present, scattering becomes stronger and more complex scattered waves appear in the gathers. The shorter the spacing and the more compliant the fracture, the stronger the scattering. When the fracture sets are not orthogonal to each other, the gathers still show coherent scattering in the fracture orientations. By capturing the azimuthal characteristics of the scattered waves, one can analyze fracture orientations, spacing, and relative compliance of intersecting fracture sets. Detailed analysis of reflected and converted wave data obtained by using the proposed modeling method, may provide insights on the applicability of effective media theory in fracture characterization. The modeling method also provides a new, widely applicable tool for understanding seismic data from fractured reservoirs.

8 Acknowledgements

This work is funded by the ERL Founding Members Consortium. Additional support comes from Shell GameChanger.

References

Auld, B. A. (1990). *Acoustic fields and waves in solids, Volume I.* Robert E. Krieger Publishing Co.

Bakulin, A., Grechka, V., and Tsvankin, I. (2000a). Estimation of fracture parameters from reflection seismic data, Part I : HTI model due to a single fracture set. *Geophysics*, 65:1788–1802.

Bakulin, A., Grechka, V., and Tsvankin, I. (2000b). Estimation of fracture parameters from reflection seismic data, Part II : Fractured models with orthorhombic symmetry. *Geophysics*, 65:1803–1817.

Bakulin, A., Grechka, V., and Tsvankin, I. (2000c). Estimation of fracture parameters from reflection seismic data, Part III : Fractured models with monoclinc symmetry. *Geophysics*, 65:1818–1830.

Coates, R. T. and Schoenberg, M. (1995). Finite-difference modeling of fdaults and fractures. *Geophysics*, 60:1514–1526.

Grechka, V. and Kachanov, M. (2005). Multiple fractures in rocks: Effectiuve orthotropy and seismic characterization. In *Exp. Abstr., 75th Ann. Internat. Mtg.*, pages 158–161. Soc. of Expl. Geoph.

Hudson, J. A. (1986). Overall properties of a material with inclusions or cavities. *Geophys. J. Int.*, 117:555–561.

Liu, E., Hudson, J. A., and Pointer, T. (2000). Equivalent medium representation of fractured rock. *J. Geophys. Res.*, (105):2981–3000.

Lynn, H. B. (2004). The winds of change. *The Leading Edge*, 21(11):1156–1268.

Marcinkovich, C. and Olsen, K. (2003). On the implementation of perfectly matched layers in a three-dimensional fourth-order velocity-stress finite-difference scheme. *J. Geophys. Res. B*, 108(5):18–1–18–16.

Nelson, R. A. (1985). *Geologic analysis of naturally fractured reservoirs*. Gulf Publishing, Houston, TX.

Nichols, D., Muir, F., and Schoenberg, M. (1989). Elastic properties of rocks with multiple sets of fractures. In *Exp. Abstr., 59th Ann. Internat. Mtg.*, pages 471–474. Soc. of Expl. Geoph.

Nihei, K. T., Nakagawa, S., and Meyer, L. R. (2002). Finite-difference modeling of seismic wave interactions with discrete, finite-length fractures. In *Exp. Abstr., 72th Ann. Internat. Mtg.*, pages 1784–1751. Soc. of Expl. Geoph.

Reiss, L. (1980). *The reservoir engineering aspects of fractured formations*. Editions Technip, Paris.

Saenger, E. H., Gold, N., and Shapiro, S. A. (2000). Modeling the propagation of elastic waves using a modified finite-difference grid. *Wave Motion*, 31:77 – 92.

Sayers, C. M. (1998). Misalignment of the orientation of fractures and the orincipal axes for P and S waves in rocks containing multiple non-orthogonal fracture sets. *Geophys. J. Int.*, 133:459–466.

Schoenberg, M., Dean, S., and Sayers, C. M. (1999). Azimuth-dependent tuning of seimsic wave reflected from fractured reservoirs. *Geophysics*, pages 1160 – 1171.

Schoenberg, M. and Helbig, K. (1997). Orthorhombic media: modeling elastic wave behavior in a vertically fractured Earth. *Geophysics*, 62:1954 – 1974.

Schoenberg, M. and Muir, F. (1989). A calculus for finely layered anisoitropic media. *Geophysics*, 54:581 – 589.

Schoenberg, M. and Sayers, C. M. (1995). Seismic anisotriopy of fractured rock. *Geophysics*, 60:204 – 211.

Shen, F., Zhu, X., and Toksöz, M. N. (2002). Effects of fractures on NMO velocities and P-wave azimuthal AVO response. *Geophysics*, 67:711 – 726.

Vetri, L., Loinger, E., Gaiser, J., Grandi, A., and Lynn, H. (2003). 3D/4C Emilio: Azimuth processing and anisotropy analysis in a fractured carbonate reservoir. *The Leading Edge*, 22:675 – 679.

Virieux, J. (1986). Velocity-stress finite-differene method. *Geophysics*, 51:889 – 901.

Vlastos, S., liu, E., Main, I. G., and Li, X.-Y. (2003). Numerical simulation of wave propagation in media with discrete distributoins of fracturesl effects of fracture sizes and spatial distributions. *Geophys. J. Int.*, 152:649–668.

Willis, M. E., Burns, D. R., Rao, R., Minsley, B., Toksöz, M. N., and Vetri, L. (2006). Spatial orientation and disrtibution of reservoir fractures from scattered seismic energy. *Geophysics, in press*.

Willis, M. E., Rao, D. R. B. R., Minsley, B., Toksöz, M. N., and Vetri, L. (2004a). Spatial orientation and distribution of reservoir fractures from scattered seismic energy. In *Ext. Abstr. 74th Ann. Intern. Mtg.* Soc. Expl. Geophys.

Willis, M. E., Rao, R., Burns, D. R., Byun, J., and Vetri, L. (2004b). Reservoir fracture orientation and density from reflected and scattered seismic energy. In *Ext. Abstr., 66th Mtg.* Europ. Assn. Geophys. Eng.

Winterstein, D. F. (1990). Velocity anisotropy terminology for geophysicists. *Geophysics*, 55:1070–1088.

Zhang, Y., Chi., S., Willis, M. E., Burns, D. R., and Toksöz, M. N. (2005). Comparison of discrete fracture and effective media representation of fractures on azumuthal avo. In *Exp. Abstr., 75th Ann. Internat. Mtg.* Soc. of Expl. Geoph.

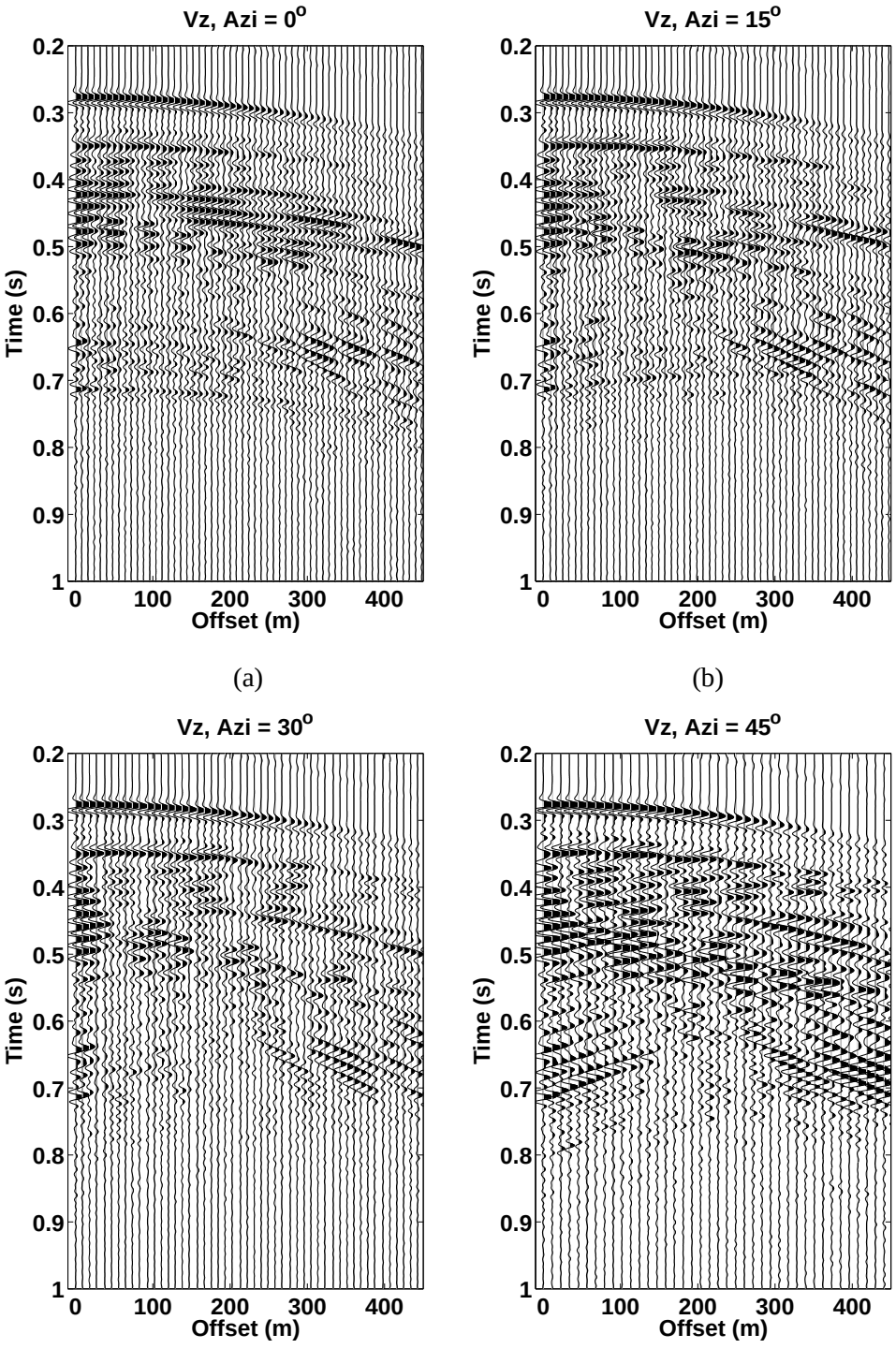

(a) (b)

(c) (d)

Figure 12: Shot gathers for two sets of orthogonally intersecting fractures embedded in the middle layer. The spacing of each set of fractures is 30 m.

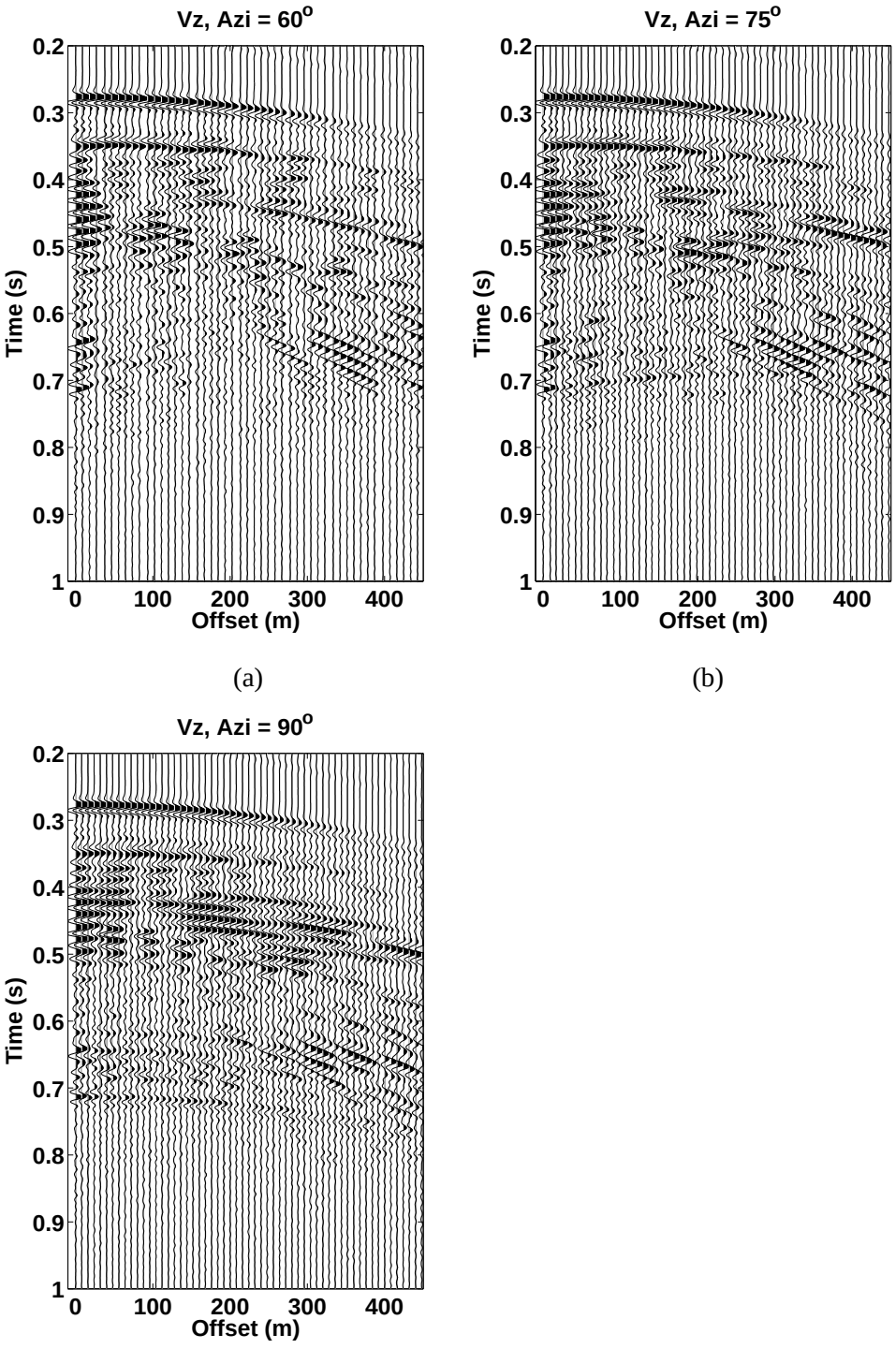

Figure 13: Shot gathers for two sets of orthogonally intersecting fractures embedded in the middle layer. The spacing of each set of fractures is 30 m.

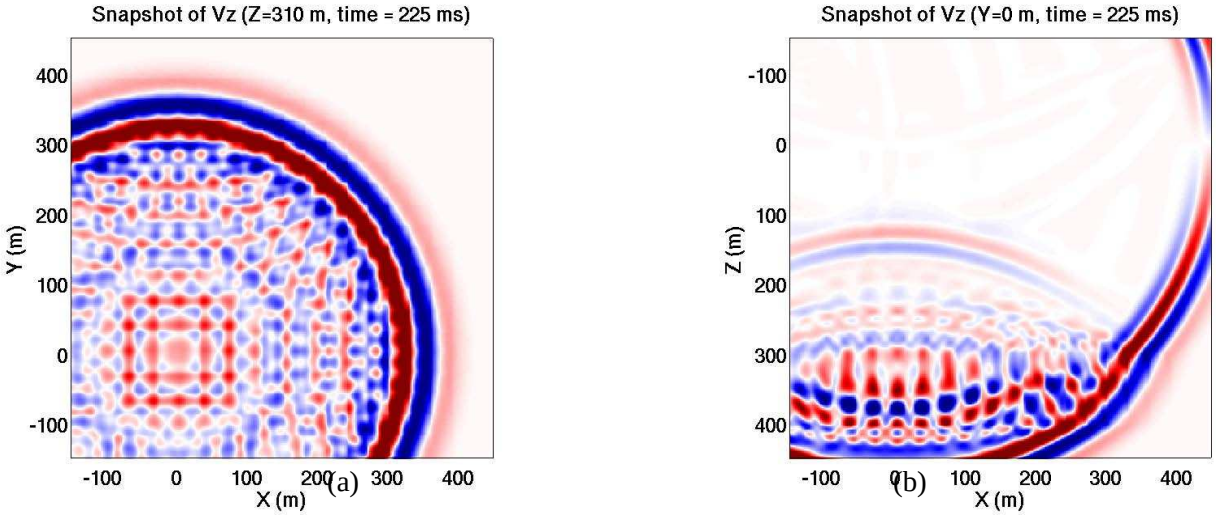

Figure 14: Snapshots of the wavefield in the fractured reservoir (a) in a horizontal plane at z=310 m; (b) in a vertical plane at y=0 m.

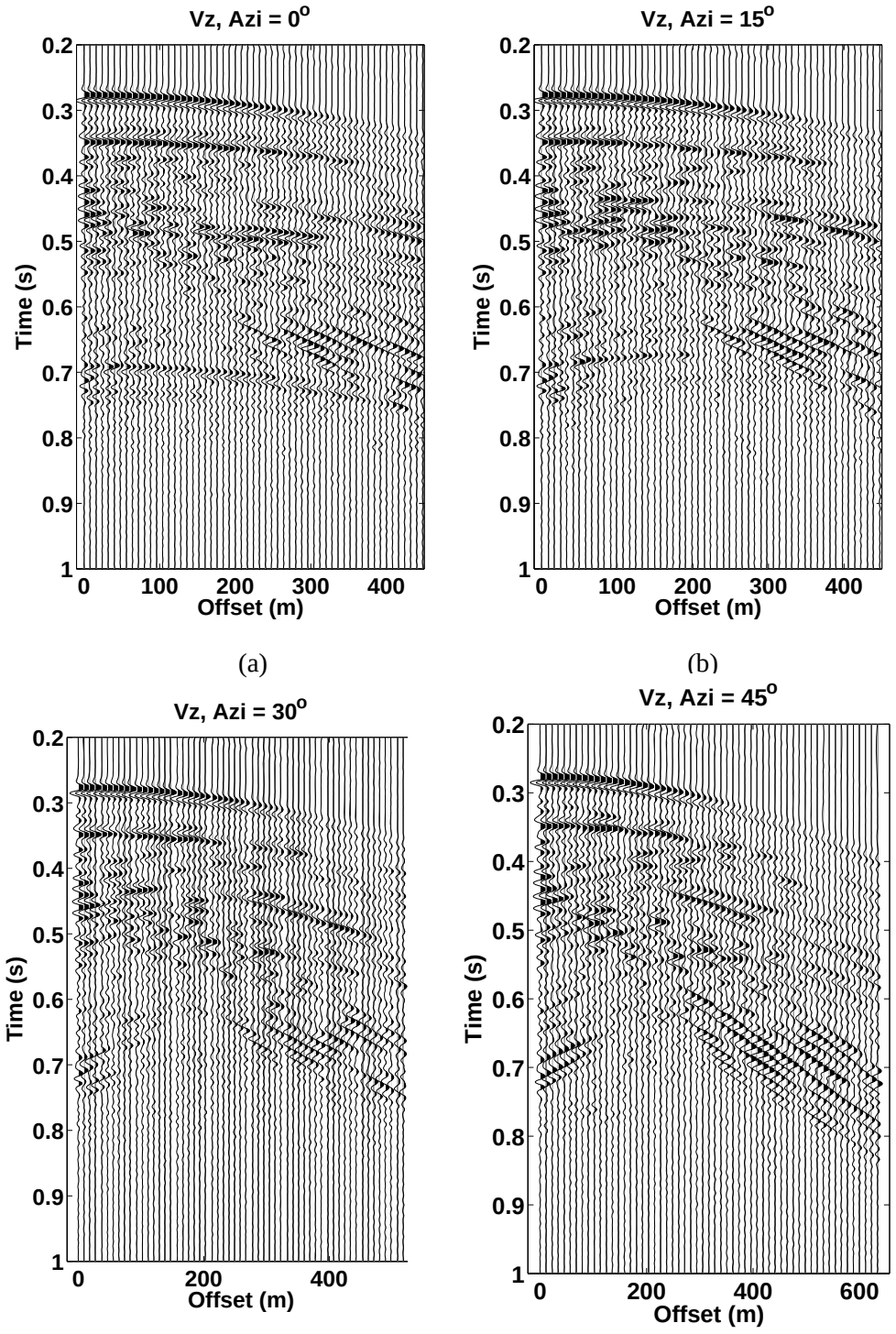

(a) (b)

(c) (d)

Figure 15: Shot gathers for two sets of orthogonally intersecting fractures embedded in the middle layer. The spacing of each set of fractures is 30 m and 42 m, respectively.

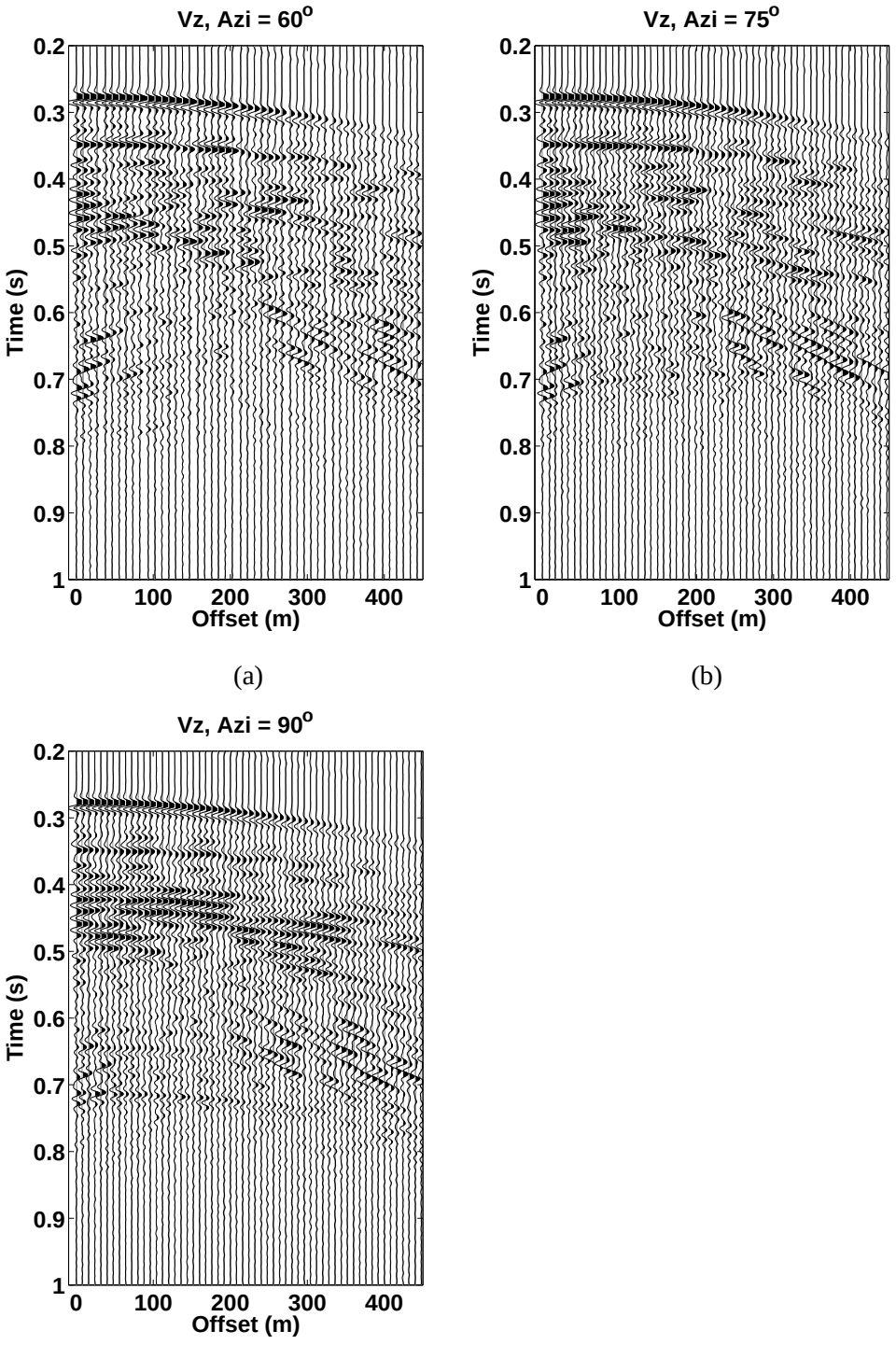

Figure 16: Shot gathers for two sets of orthogonally intersecting fractures embedded in the middle layer. The spacing of each set of fractures is 30 m and 42 m, respectively.

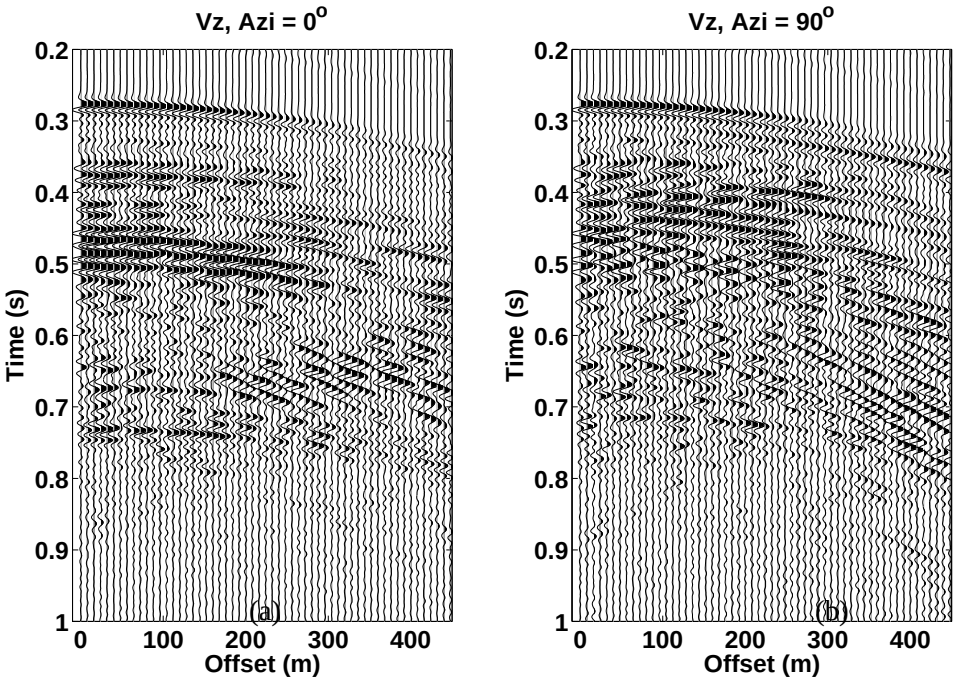

Figure 17: Shot gathers for two sets of orthogonally intersecting fractures embedded in the middle layer. The spacing of each set of fractures both is 30 m. The fracture set oriented at the 0 degree azimuth is four times as compliant as the one oriented at the 90-degree azimuth.

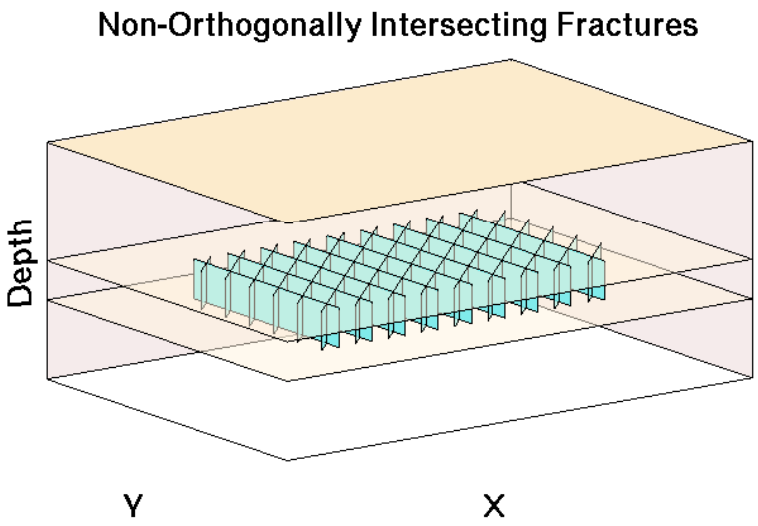

Figure 18: A 3D schematic of the reservoir model with two sets of intersecting fractures with an angle of 45 degrees.

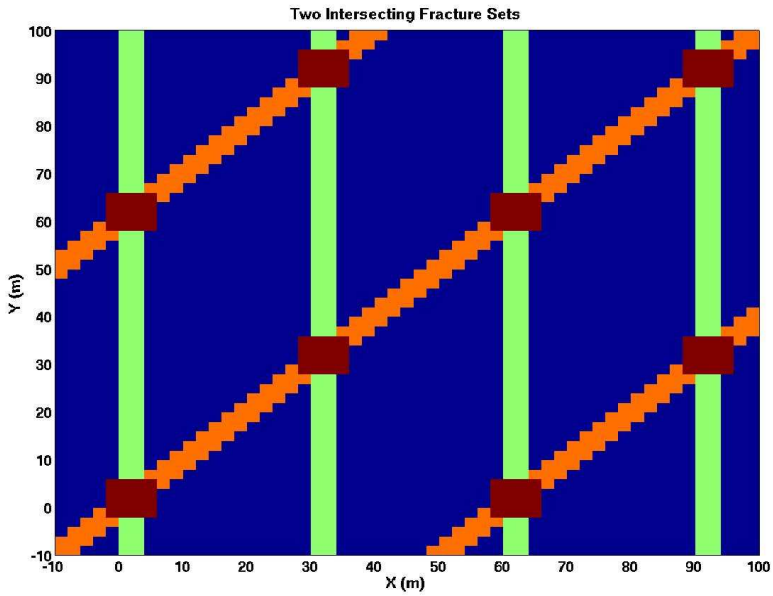

Figure 19: Elastic property distribution of two sets of 45 degrees intersecting fractures as indicated by different colors.

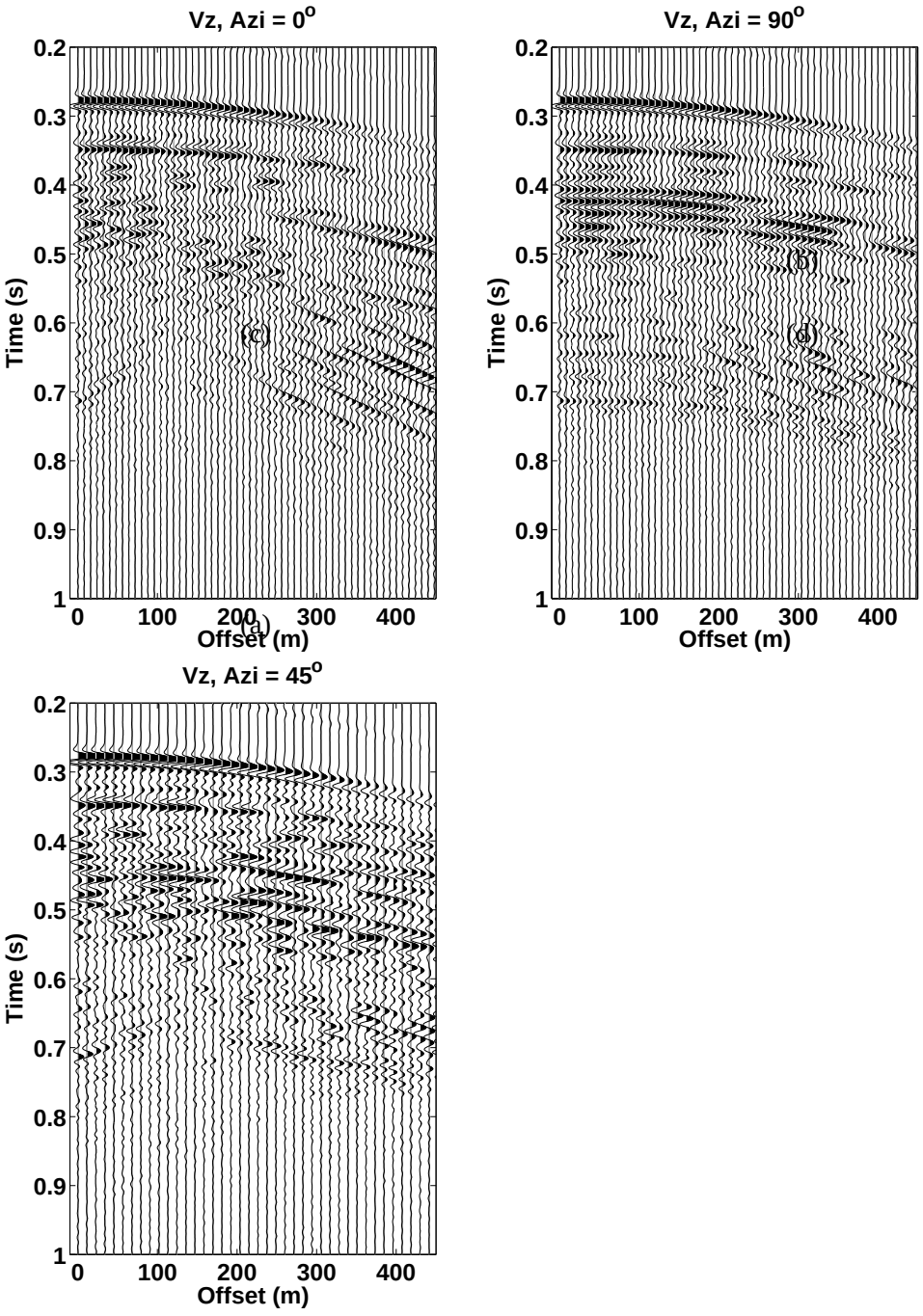

Figure 20: Shot gathers of vertical velocity measured on the surface of a fractured reservoir at 0, 90 and 45-degree azimuths.

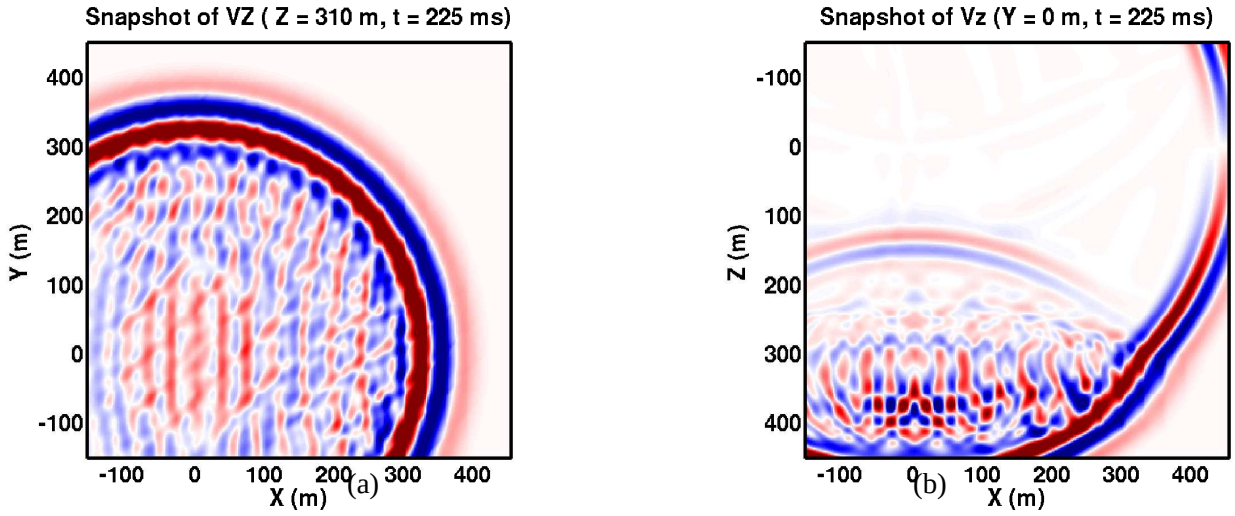

Figure 21: Snapshots of the wavefield in the fractured reservoir (a) in a horizontal plane at z=310 m; (b) in a vertical plane at y=0 m.

APPENDIX D

Orientation Estimation for Multiple Large Fractures by Scattering Energy

Yang Zhang, Shihong Chi, Mark E. Willis, M. Nafi Toksöz, and Dan Burns

Earth Resources Laboratory
Dept. of Earth, Atmospheric and Planetary Sciences
Massachusetts Institute of Technology
Cambridge, MA 02139

Abstract

We have done the numerical modeling of seismic response to multiple sets of vertical large fractures by using finite-difference method (FD), which can easily handle media with monoclinic anisotropy. We consider three types of fracture distributions: a set of parallel fractures, two sets of orthogonal fractures and two sets of non-orthogonal fractures intersecting at 45 degrees. We address the seismic scattering response to large fractures by using a 3-layer model and a 5-layer model, where a fractured reservoir is in the middle layer of these two models. Seismic scattered energy is analyzed by the Scattering Index (SI) method to estimate the orientation of these multiple fractures. In both models, SI indicates the correct orientation of the two orthogonal fracture sets but is ambiguous for non-orthogonal fracture sets. Information about the fracture spacing and compliance can also be extracted from the azimuthal SI in some situations. More compliant fracture sets result in higher SI values while the relationship between fracture spacing and SI depends on the source wavelength. Variations in the SI energy can be caused by fracture spacing and compliance variations, and these relationships need further investigation.

1. Introduction

With increasing interest in carbonate and unconventional (e.g., tight gas) reservoirs, fracture characterization has become an important research topic. When the seismic wavelength is much larger than the scale of the cracks or fractures in length and spacing, effective media theories can be used to describe the seismic response to fractures in the reservoir (e.g., Hudson, 1980, 1981; Schoenberg et al., 1980, 1988, 1995, 1997; Kachanov, 1980, 1992, 1993). Due to natural stress fields, the fractures in a reservoir usually are vertical or sub-vertical and have a preferred orientation parallel to the maximum horizontal stress direction, which could induce the seismic anisotropy. When a seismic wave propagates through an anisotropic medium the P wave shows an AVOAz (amplitude variation with offset and azimuth) response, an elliptical NMO velocity response with azimuth, and shear wave splitting. To take advantage of these seismic signatures, effective media theories provide the mathematical framework which has been used for inversion processes to get the parameters related to the fractured reservoir, such as fracture orientation, crack density and even properties of the fracture fill material.

However, cracks or fractures seldom distribute evenly in the subsurface as assumed in effective media theories. Often fractures will cluster onto large scale fracture corridors or zones, which can have much more impact on production. Recent research shows that the seismic response to such large fracture zones is quite different from that described by effective media theories. The response depends on fracture size, spacing, and distribution (Vlastos, et al., 2003; Chi, et al., 2006). Since the scale of fractures in such settings is comparable to the seismic wavelength, the prominent characteristic of seismic response is seismic scattering, which includes energy diffracted from fractures and reverberating within fracture zones. The strong scattered energy can make it difficult to identify coherent events in the seismic section (Willis, et al., 2006; Chi, et al., 2006). Zhang et al. (2005) numerically studied the AVOaz responses of PP reflections from the top of a reservoir containing large scale discrete fractures, and compared them to the responses obtained from reservoirs containing small cracks (i.e., effective media representation). They showed that in the case with large discrete fractures, the AVOaz for the PP reflections from the top of the reservoir had noticeable differences in magnitude and phase from those of the effective media case. Willis et al. (2006) studied the features of seismic scattering from one set of aligned discrete fractures, and estimated the orientation of the fractures by analyzing the scattered energy at different azimuths. Also

Willis et al. (2005) used the spectral notches of the scattered energy to estimate the fracture spacing. Grandi et al. (2005) and Zhang et al. (2006) estimated the fracture spacing by FK analysis of the backscattered energy from discrete fracture zones from P to P and P to S scattered energy.

These previous studies suggest that scattered energy from discrete fracture zones can be useful for fracture characterization, however most have focused on one set of aligned fractures. It is more likely that multiple sets of fractures are present in field settings, even if one set is more dominant due to the in-situ stress field. Much effort has been spent in considering the effect of multiple fracture sets in effective media theories (e.g., Nichols, et al., 1989; Grechka, et al., 2003; Grechka and Kachanov, 2006). A promising conclusion drawn by Grechka and Kachanov (2006) is that no matter how many vertical small cracks there are and how they orient and what types of infill they contain, the effective medium can be approximately described as orthorhombic. Geological observation suggests that there could be two or more sets, depending on the geological history in that particular area, of conjugate fractures coexisting. These sets of large fractures can be orthogonal or non-orthogonal to each other. For vertical large fracture sets in one fixed Cartesian coordinate system, such sets would give rise to media with different anisotropic symmetry, such as HTI, orthorhombic and monoclinic.

Chi et al. (2006) carried out a numerical study of the seismic scattering from multiple sets of vertical large fractures by using the finite difference method. They carefully handled these anisotropic media by assigning different effective elastic constants to the grid cells where fractures or the intersection of fractures were located. The effective constants for the fracture grid cells were calculated by the method developed by Coates and Schoenberg (1995). A simple 3-layer model with a fractured reservoir in the middle layer was used to emphasize on the scattering patterns due to multiple fracture sets. By analyzing the forward modeling results from different configurations of fractures sets, they addressed qualitatively the relationship between the patterns of scattered energy and the orientations, elastic properties, and spacing of the fracture sets. We might note that Willis et al (2004) had considered the case with dual fracture sets but simplified the fracture properties by using homogeneous and isotropic media directly. As mentioned earlier, Willis et al (2006) developed a method, called the Scattering Index (SI), to extract the orientation information of one single set of aligned fractures from variations in the scattered energy as a function of azimuth. The question we want to answer in this paper is whether the SI method can work on cases with multiple sets of fractures, and further to discuss whether the transfer function or the stacked traces can give us some new information about such multiple fracture sets.

This paper is organized in four sections: 1) a brief review of the numerical modeling work done by Chi et al (2006), since we will use their data for our SI analyses; 2) the analysis of the 3-layer model data by the SI method; 3) the analysis of one 5-layer model with multiple fracture sets; and 4) a discussion of the results.

2. Numerical Modeling of Multiple Sets of Fractures

Although the length and spacing of large fracture zones are comparable to the seismic wavelength, they are composed of many cracks that may contain weaker material such as oil, water and gas. These infill materials cause the fracture zones to be much more compliant than the background matrix material. As a result, fractures can behave mechanically as discontinuous interfaces, through which seismic wave induced displacements are discontinuous while tractions are continuous (Schoenberg, 1980). Schoenberg and Sayers (1995) mathematically derived a linear slip relationship to link the displacements and tractions with a factor **Z**, the fracture compliance, which describes the mechanical properties of fractures. Schoenberg and Sayers (1995) showed that the effective properties of media containing multiple fracture sets can be gotten by adding each set of fractures sequentially. Chi et al (2006) used a similar procedure, treating the finite difference cells containing intersecting fractures as multiple sets of fractures, while all other cells contained either a single fracture or the background material. In this paper, we only consider vertical fractures and a maximum of two fracture sets.

For a given coordinate system, the anisotropy for a single fracture set aligned with the coordinate axes would be HTI (horizontal transverse isotropy), and for a single fracture set oriented at an angle to the

axes the anisotropy would be monoclinic. For two sets of orthogonal fractures, the material at the intersection would be orthorhombic, and for those of non-orthogonal intersecting fractures, monoclinic it would be (Chi et al., 2006). Coates and Schoenberg (1995) introduced a method to represent the fractures in finite difference grids by calculating the effective constants for grid cells where fractures intersect. Once we get these effective constants, we can assign them onto grid cells corresponding to the locations of fractures. Figure 1 shows three types of fracture models considered in this paper: one set of aligned fractures, two orthogonal fracture sets and two non-orthogonal fracture sets intersecting at 45 degrees. Different colors represent materials with different anisotropic properties.

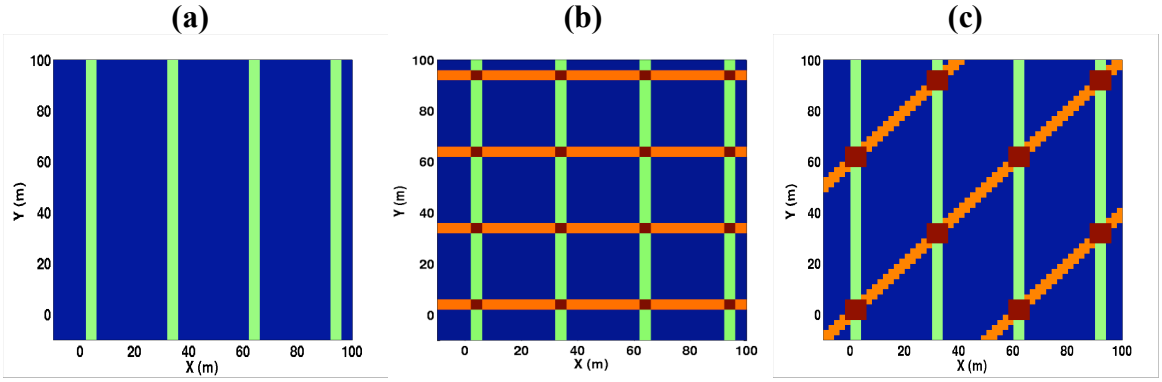

Figure 1: Three fracture models: (a) one set of aligned fractures; (b) two orthogonal fracture sets; (c) two non-orthogonal fracture sets intersecting at 45 degrees.

3. Orientation Estimation for Multiple Sets of Fractures with SI Method

The Scattering Index (SI) method developed by Willis et al. (2006) is a technique to estimate the orientation of aligned large fractures by capturing the azimuthal variation of the coherence of seismic scattering energy from fracture zones. The method was derived from numerical data analysis and has been successfully applied to onshore and offshore field data from fractured carbonate reservoirs. However, the methodology was developed with the assumption of a single set of aligned fractures and it is not clear if the method will work if there are multiple fracture sets present. Chi et al (2006) showed that the scattered wavefield generated from multiple sets of fractures is much more complicated than that of a single set of fractures, adding to this concern. To answer this question, we generate numerical waveforms for a 3 layered and 5 layered model. The middle layer in each contains fractures with one of the three types of fracture distributions shown in Figure 1. Figure 2 shows the model configuration for 3-layer model, in which source and receivers are at the surface, and the acquisition azimuths have been defined.

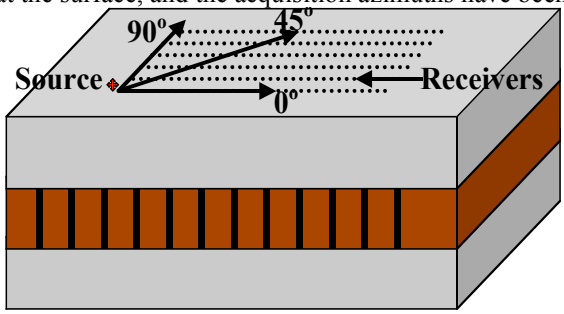

Figure 2: A three-layered model for fractured reservoir.

4. Results and Discussion

4.1 Model with 3 Layers

For this case, as shown in Figure 2, one fractured layer is embedded within two homogenous, isotropic layers. Large fractures in this layer are distributed in form of each of the models shown in Figure 1. The spacing for fracture set aligning at 90 degrees is set to 30 m (Figure 1a), denoted as $\mathbf{X30}$, while the spacing for the one orthogonally aligned is set to 30 m ($\mathbf{X30 \perp Y30}$) and 42 m ($\mathbf{X30 \perp Y42}$) respectively as shown in Figure 1b. For non-orthogonal fracture sets, the fractures oriented at 45 degrees have a spacing of $\mathbf{30 \cdot \sqrt{2} \approx 42}$ m ($\mathbf{X30 \angle 45}$), as shown in Figure 1c. The fractures we consider are rotationally invariant with normal and transverse compliance being equal. For most cases considered here, we choose fracture compliances $Z_N = Z_T = 2 \times 10^{-10}$ m/Pa for all fracture sets. For the case of $\mathbf{X30 \perp Y30}$ we also investigate unequal compliance for different fracture sets. We set the compliance value for the fracture set aligned at 0 degree ($\mathbf{Y30}$) to be four (4) times large than the fractures at 90 degrees ($\mathbf{X30}$). This situation is denoted as $\mathbf{X30 \perp Y30Z4\times}$. One case without fractures (**NoFrac**) is used as a reference (Figure 3a). For More details about the numerical modeling, please refer to the work by Chi et al. (2006).

For models without fractures and with parallel and orthogonal fractures, we sort the common-shot gathers in azimuths from 0 to 90 degrees at an increment of 10 degrees. A gather at an azimuth 45 degrees is also included. Especially for multiple non-orthogonal fracture sets intersecting in 45 degrees to each other, the range of azimuth should vary from 0 to 180 degrees because of the lower symmetry of the model configuration. Following the method of Willis et al (2006), we first use the shot gathers of the **NoFrac** model to do a velocity analysis and obtain the NMO velocities of the PP events at each azimuth (which should be equal theoretically). We then apply these NMO velocities on the azimuthal shot gathers for the rest models. We stack the traces of these NMOed shot gathers at offsets within 400 m. Figure 3a shows the stacked traces in azimuth for the model without fractures. Two strong events at times of about 550 ms and 650 ms represent the reflected PP wave from the top and bottom of the reservoir. The amplitudes of these arrivals have no azimuthal variation and no scattering energy arrives at later times. For using the SI method on the models containing fractures, we pick two time windows, the input and output windows, which are indicated by red and blue boxes respectively in Figure 3a. The longer output window is chosen to capture most of the scattering energy due to large fractures in the other models.

Applying the NMO velocities for the model without fractures on the data for models with fractures we get the stacked traces shown in Figure 3b to 3f. The most significant phenomenon for these traces is the coda energy existing at later times due to the scattering from the large fractures. For models with only one set of parallel fractures (Figure 3b), strong scattered energy is seen at the azimuth of 90 degrees, which is parallel to the fractures. After stacking, coherent scattered energy gets strong, while incoherent energy (that is, the combination of forward and back scattering) gets cancelled out. The result is that scattered energy stacks in at the azimuth that is parallel to the fracture direction. Due to symmetry of the configuration, the model with two sets of orthogonal fractures with equal compliances and spacing gives equally strong scattered energy at 0 and 90 degree azimuths, which are parallel to each set of fracture respectively (Figure 3c). Relatively small scattered energy is seen in the middle range of azimuths. For models with one set of more compliant fractures (Figure 3d), we see that the PP reflection from the bottom of the reservoir is mostly contaminated by the scattered wave energy. Strong scattered energy shows at all azimuths, and the scattered energy at 0 degrees is stronger than that at 90 degrees. This suggests that the more compliant fracture set contributes much more to the scattered wavefield. For models with two sets of fractures but with different spacing (Figure 3e), the azimuthal variation of scattered energy is somewhat similar to that for one set of parallel fractures (Figure 3b) except that a small amount of scattering is also seen at 0 degree azimuth, which is due to the second fracture set with larger spacing. Comparing energy in Figure 3d and 3e, we see that spacing and compliance both have an effect on stacked energy, but the compliance factor has the larger effect. The final model has two sets of non-orthogonal fractures at 45 degrees to one another. Figures 4f shows that the scattered energy varies azimuthally from 0 to 180 degrees. The strongest scattered

energy is seen at 90 degrees, which is parallel to the fracture set with 30 m spacing. There is a small amount of scattered energy visible at 45 degrees arriving at 900 ms.

To compute the SI attribute we can apply the input and output time windows to the azimuthal stacks in Figure 3 to isolate the signals for the deconvolutional process, which at the end gives us the transfer function linking these two signals (Willis et al., 2006). Being like a filter, the fractured reservoir takes in the simple input signal and converts it into the more complicated output signal. The transfer function describing the filter characterizes the degree of scattering due to the discrete large fractures in the reservoir. By calculating the L1-norm of the transfer function, Willis et al (2006) derived a quantity, scattering index (SI), as a seismic attribute of scattering to determine the orientation of fractures.

Figure 4 shows the scattering index (SI) values as a function of azimuth for cases with and without fractures. The SI values are calculated for azimuths between 0 and 90 degrees, and these values are then projected into the other quadrants based on symmetry. For the model without fractures there is no scattered energy and the SI values show no azimuthal variation (Figure 4a). For the model with one set of aligned fractures (Figure 4b), there is a large SI amplitude at an azimuth of 90 degrees, which is the orientation direction of the fracture set. Figure 4c shows the SI values for the model with two sets of orthogonal fractures having equal fracture spacing. High amplitudes are seen at azimuths of 0 and 90 degrees, indicating the orientation of the two sets of fractures respectively. This result, where the two fracture sets have the same compliance, can be compared to the case where the fracture compliance values are different. Figure 4d shows the results for the same two sets of orthogonal fractures as shown in Figure 4c, however in this case the fracture set oriented at 0 degrees has a compliance that is four times larger than the set oriented at 90 degrees. In the direction parallel to the more compliant set of fractures (0 degrees) the SI amplitude is about four times larger than the amplitude at 90 degrees, which is parallel to the less compliant fracture set. This is an encouraging result that suggests the possibility of using the scattered energy amplitude as a measure of fracture compliance, which could be related to fracture aperture and therefore permeability. However, such an approach must be entered into cautiously because of the ambiguity between fracture spacing and compliance. Figure 4e illustrates this point. For a model with two sets of orthogonal fractures but having unequal spacing, we see a pattern in the SI values that is similar to that seen with different compliance values. In this situation the highest SI amplitudes are in the direction parallel to the smaller fracture spacing (90 degree orientation, 30 m spacing), with a much smaller SI value peak (about a factor of three smaller) in the direction of the fracture set with larger spacing (0 degrees, 42 m spacing). The relationship between scattered wave energy and fracture spacing will be a function of the seismic wavelength. Because of the similar response of the SI attribute to changes in fracture compliance and spacing, it is important to find ways to differentiate between these two effects. Zhang et al. (2006) and Willis et al. (2006) have used the backscattered energy and spectral notches respectively to estimate the fracture spacing from the scattered wave energy. Such approaches might provide us with a means of separating the effects of spacing and compliance and allow us to isolate the effect of fracture compliance. The final model is for two sets of non-orthogonal fractures, one set oriented at 90 degrees and the second set oriented at 45 degrees. Both fracture sets have the same compliance, but the spacing is different (larger spacing for the fracture set at 45 degrees). In this case we need to investigate the scattering in the azimuth range from 0 to 180 degrees in order to cover fully the scattering for both fracture sets. The resulting SI values are plotted from 0 to 180 degrees, which is symmetric for the 180 to 360 degree azimuths. Figure 4f shows that the SI values are largest at 90 degrees, the orientation of one set of fractures (with the smaller spacing), while the other azimuths show much smaller values. We can infer that another set of fracture is present, which could be oriented at 30, 45, or 135 degrees based on the SI distribution (which is clearly different from that seen for a single set of fractures as in Figure 5b). For this simple 3-layer model, the stacked traces in Figure 3f would suggest that the second fracture set is at 45 degrees, however the SI values are less clear.

4.2 Model with 5 layers

In the three layer model, it is quite easy to pick out the reflections from the top and base of the reservoir, even in the presence of significant scattering. However, in actual field situations there will be many reflectors present and it will not be easy to isolate these reflectors for SI analysis. In order to test the methodology in a slightly more realistic situation we generate a second set of models containing 5 layers.

In these models we will use a larger sampling window containing several reflected events for the SI analysis, as was shown by Willis et al. (2006). The 'input' wavelet is estimated from a window containing reflection events above the reservoir level, and the 'output' wavelet is estimated from a window containing reflection events below the reservoir level. The transfer function is estimated from these wavelets via a deconvolutional process.

Choosing the same parameters for the background media and fracture compliance used by Willis et al. (2006), we modeled the seismic response to discrete large fractures embedded in the middle layer. The same three types of fracture model shown in Figure 1 are considered, but for these models the fracture spacing is set at 35 m to provide maximum scattering for this set of parameters (Willis et al., 2006). In this case the spacing between fractures orientated at 45 degrees is about 50 m, so there are a total of six cases considered in this section: **NoFrac**, **X35** , **X35 ⊥ Y35** , **X35 ⊥ Y35Z4×** , **X35 ⊥ Y50** and **X35∠45** .

Figure 5a shows the azimuthal stacked traces for the model without fractures. Four arrivals are seen, which correspond to the PP reflected waves at each interface in the model. We take a window (red) including first two reflected PP events as the input signal, and then another window (blue) including the last two as the output signal. These two time windows will be applied on the azimuthal stacked traces for the other models as well.

Azimuthal stacked traces for all the different models are shown in Figure 5 and most of the same trends seen for the 3-layer models are present. For the model with a single set of parallel fractures (Figure 5b), strong scattered energy remains after stacking in the direction parallel to the fracture strike. For the model with two sets of orthogonal fractures with the same spacing (Figure 5c) strong energy is seen in the two directions parallel to the two sets of fractures. When one fracture set is four times more compliant, the more compliant fracture set induces stronger scattered energy in the direction parallel to its strike (Figure 5d), although the difference in amplitude is not as great as it was in the 3-layer model (Figure 3d). Figure 5e shows the results for a model with two sets of orthogonal fractures but with different spacing. For the 3-layer model we observed that the fracture set with smaller spacing (30 m) induced stronger scattered energy than the one with larger spacing (42 m). However for the 5-layer model, the fracture set with the larger spacing (50 m) seems to give slightly stronger energy than smaller spacing does (35 m), although the difference is quite small. This may be due to somewhat different source wavelengths in the two models. The final model is for two sets of non-orthogonal fractures, oriented at 90 and 45 degrees (Figure 5f). We still see strong scattered energy in the 90 degree direction along with significant scattered energy at most other azimuths although higher amplitudes are seen around 45 degrees, the orientation of the second set of fractures.

Applying the time windows defined in Figure 5a to each set of model azimuthal stacks we compute the SI values, which are shown in Figure 6. For the model without fractures (Figure 6a), the SI values are small and approximately equal at all azimuths. For one single set of parallel fractures, the SI value is a maximum in the direction of the fracture strike (Figure 6b). The three cases with orthogonal fracture sets are shown in Figures 6c, d and e respectively. All of them give a clear indication of the orientations for both sets of fractures. We notice that the SI plots in Figures 6d and 6e look similar, with the maximum SI value being at 0 degrees. In Figure 6d this direction corresponds to the fracture set with largest compliance, while in Figure 6e this direction corresponds to the fracture set with the larger spacing, which shows again the ambiguity between compliance and spacing. In Figure 6f, the SI peak is at 90 degrees indicating the set of fracture with 35 m spacing with a broad area of increase SI values around is at 30 to 50 degrees.

Acknowledgements

This work was supported by the Founding Member Consortium at the Earth Resources Lab, and DOE Award No. DE-FC26-02NT15346.

References:

Chi, S. H., Zhang, Y., Campman, X. and Toksöz, M. N., 2006 Finite difference modeling seismic responses to intersecting fractures, 2006 ERL Consortium Meeting Repoert

Coates, R. T. and Schoenberg, M., 1995, Finite-difference modeling of faults and fractures, *Geophysics*, 60, 5, 1514-1526

Grandi, S., Willis, M. E., Burns, D. R. and Toksöz, M. N., 2005, F-K analysis of backscattered signal to estimate fracture orientation and spacing, 2005 ERL Consortium Meeting Report

Grechka, V. and Tsvankin, I., 2003, Feasibility of seismic characterization of multiple fracture sets, *Geophysics*, 68, 1399-1407

Grechka, V. and Kachanov, M., 2006, Seismic characterization of multiple fracture sets: Does orthotropy suffice?, Geophysics, 71, …

Hudson, J. A., 1980, Overall properties of a cracked solid, *Math. Proc. Camb. Phil. Soc*., 88, 371-384

Hudson, J. A., 1981, Wavespeeds and attenumation of elastic waves in material containing cracks, *Geophys. J. Roy. Astr. Soc*., 64, 133-150

Kachanov, M., 1980, Continuum model of medium with cracks, *J. Eng. Mech. Div., ASCE*, 106, EM5, 1039-1051

Kachanov, M., 1992, Effective elastic properties of cracked solids: Critical review of some basic concepts, *Appl. Mech. Rev.*, 45, 304-335

Kachanov, M., 1993, Elastic solids with many cracks and related problems, *Adv. Appl. Mech*., 30, 259-445

Nichols, D., Muir, F., and Schoenberg, M., 1989, Elastic properties of rocks with multiple sets of fractures, *59th SEG Expanded Abstracts*, 471-474.

Schoenberg, M., 1980, Elastic wave behavior across linear slip interfaces, *J. Acous. Soc. Am.*, 68, 1516-1521

Schoenberg, M. and Douma, J., 1988, Elastic wave propagation in media with parallel fractures and aligned cracks, *Geophysical Prosp.,* 36, 571-590

Schoenberg, M. and Sayers, C. M., 1995, Seismic anisotropy of fractured rock, *Geophysics*, 60, 1, 204-211

Schoenberg, M., and Helbig, K., 1997, Orthorhombic media: modeling elastic wave behavior in a vertically fractured earth, Geophysics, 62(6), 1954-1974.

Vlastos, S., Liu, E., Main, I. G. and Li, X. Y., 2003, Numerical simulation of wave propagation in media with discrete distributions of fractures: effects of fracture sizes and spatial distributions, *Geophysical J. International*, 152, 3, 649-668

Willis, M., Rao, R., Burns, D. and Byun, J., 2004, Spatial orientation and distribution of reservoir fractures from scattered seismic energy, 2004 ERL Consortium Meeting Report.

Willis, M., Rao, R., Burns, D. and Toksoz, M. N., 2005, Fracture spacing and orientation estimation from spectral analyses of azimuth stacks, Expanded abstract, EAGE meeting, Madrid.

Willis, M., Burns, D. R., Rao, R., Minsley, B., Toksoz, M. N., Vetri, L., 2006, Spatial orientation and distribution of reservoir fractures from scattered seismic energy, *Geophysics, in press*.

Zhang, Y., Chi, S., Willis, M. E., Burns D. R. and Toksöz, M. N., 2005, Comparison of discrete fracture and effective media representation of fractures on azimuthal AVO, *75th SEG Expanded Abstracts*

Zhang, Y., Campman, X., Grandi, S., Chi, S. H., Willis, M. E., Toksöz, M. N. and Burns, D., 2006, Wavenumber-Frequency domain characteristics of the seismic response of a set of parallel discrete fractures, *76th SEG Expanded Abstracts* submitted

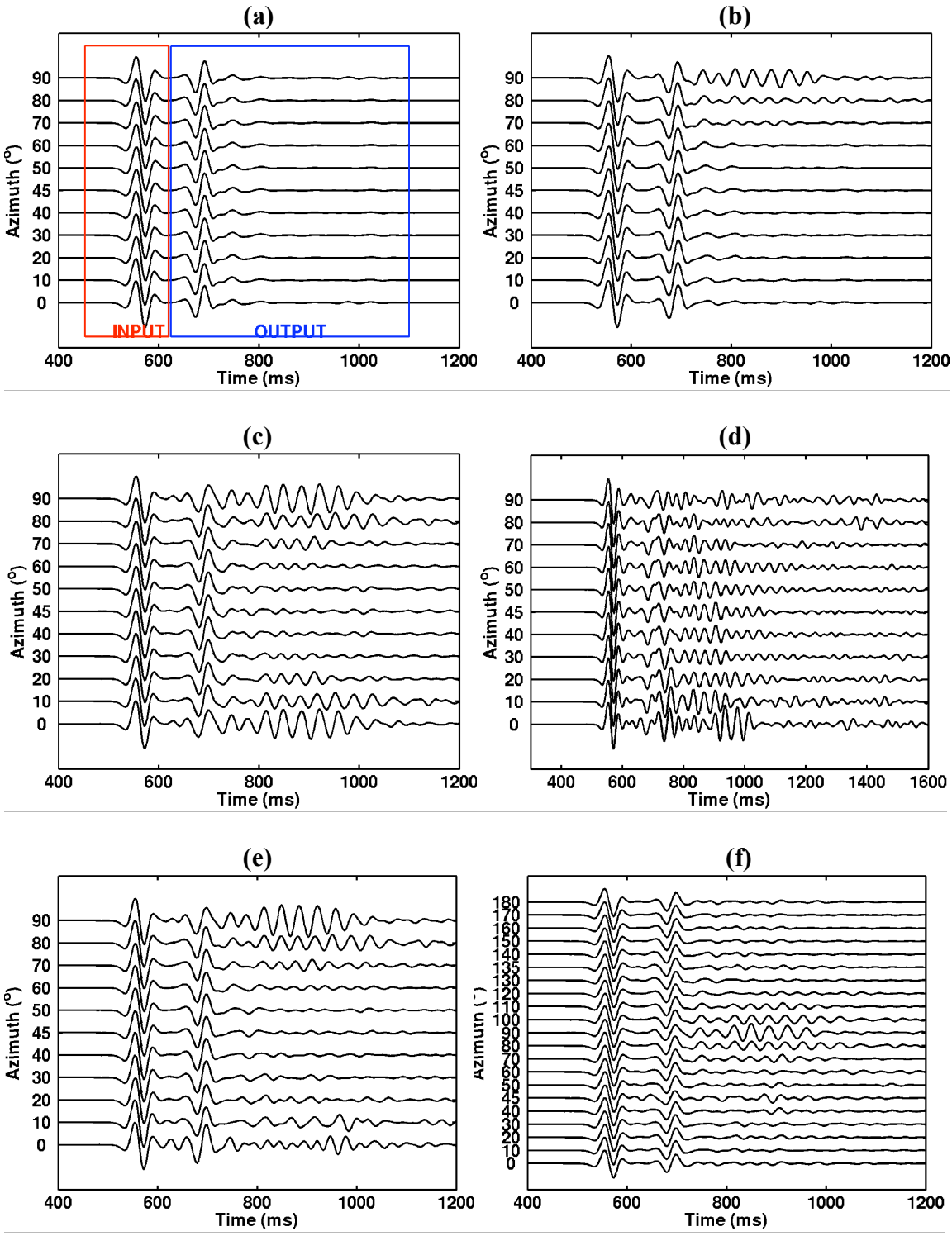

Figure 3: Azimuthal stacked traces for the 3-layer models. (a) no fractures; (b) single fracture set with a strike of 90 degrees (**X30**); (c) two sets of orthogonal fractures with the same fracture compliance and spacing (**X30** ⊥ **Y30**); (d) same as (b) except compliance for fracture set aligned at 0 degrees is 4 times large than that at 90 degrees (**X30** ⊥ **Y30Z4**×); (e) two sets of orthogonal fractures with different spacing (**X30** ⊥ **Y42**); (f) two sets of non-orthogonal fractures at 45 degrees, 0 to 180 degrees azimuth (**X30**∠**45**);

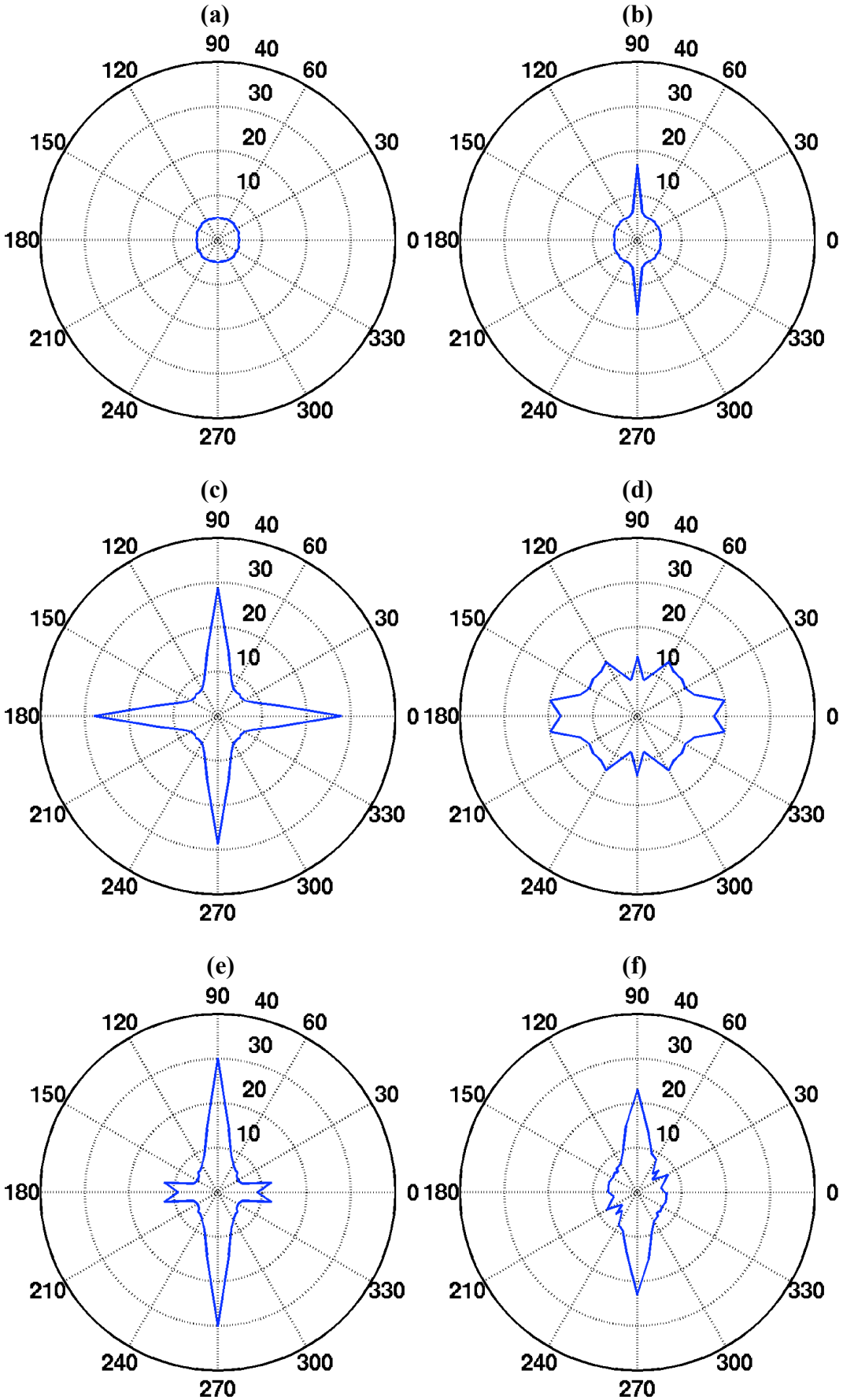

Figure 4: Azimuthal scattering index for 3-layer models (a) **NoFrac**; (b) **X30**; (c) **X30 ⊥ Y30**; (d) **X30 ⊥ Y30Z4×**; (e) **X30 ⊥ Y42**; (f) **X30∠45**.

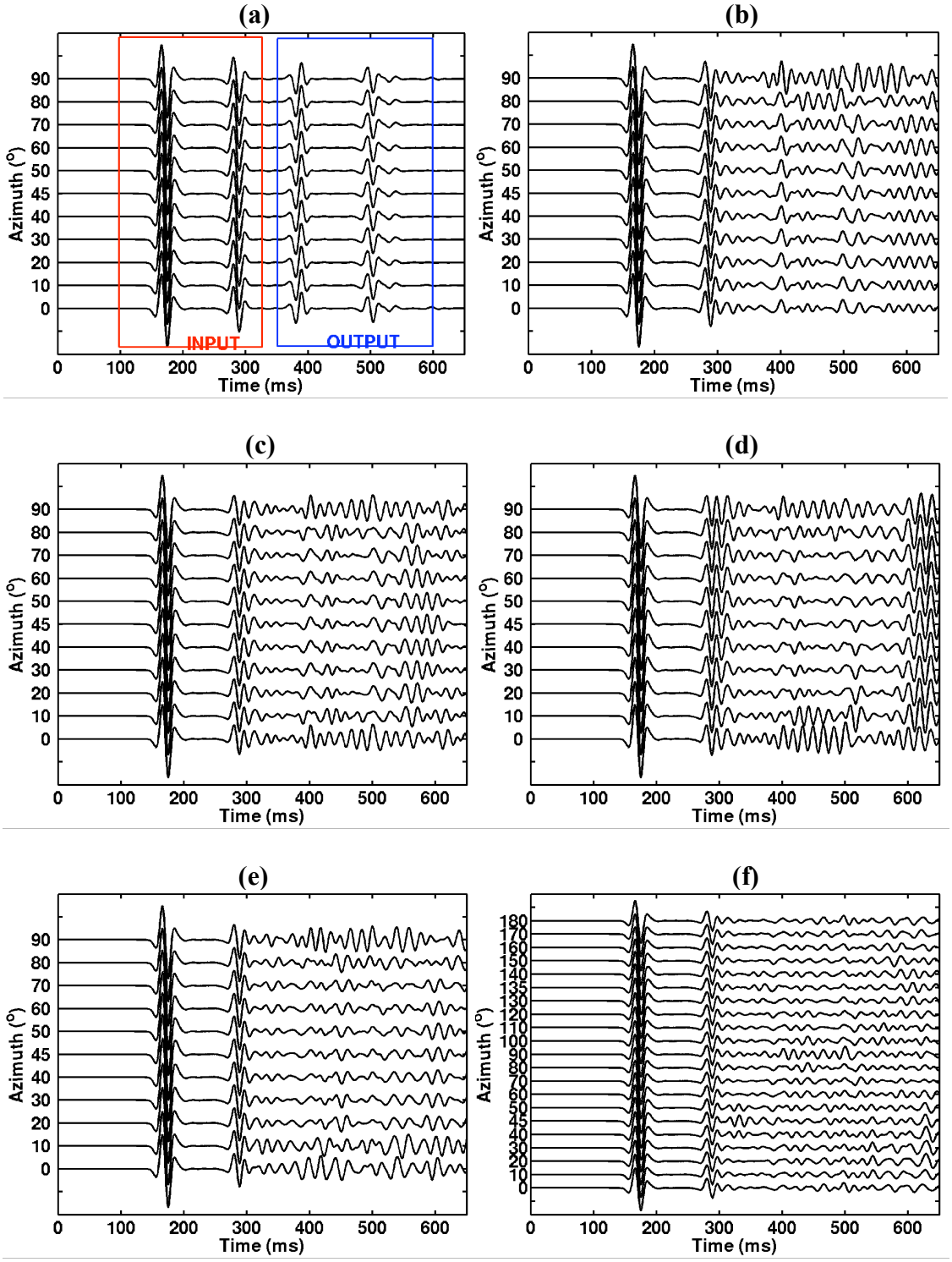

Figure 5: Azimuthal stacked traces for 5-layer models. (a) no fractures; (b) single fracture set with strike of 90 degrees (**X35**); (c) two sets of orthogonal fractures with the same fracture compliance and spacing (**X35** ⊥ **Y35**); (d) same as (b) except compliance for fracture set aligned at 0 degrees is 4 times large than that at 90 degrees (**X35** ⊥ **Y35Z4**×); (e) two sets of orthogonal fractures with different spacing (**X35** ⊥ **Y50**); (f) two sets of non-orthogonal fractures at 45 degrees, 0 to 180 degrees azimuth.

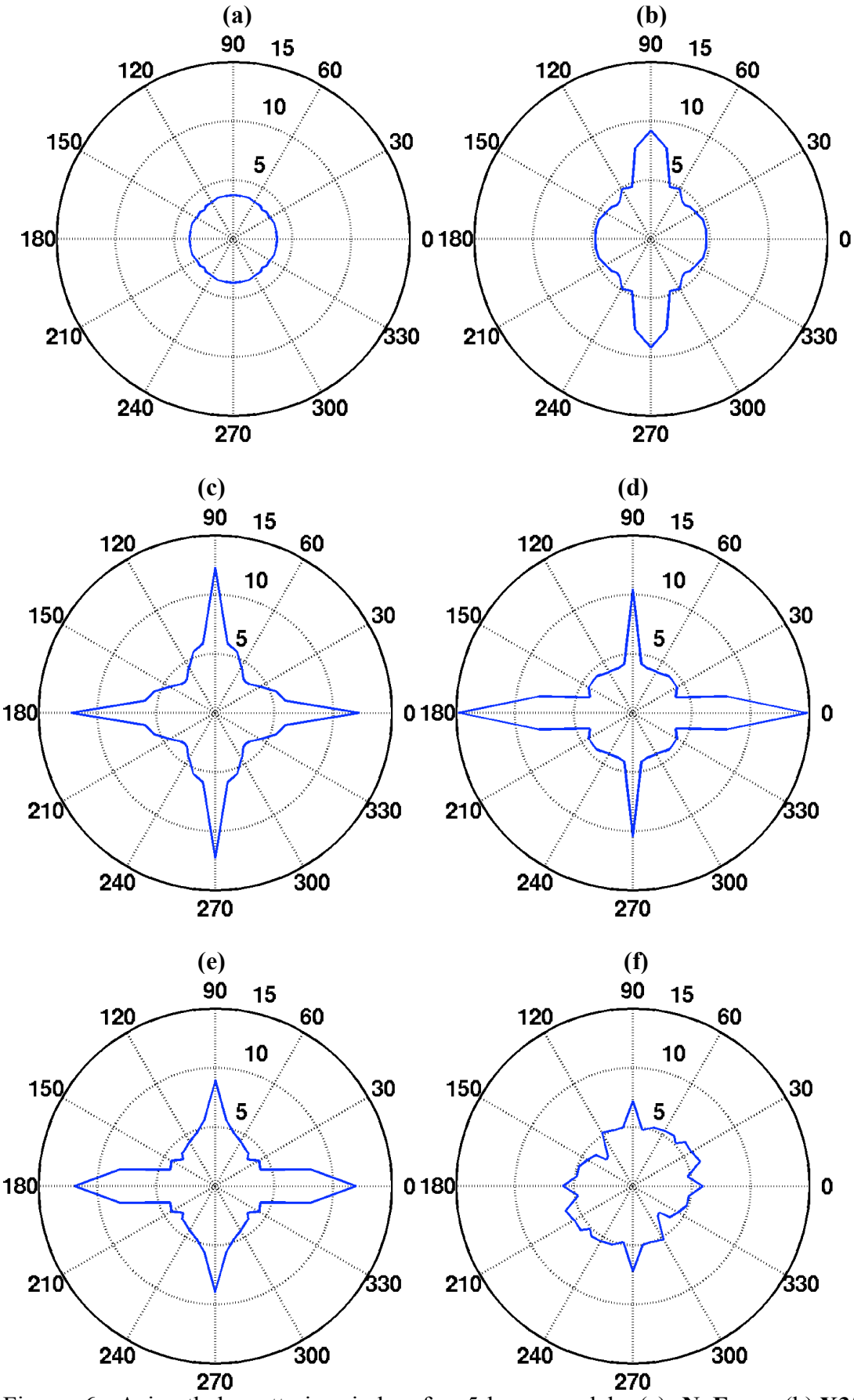

Figure 6: Azimuthal scattering index for 5-layer models (a) **NoFrac**; (b) **X35**; (c) **X35 ⊥ Y35**; (d) **X35 ⊥ Y35Z4×**; (e) **X35 ⊥ Y50**; (f) **X35∠45**.